Round 1

Reviewer #1

The manuscript titled "The 1804 Alborán seismic series: search for the source using seismic scenarios and static stress interactions" by Y. de Pro-Díaz, J. J. Martínez-Díaz and C. Canora-Catalán presents the research carried to associate the historical 1804 Alboran earthquake to a recognized active fault. The manuscript focuses in the use of a methodology, already used in previous works, based on the comparisson between a modeled intensity field, using GMM and GMICE, and the distribution of the intensity data points. In addition, they complement this discussion using the changes on the coulomb stress produce by these event on the proposed source of the 1804 Dalias earthquake. Finally, they compare the coulomb stress change produced by the 1804 Dalias earthquake with the distribution of the recorded seismicity since then.

The manuscript would be of interest to researchers involved in seismotectonics, active tectonics and seismic hazard in south Iberia and Alboarn sea regions. If authors made an effort to define an approche more focused on offshore areas it could be of interest for a larger audience.

The data and results presented are of interest and bear significant outcomes in terms of identifying the causative fault of an historical earthquake that produced damage and was felt in south Iberia and north Morocoo. However, some rather weak points affect the manuscript. In this view, the models presented in the manuscript need to be better described and, then, base the discussion on the differences between the models. In addition, they model some but not all of the known active faults in the northern Alboran sea, so their conclusions about the fault that caused the 1804 eaqrthauqek may not be quite strong considering the present knowledge of active faults in the area. There are is much room for improvement.

Despite my criticism, to be intended solely as constructive, I warmly encourage the authors to make any effort for the publication of their data in a future improved manuscript.

General comments:

The following observations are possibly the main problems that I have found in the manuscrpt, but I have included further comments in the reviwed manuscript.

1. To me all the sections related to th Gasperini's method is not valuable, nor necessary. It is known that this method uses the maximum intensity data to evaluate earquake's source area location and its magnitude. If all the previous works on the 1804 Alboran earthquake have located the source offshore, it is clear that the distribution of the intensity data points will not be complete and distributed just on the onshore areas, and the results will not be relevant.

2. The authors just consider the faults on the Quaternary Active Faults of Iberia (QAFI) database, but have not look for other possible sources in the area that are mapped and referred in other more recent publications. I would say that if this work wants to be relevant, all the possible sources must be considered. So a review of the recent references must be done.

3. The description of the results (different models) has to be greatly imporved. In the discussion is mention that a source is preferred over the others because the modeled intensity field is more in agreement with intensity data points distribution, but this is not described in the results section.

4. The authors discuss about the influence of the GMM in the final model results, but they do not dicuss anything about the GMICE. This could also be responsible of some differences in between the real data and the modeled fields.

5. To me the part related to the Dalias 1804 Coulom stress change modeling is not relevant in this work. Even the discussion is quite poor about this event. Authors may consider the interest in including this earthquake and they decide to include it, then improve the results description and the discussion.

Reviewer #2

This study tries to identify the best candidate as fault source of the 1804 Alboran earthquake (Iberia). An approach involving the Boxer method, seismic scenarios built in OpenQuake and Coulomb stress transfer is pursued. Ten candidate faults are examined and 6 are ruled out. The topic is of interest to the potential readers of the journal.

The work presents interesting results, even though not conclusive. I suggest below some comments on how to improve the data/results, and some request for clarification.

Line-by-line comments:

- The final part of the abstract is quite weak, or too vague, since it doesn't capture the attention of the reader. Even though the results of this study are not conclusive, you can better emphasize the knowledge you gained, or that you were able to rule out some candidate faults.
- Lines 95-96: EMS, ESI – define all the acronyms the first time you use it
- Section 2.1: there are quite a lot of acronyms, some of them very similar to each other. Try to limit the number of acronyms; my suggestion is to keep the acronyms only for the faults that were used as scenarios. This already brings the count to 5 (Table 1). Write out all the other fault names in the text; keep the acronyms in the figures and write out in the captions.
- Line 190 caption fig 1: write out EBSZ and TASZ
- Line 259: describe the input data and Boxer procedure, as done at line 270-275 for the Openquake scenarios.
- Line 292: which is the threshold for "enough data points"?
- Lines 345-355: different user choices were made on different faults, namely whole length for 3 faults, area-magnitude scaling relations (Carboneras) and an ad-hoc choice (Al Idrissi). This seems rather ambiguous and poorly justified from the methodological point of view, implying a non-negligible amount of subjectivity. If the scope is to test different scenarios to identify the most reliable candidate ruptures, the user choices should be kept to a minimum.
- Line 365 (table 1): not clear why A1, A2 and A3 scenarios have different M but the same area. Maybe I'm missing something, in the text you mention the Stirling and Wells&Coppersmith' equations. Table 1 caption: add Al-Idrissi fault
- Figures 4 and 5: the use of the same color palette for seismic scenarios and observed intensity data points makes it challenging to discern the colors. Maybe try a different color scheme, or contour plot for the scenarios
- Lines 375-376: the max observed intensity is VII-VIII (Table AP1) while seismic scenarios have max intensity IX (Figures 4-5). I would have expected more R(obs-rup) negative values, while in figure 6 there are only a few standard deviation bars > 0. This points to a GMM which attenuates faster than what has been observed in the 1804 earthquake.
- Lines 378 vs 381: the Al-Idrissi scenario is considered among the competing scenarios or not?
- Lines 388-394: I agree with your reasoning, but the text could be improved: now it seems that you chose a GMM but it didn't work well, so you moved to another GMM. This looks too subjective. If you change the phrasing into "we tested 2 GMM and the Akkar&Bommer is consistently better in terms of residual", it looks better constrained.
- Lines 437-438: for all the 3 comparisons you say there are no enough points to perform statistical analysis; since this holds for all the scenarios, just delete this part.
- Section 4.5 and figure 14: I'm not fully convinced by the claim that the Dalias earthquake could have influenced the posterior earthquake distribution. Seismicity in fig 14 does not have a strong spatial pattern. Can you show a histogram with the frequency of earthquakes vs DCFS?

- Line 526: I think Boxer needs to be calibrated with a dataset of earthquakes from the region under investigation. One reason for the poor performance of Boxer could be that it was not calibrated with earthquakes in the Betics area.
- Line 538: you present 4 possible explanations, not 3.
- Line 556: a sentence about the datasets used to build the 2 GMMs (geographic distribution, kinematics, magnitude range) is needed much earlier in the manuscript. If Akkar & Bommer is built using data from the study area, why did you first tried another GMM?

Reviewer #3

Review of the manuscript entitled “The 1804 Alborán seismic series: search for the source using seismic scenarios and static stress interactions” by Y. de Pro-Díaz et al.

In this manuscript, the authors investigate the 1804 Alborán seismic sequence using intensity data. In particular, they use the Gasperini method, the seismic scenario method and a Coulomb stress transfer analysis to try to understand which fault, or faults, may have been responsible for the main earthquakes and potential subsequent seismicity. The results are not conclusive but allow the elimination of possible sources (six out of ten), leaving four possible faults as potential sources. This work may contribute to informing us of the seismic hazard of the region.

Overall, this is a good and informative contribution. I would recommend this manuscript for publication, but it still needs some work, in particular in terms of quality and clarity of the writing. Some parts are better written than others, so it would be good a couple of rounds of polishing. The parts that are poorly written are really hard to read and the reader has to read each sentence a few times before being able to move forward. There are also several loose/informal terms and, in some places, the links between text and figures can be improved. The figures are in general ok, but a few may need some attention (either small amendments or clarifications in the captions).

I am sending a PDF file with many comments and suggestions that the authors can use to work on an improved version of the text.

Hope the author can find my comments useful. They were written with a positive and constructive spirit. In the end, I enjoyed reading the manuscript and I think this is a very nice work. These improvements will likely help the reading of others.

João Duarte

University of Lisbon

Reviewer #4

The paper cannot be published at the present stage. The reasons for this opinion are presented on the attached document.

Given this opinion, I am not presenting a commented document that I praise to be well written.

The subject is relevant because the authors address the problem of identifying the source of historical earthquakes which source faults are probably offshore.

The authors are encouraged to resubmit a paper, whence the major comments are addressed. The conclusions of the current version of the work are not very satisfactory, of the 5 faults investigated the authors only managed to discard one as a probable source for the Alborán earthquake. But the methodology is interesting and maybe using some of the suggestions mentioned in the attached document, a more restricted conclusion may be obtained.

The 1804 Alborán seismic series: search for the source using seismic scenarios and static stress interactions

Y. de Pro-Díaz[1,*], J. J. Martínez-Díaz[1-2], and C. Canora-Catalán[3]

[1]Department of Geodynamics, Stratigraphy and Paleontology, Universidad Complutense de Madrid, Madrid, Spain
[2]Instituto de Geociencias (CSIC, UCM)
[3]Department of Geology and Geochemistry, Universidad Autónoma de Madrid, Cantoblanco, Spain
[*]Corresponding author: ypro@ucm.es

Author ORCIDs

Y. de Pro-Díaz: 0000-0001-9807-3627
J. J. Martínez-Díaz: 0000-0003-4846-0279
C. Canora-Catalán: 0000-0003-2480-3679

Author contributions

Conceptualization: Y. de Pro-Díaz
Data Curation: Y. de Pro-Díaz
Formal Analysis: Y. de Pro-Díaz
Funding Acquisition: Y. de Pro-Díaz, J. J. Martínez-Díaz, C. Canora-Catalán
Investigation: Y. de Pro-Díaz, J. J. Martínez-Díaz, C. Canora-Catalán
Methodology: Y. de Pro-Díaz
Project Administration: J. J. Martínez-Díaz
Supervision: J. J. Martínez-Díaz, C. Canora-Catalán
Validation: J. J. Martínez-Díaz, C. Canora-Catalán
Visualization: Y. de Pro-Díaz
Writing – original draft: Y. de Pro-Díaz
Writing – review & editing: Y. de Pro-Díaz, J. J. Martínez-Díaz, C. Canora-Catalán

Abstract

Linking historical earthquakes with the faults that caused them is crucial for seismic hazard assessment. Historical documentation describing the effects of an earthquake is a useful information source, from which we can compile the observed intensity field of the earthquake. In this work we use intensity data from the catastrophic 1804 Alborán earthquake (south of Iberia) along with intensity simulations and coseismic stress transfer analysis to search for this earthquake's seismic source. We build intensity simulations for each "candidate" fault to be the source, and compare these simulations with the intensity field. We also propose a possible triggering between the Alborán 1804 earthquake and the Dalías earthquake (I_{EMS-98} IX) occurred seven months after, and analyze stress transfer between the two faults. Finally, we investigate the possible influence of the coseismic stress transfer caused by the Dalías earthquake in the subsequent local seismicity.

The Alborán earthquake could be linked to the Adra Fault, the Al-Idrissi Fault, the Balanegra Fault or the Loma del Viento Fault. The influence of the Dalías earthquake might still linger nowadays.

Second language abstract: Resumen (Español)

Relacionar los terremotos históricos con sus fallas responsables es crucial para las evaluaciones de peligrosidad sísmica. Una fuente de información sobre estos terremotos es la documentación histórica que describe sus efectos, a partir de la cual se puede recopilar el campo de intensidad observada del terremoto.

En este trabajo utilizamos los datos de intensidad del terremoto de Alborán de 1804 (al sur de Iberia) junto con simulaciones y análisis del cambio de esfuerzos cosísmico para buscar su falla responsable. Construimos simulaciones de intensidad para las distintas fallas "candidatas" a ser la fuente y las comparamos con el campo de intensidad. También proponemos un posible *triggering* entre el terremoto de Alborán y el terremoto de Dalías (I_{EMS-98} IX) ocurrido siete meses después, y analizamos la posible transferencia de esfuerzos entre ambas fallas. Finalmente, investigamos la influencia que el cambio de esfuerzos cosísmico del terremoto de Dalías haya podido tener en la sismicidad local posterior.

El terremoto de Alborán puede relacionarse con la Falla de Adra, la Falla de Al-Idrissi, la Falla de Balanegra o la Falla de Loma del Viento. La influencia del terremoto de Dalías en la tasa de sismicidad podría perdurar a día de hoy.

Non-technical summary

To avoid earthquake damage, we must first know as best as we can the faults that cause earthquakes and how they behave over time. Studying the effects caused by historical earthquakes is one way to achieve this.

We use data from effects of the 1804 Alborán earthquake (south of Spain) to search for the fault that most likely caused this earthquake. We recreate the earthquake effects trying out different possible faults as sources and compare the hypothetical effects caused by each one with the historically documented effects. The recreation which best fits the historical effects will also be the one built on a source which is the most similar to the actual earthquake source. We also propose the Alborán earthquake could have triggered another one which occurred nearby seven months later, the Dalías earthquake, and explore this possibility. Finally, we explore whether or not the Dalías earthquake could have boosted seismicity afterwards in the nearby region.

The faults that could have caused the Alborán earthquake are: Adra, Al-Idrissi, Balanegra and Loma del Viento. The influence of the Dalías earthquake might still linger nowadays.

1. Introduction

Linking historical earthquakes to their fault sources has become crucial in modern seismic hazard assessment (SHA) studies, particularly in regions with slow-to-moderate moving faults such as the Iberian Peninsula. In these regions, including accurate historical earthquake data in SHA studies can make a difference when considering whether or not a particular fault might rupture in the future. The importance of addressing faults as seismogenic sources in SHA studies and extend back their known seismic history beyond the instrumental record has been rising in the recent years (e. g. Ambraseys & Jackson, 1998; Basili et al., 2008; Caputo et al., 2015; Gómez-Novell et

al., 2020). Paleoseismology, which studies geological evidence of past earthquakes, is one way to achieve this; however, there are seismically active areas where paleoseismological analysis cannot be performed. This happens either because the structures which expose an earthquake occurrence never formed in the first place due to the site's geological conditions, or these structures did form but high erosion rates immediately dismantled them, or the human activity has destroyed these structures, or they are located in a not easily accessed area (McCalpin & Nelson, 1996). An alternative approach to paleoseismology in these cases can be the analysis of the effects caused by the earthquake on the human communities and their building stock. Documents such as personal diaries, letters to the authorities and reconstruction bills provide present researchers with a lot of information about earthquakes occurred in historical times (Teves-Costa & Batlló, 2011; Muñoz Clares et al., 2012; Murphy Corella, 2019). Sometimes, historical documents also preserve descriptions of geological evidence even after the geological structure itself has been lost due to erosion or anthropic activities (Huerta et al., 2015; Murphy Corella, 2019). Damage and effects reported on these documents can be addressed using modern intensity scales such as the EMS-98 (Grünthal, 1998) or the ESI-07 (Michetti et al., 2007) to assign each site a numeric value and compile the observed intensity field of historical earthquakes.

It has been noted in many studies how seismic intensity correlates quite well with strong ground motion parameters such as peak ground acceleration (PGA) and peak ground velocity (PGV) (Trifunac & Brady, 1975; Wald et al., 1999; Atkinson & Wald, 2007; Delavaud et al., 2009). Because of this correlation, several authors have developed ground-motion-to intensity-conversion equations (GMICE) which allow us to "translate"

ground motion into intensity values and vice versa (e. g. Kaka & Atkinson, 2004; Atkinson & Kaka, 2007; Tselentis & Danciu, 2008; Worden et al., 2012; Caprio et al., 2015). Additionally, plethora of authors have also developed ground motion models (GMM), which calculate the ground motion on a certain point considering a certain seismic source (e. g. Campbell, 2003; Ambraseys et al., 2005; Akkar & Bommer, 2010; Abrahamson et al., 2014; Akkar et al., 2014; Campbell & Bozorgnia, 2014; Pezeshk et al., 2018). A lot of research has also been done on the effect that an earthquake causes in the local stress state and how it can influence the occurrence of future shocks. One of the most successful approaches is the analysis of Coulomb failure static stress change (ΔCFS) (e. g. Okada, 1992; King et al., 1994; Harris, 1998; Stein, 1999, 2003).

Through the combined use of GMM, GMICE, and/or ΔCFS, we can build a simulation of the effects caused by any given earthquake on the building stock, on geological terrain and on the local stress field as long as we know the source parameters, so that we know what to expect of a well-known fault in the future. But we can also use this approach to look into the past and search for the source of historical earthquakes when the responsible fault is unclear and no other evidence is found. The premise is as follows: if we build a simulation which matches the observed effects, the seismic source on which we built that simulation will also match the actual source of the earthquake. Using this approach, the source of many historical earthquakes has been searched for before this work, for instance: the seismic crisis of 1456 on Italy (Fracassi & Valensise, 2007), the Catalan seismic series of 1427-1428 (Perea, 2009), the 2001 El Salvador earthquake (Canora et al., 2010), the California earthquake of 1812 (Lozos, 2016), the 1829, 1863 and 1755 earthquakes of Torrevieja, Huércal-Overa and Lisbon, respectively (Silva et al., 2017),

the Arenas del Rey earthquake of 1884 (Rodríguez-Pascua et al., 2017), several historical earthquakes east of the Sunda Arc (Griffin et al., 2019), the 1933 Long Beach earthquake (Hough & Graves, 2020), the 2019 Jijel and 2014 Ziama earthquakes (Yelles-Chaouche et al., 2021) or the 1531 Lisbon earthquake (Canora et al., 2021).

In this work, we search for the most likely source of the Almería earthquake of 13th January 1804, also known as the Alborán earthquake of 1804, which caused significant damage at both the Spanish and Moroccan coasts as well as at several inland locations. The greatest damage occurred in the building stock from the provinces of Granada and especially Almería (Murphy Corella, 2019). This earthquake has been assigned M_w 6,3-6,7 by different authors, mostly based on the damage (Martínez Solares & Mezcua Rodríguez, 2002; Posadas et al., 2006; Mezcua et al., 2013). To investigate its source, we use a methodology based on simulations of earthquake effects caused by different possible seismic sources and comparing these simulations with the observed effects in search of the scenario that better fits reality. We use a methodology proposed by de Pro-Díaz et al. (2022, 2023) and incorporate a new extra step using ΔCFS analysis to better constrain the results.

2. Neotectonic and seismic context

2.1. The Betics and Alborán Sea area

The Betic Cordillera, also known as the Betics, is an ENE-WSW orogen located south of the Iberian Peninsula. During the neotectonic period (Late Miocene to Present), tectonic activity in the Eastern Betics is dominated by the convergence between Iberia and Nubia plates (DeMets et al., 2010; Serpelloni et al., 2007; Nocquet & Calais, 2004). The study area is located in the Eastern Betics where a compressional stress field with NNW-SSE

shortening has been dominant during the Quaternary (Echeverria et al., 2015). This strain regime is consistent with the kinematics of the largest active faults in this area (Martínez-Díaz et al., 2012).

Along the Eastern Betics, active faults show three main orientations: NE-SW, E-W and NW-SE (Sanz de Galdeano, 1983; Sanz de Galdeano et al., 2020). One of the most important fault systems is the Eastern Betics Shear Zone (EBSZ) (Silva et al., 1993), the continental part of the Trans-Alborán Shear Zone (TASZ) (De Larouzière et al., 1988), a sigmoidal, NE-SW, transpressive fault zone formed mainly by left-lateral strike-slip faults, and reverse faults on the northern sector (Silva et al., 1993). The EBSZ has been largely studied, including plethora of paleoseismological work (e. g. Ortuño et al., 2012; Insua-Arévalo et al., 2015; Martín-Banda et al., 2016; Ferrater et al., 2016, 2017; Herrero Barbero, 2021). The Carboneras Fault (CF) is one of the major faults of the TASZ, and part of its trace runs south of the epicentral area of the earthquakes addressed in this work (Figure 1) (Gràcia et al., 2006; Moreno Mota, 2011; Moreno et al., 2015, 2016; Álvarez-Gómez et al., 2023). Another major fault near the epicentral area is the Al-Idrissi Fault (AIF), a young, NE-SW oriented, subvertical, left-lateral strike-slip fault which has been related to three $M_w \geq 6$ earthquakes occurred near the African coast in 1994, 2004 and 2016 (Figure 1), as well as the seismic series of 2021-2022 near Al Hoceima (Ammar et al., 2007; Martínez-García et al., 2011, 2013; d'Acremont et al., 2014; Álvarez-Gómez et al., 2016; Gràcia et al., 2019; Lafosse et al., 2020; Perea et al., 2022). Both the CF and AIF are considered not only active and seismogenic, but also potentially tsunamigenic (Gómez de la Peña et al., 2022). The Alpujarras Fault Zone (AFZ) is also an important structure in this area: an E-W, strike-slip, right-lateral corridor composed of several

faults, some of which have been active in the Quaternary (Martínez-Martínez, 2006; Echeverria et al., 2015; Sanz de Galdeano et al., 1985, 2020). The AFZ and the CF are the northern and south-eastern limits of a complex crustal block which is divided in smaller, rotating blocks delimited by oblique (normal-strike-slip) faults trending NW-SE (Martínez-Díaz & Hernández-Enrile, 2004). The smaller NW-SE faults control several Neogene basins, such as the Campo de Dalías. Among these NW-SE faults are the Loma del Viento Fault (LVF) (Martínez-Díaz, 1999; Marín-Lechado et al., 2005; García-Mayordomo et al., 2012; Pedrera et al., 2012; Murphy Corella, 2019), the Llano del Águila Fault (LLAF) (Molins-Vigatà et al., 2022), the Adra Fault (AF), the Balanegra Fault (BF) (Martínez-Díaz & Hernández-Enrile, 2004; Gràcia et al., 2006, 2012; Marín-Lechado et al., 2010; Sanz de Galdeano et al., 2020) and the Punta Entinas Fault (PEF) (Gràcia et al., 2006, 2012; García-Mayordomo et al., 2012), which all share normal-dextral kinematics.

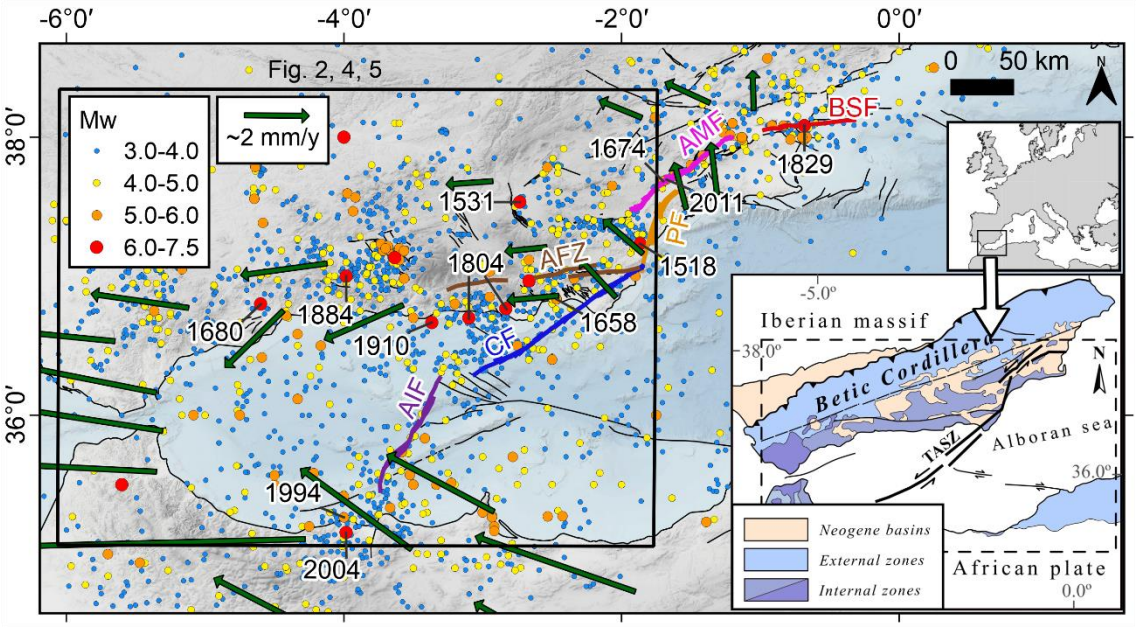

Figure 1. Seismotectonic context for the study region. Inset modified from Herrero-Barbero et al. (2021). Seismic catalog from IGN-UCM (2013), represented as dots with the dates of the main earthquakes. Geodetic velocity trends from GNSS networks are represented as green arrows, from

Palano et al. (2015). Fault traces from the QAFI database (García-Mayordomo et al., 2012) are represented as black lines, with the main faults of the EBSZ and TASZ highlighted in color. CF: Carboneras Fault. AFZ: Alpujarras Fault Zone. PF: Palomares Fault. AMF: Alhama de Murcia Fault. BSF: Bajo Segura Fault. AIF: Al-Idrissi Fault.

2.2. The 1804 Almería seismic series

In 1804, two seismic series occurred in the Campo de Dalías area, one in January and the other in August. The mainshock of the August series occurred on the 25th near the city of Dalías and its most likely source appears to be a conjunct rupture of the LVF and LLAF (de Pro-Díaz et al., 2023). The mainshock of the January series, which is the focus of this work, occurred on the 13th and was felt at several locations along both the south Iberian Peninsula's and north African coasts (Espinar Moreno, 1994; Murphy Corella, 2019).

The 1804 Almería seismic series was extensively researched by Murphy Corella (2019). This author recovered historical documents describing the effects of the earthquakes and their aftermath in the affected areas and analyzed these records in order to assign EMS-98 intensity values to each site. He also includes data from geological effects to assign ESI-07 intensity values. Although he focuses mainly on the 25th August shock, which was the most damaging of the series, he also addresses the 13th January shock in his analysis, as well as the strongest aftershocks in both the January and August series. In the following paragraph, we translate and resume some of Murphy Corella (2019)'s research regarding the 13th January shock.

In Berja and Dalías, historical records analyzed by Murphy Corella (2019) describe damage in several buildings after the January mainshock, including the four churches of these two towns. This earthquake and its subsequent aftershocks forced the people of these two localities to camp outside town for a whole month until the tremors stopped, and damage could be fixed during spring season. Records from the coastal town of Adra

describe how the earthquake was felt by the population, as well as a “disturbance in the sea, which was shaken with noisy movement, which completely ceased” after each shock of the series. The earthquake was also felt in Málaga, where “startled people occupied the streets and squares”, as well as in several cities far from the epicentral area, like Sevilla, Melilla or even Madrid, more than 400 km north of the epicentral area. Certain buildings were also severely damaged in Roquetas. Records from the city of Almería’s municipal archive report extensive damage to the whole building stock, although there were no casualties. In Motril, another coastal town, the sea was described to withdraw 22 varas (~18 m), and the earthquake caused “ruins and two deaths”, being this the only site with confirmed casualties for the 13th January earthquake. Records addressing the effects in Motril also identify the different seismic phases, which is why this earthquake was known as the Motril earthquake for some time. As it happened in Berja and Dalías, Motril’s citizens also camped outside town until the aftershocks stopped by the end of February (Murphy Corella, 2019).

These are the most known sites where the earthquake was felt, but its effects are reported in more localities which were all addressed by Murphy Corella (2019) in his work. A more detailed translation of the reported effects in these sites and some others can be found in Table AP1 of the *Appendix* of this article. From these records, he compiled an intensity field of 30 data points which is shown in Figure 2. This is the intensity field we will be using for our analysis of this earthquake.

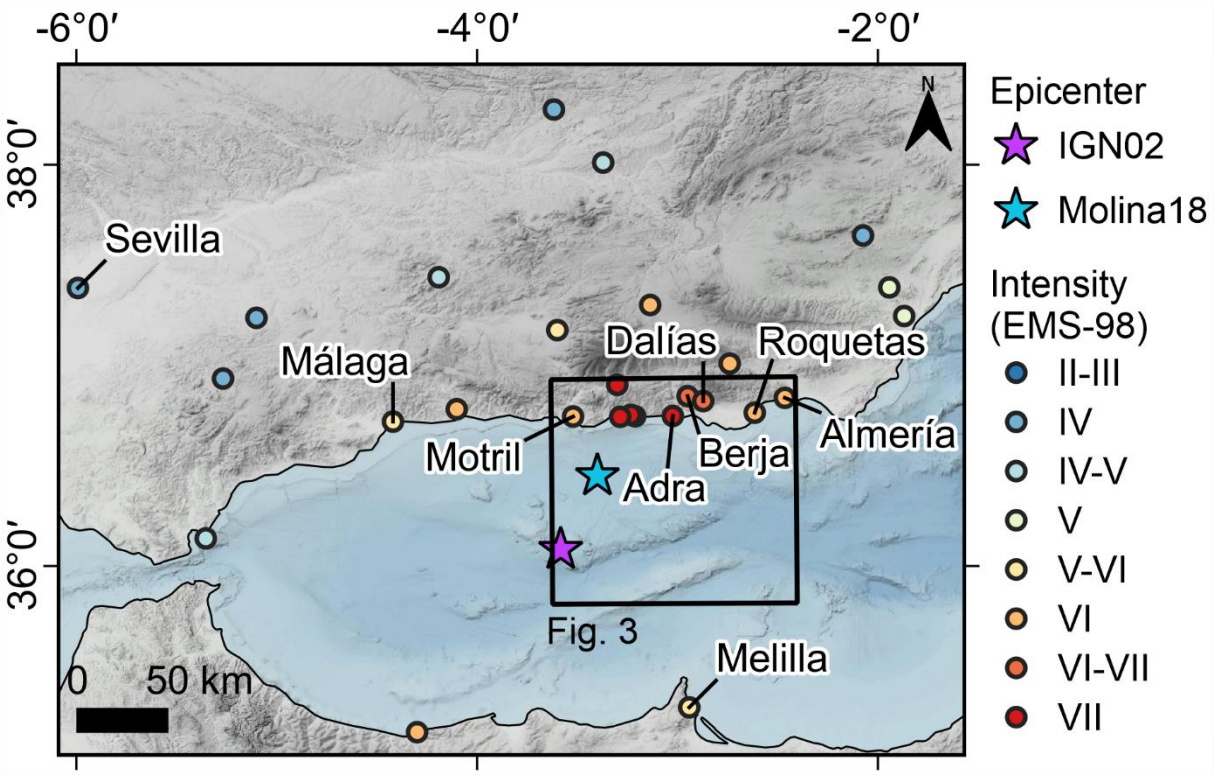

Figure 2. Intensity field of the Alborán earthquake of 13th January, 1804, compiled by Murphy Corella (2019). IGN02: epicenter estimated by Martínez Solares & Mezcua Rodríguez (2002). Molina18: epicenter estimated by Molina et al. (2018).

Two different locations have been proposed for the epicenter using intensity data: 36.083 ºN, 3.583 ºW by Martínez Solares & Mezcua Rodríguez (2002), estimated from the center of the highest intensity area with a previous and less rich dataset; and 36.45 ºN, 3.40 º W by Molina et al. (2018), who used Murphy Corella (2019)'s data and also considered the reported S-P arrival time difference from Motril (Figure 2). As stated before, different authors have proposed magnitudes of M_w 6,3-6,7 for this earthquake using also intensity data for their estimations (Martínez Solares & Mezcua Rodríguez, 2002; Posadas et al., 2006; Mezcua et al., 2013). As for the seismic source, Espinar Moreno (1994), Martínez Solares & Mezcua Rodríguez (2002), Molina et al. (2018) and Murphy Corella (2019) all agree on an offshore source based on the damage distribution at both the Spanish and Moroccan coasts, as well as the tsunami reports. Murphy Corella

(2019) proposed the offshore extension of the LVF as a possible source for this earthquake, although this is not the closest fault to the epicenters estimated by Martínez Solares & Mezcua Rodríguez (2002) and Molina et al. (2018) (Figures 2 and 3). No evidence of surface rupture has been found so far for this earthquake.

3. Methodology

In this work we have used the seismic scenario method proposed by de Pro-Díaz et al. (2022, 2023) for constraining the earthquake source through the use of seismic scenarios and the observed intensity field. We have also added an extra step using Coulomb stress transfer analysis to be used as an additional criterion to rank the preferred scenarios. Methodology is composed of four steps:

1. Boxer calculation. We use Gasperini et al. (1999, 2010)'s method and their Boxer software to calculate the most likely area of the surface where the seismic source might be located. This area is called "boxer". The boxer is then compared with the known seismogenic faults in the area. The faults which partially or totally overlap the boxer become possible candidates to be the source of the earthquake (from now on, "candidate ruptures"). If the boxer does not fit any known seismogenic fault and shows no overlap with any of the epicenters proposed by other authors, candidate ruptures are selected using sources proposed by other authors and the local known faults which are close to the epicenter.

2. Seismic scenarios. We build seismic scenarios for each one of the candidate ruptures using the OpenQuake software (Pagani et al., 2014). OpenQuake takes M_w, geometry and position of the rupture, as well as position of the hypocenter as input data, and

using a ground-motion model (GMM) produces a regular grid of points over the study area, each containing values of ground motion – in this work, peak ground acceleration (PGA) and peak ground velocity (PGV). Then, using ground-motion-to-intensity conversion equations (GMICE), we translate the ground motion into simulated intensity values. In this work, we initially used Campbell & Bozorgnia (2014)'s GMM and Worden et al. (2012)'s GMICE, following de Pro-Díaz et al. (2023), although we had to switch to Akkar & Bommer (2010)'s GMM (this change will be addressed later on in the *Results* and *Discussion*). Each scenario is then compared to the observed intensity field using this equation:

$$R_{obs\text{-}rup} = I_{obs} - I_{rup}$$

where I_{obs} is the observed intensity value and I_{rup} is the simulated intensity value sampled from the same location as I_{obs}. The scenario which shows $R_{obs\text{-}rup}$ closest to 0 is the one which better fits the observed effects of the earthquake. This means the candidate rupture upon which the best-performing scenario was built is the closest to the actual seismic source of the earthquake. If two or more scenarios show $R_{obs\text{-}rup}$ equally closer to 0, we proceed on to step 3 with those (from now on, "competing scenarios").

3. Differential zones. We compare the competing scenarios to find the areas in which they differ from each other, or "differential zones". If there are enough I_{obs} data points inside the differential zones, we perform a statistical test to evaluate the likeness of the data distributions sampled inside these areas from I_{obs} and each seismic scenario. The aim is to find the scenario which is statistically similar to I_{obs}. If there are not enough

data points inside the differential areas, we proceed on to step 4 with the candidate ruptures for the competing scenarios.

4. Coulomb stress transfer. We model the static stress change (ΔCFS) associated with the ruptures selected as candidates using the Okada (1992) equations for dislocations in an elastic half-space following the methodology described by King et al. (1994) and Harris (1998) and the Coulomb 3.4 software (Toda et al., 2011). We also model the source for the 25th August earthquake proposed by de Pro-Díaz et al. (2023), which we call rupture D, and taper it into 539 tiles measuring 1 km^2 each. We then calculate the ΔCFS produced in rupture D by each of the modeled candidate ruptures. Based on their closeness in space and time, if we assume that the 13th January shock might have triggered the 25th August shock, the rupture which produces the largest area of positive ΔCFS in rupture D will be considered as the closest to the actual source of the 13th January shock.

Additionally, we model the local ΔCFS produced by rupture D after the 25th August shock on ideally oriented fault planes and compare it with the seismicity occurred in the study area after 1804. The aim is to tentatively search for a possible influence of the local ΔCFS caused by the 25th August shock on the spatial distribution of the seismicity afterwards in the area.

For the ΔCFS calculations, we use a 0.4 apparent friction coefficient (Harris, 1998) and a regional stress field with σ_1 00º//158º and σ_3 00º//068º.

4. Results

4.1. Boxer calculation

The boxer calculated with Gasperini's method is presented as a red rectangle in Figure 3. The boxer has an area of 81 km^2 and strikes N93ºE. The computed epicenter is located at 36.7499ºN, 3.2436ºW, which is 38 km away from the epicenter proposed by Molina et al. (2018) and 83 km away from the one proposed by Martínez Solares & Mezcua Rodríguez (2002). Magnitude estimated by Boxer is M_w 5.88±0.10, which is lower than both M_w 6.3 assigned by Molina et al. (2018) and M_w 6.7 calculated by Martínez Solares & Mezcua Rodríguez (2002).

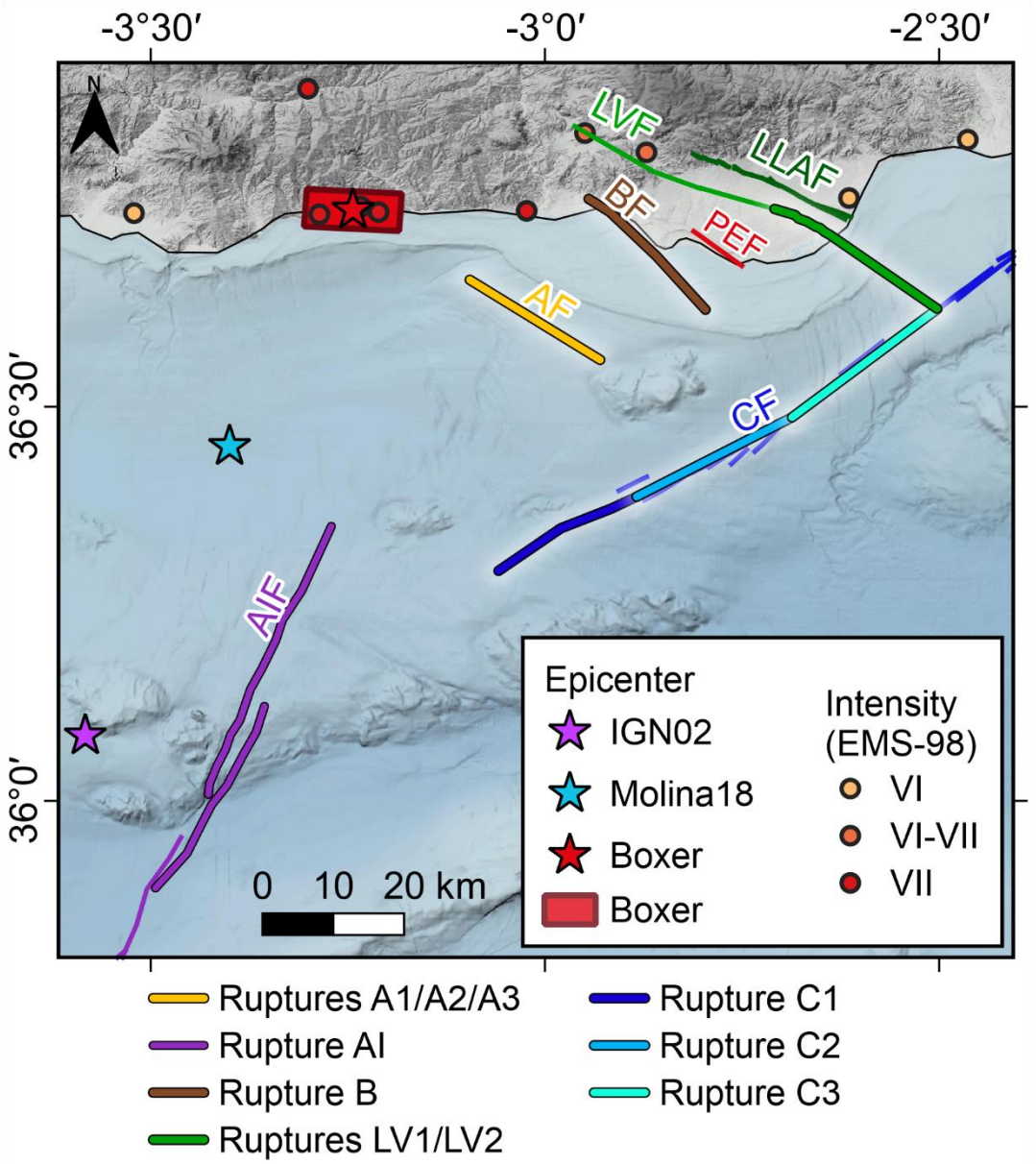

Figure 3. Boxer calculation result and known active faults in the area. Selected candidate ruptures for the Alborán earthquake are highlighted in thicker lines than the known active fault traces, and named with the fault's initial letter: A for Adra Fault, B for Balanegra Fault, C for Carboneras Fault and LV for Loma del Viento Fault). Parameters for the candidate ruptures are shown in Table 1. Molina18: Molina et al. (2018). IGN02: Martínez Solares & Mezcua Rodríguez (2002). LLAF: Llano del Águila Fault. LVF: Loma del Viento Fault. BF: Balanegra Fault. AF: Adra Fault. CF: Carboneras Fault. AIF: Al-Idrissi Fault. PEF: Punta Entinas Fault.

Despite intensive geomorphological and seismologic study in the past, no active fault has been described yet in the area around the boxer, not even smaller ones than the size required for an earthquake such as the one studied here (Figure 3). Additionally, Espinar Moreno (1994), Martínez Solares & Mezcua Rodríguez (2002), Molina et al. (2018) and

Murphy Corella (2019) all agree on an offshore source for this earthquake considering the damage distribution, yet the boxer is located mostly inland. Because of this discrepancy with the bibliography, we decided not to consider the boxer calculation result to select the candidate ruptures for the Alborán earthquake. This discrepancy will be further addressed later in the *Discussion*.

Following the hypothesis of the offshore source, candidate faults have been selected among faults with Quaternary activity evidence included in the QAFI database compiled by García-Mayordomo et al. (2012) which are also located less than 40 km away from either the highest intensity points or the epicenter proposed by Molina et al. (2018), since these authors consider the S-P arrival time in their calculations. The selected faults are the Balanegra Fault (BF), the Adra Fault (AF), the northern sector of the Al-Idrissi Fault (AIF), the sea extension of the Loma del Viento Fault (LVF), and three different sectors of the Carboneras Fault (CF). For the AF, BF and LVF we use the maximum mapped length for which geomorphological evidence has been found. For the CF, we select sectors with lengths according to the earthquake's magnitude using the empirical relations of Stirling et al. (2002) and Wells & Coppersmith (1994). For the AIF scenario, we selected a slightly bigger area comprising the north and central segments, with a higher magnitude (M_w 7.0) to compensate for the rupture being further from the coast and the subsequent intensity attenuation at the intensity field sites. Initially, for the other ruptures we tried magnitudes proposed by the already cited authors, but some ruptures had areas which could generate higher M_w according to Stirling et al. (2002)'s and Wells & Coppersmith (1994)'s empirical relationships. For these ruptures, we also try these higher magnitudes. All of this results in a total of ten different candidate ruptures which

are presented in Figure 3. Each candidate's fault parameters are presented in Table 1. Ruptures have been named using the initial letters of the rupturing fault, so rupture AI for instance corresponds to the Al-Idrissi Fault. In the case of the Adra Fault, ruptures A1, A2 and A3 correspond to the same area with different possible magnitudes. The same applies for the Loma del Viento Fault and ruptures LV1 and LV2. As for the Carboneras Fault, ruptures C1, C2 and C3 correspond to three consecutive sectors of the fault with similar areas and thus similar magnitudes.

Rupture	Strike (º)	Dip (º)	Rake (º)	Area (km^2)	Length (km)	Coordinates	SD (km)	Epicenter	M_w
A1	122	80	-135	285	19	36.6613ºN 3.0956ºW	0-15	36.6613ºN 3.0956ºW	6.5
A2	122	80	-135	285	19	36.6613ºN 3.0956ºW	0-15	36.6613ºN 3.0956ºW	6.7
A3	122	80	-135	285	19	36.6613ºN 3.0956ºW	0-15	36.6613ºN 3.0956ºW	6.9
AI	205	80	5	1100	55	36.348ºN 3.271ºW	0-20	36.348ºN 3.271ºW	7.0
B	134	70	-135	240	20	36.6233ºN 2.7967ºW	0-12	36.6233ºN 2.7967ºW	6.6

C1	62	90	0	228	19	36.292ºN 3.059ºW	0-12	36.346º N 2.98ºW	6.5
C2	63	90	0	240	21	36.387ºN 2.885ºW	0-12	36.387ºN 2.885ºW	6.5
C3	53	90	0	264	22	36.4868º N 2.6869ºW	0-12	36.4868ºN 2.6869ºW	6.4
LV1	121	80	35	297	27	36.7511ºN 2.7089ºW	0-12	36.7511ºN 2.7089ºW	6.4
LV2	121	80	35	297	27	36.7511ºN 2.7089ºW	0-12	36.751ºN 2.7089ºW	6.9

Table 1. Fault parameters for the eight proposed candidate ruptures considered as possible sources for the Alborán earthquake. The fault traces are presented in Figure 3, and named as follows: A1, A2, A3: Adra Fault ruptures; B: Balanegra Fault rupture; C1, C2, C3: Carboneras Fault ruptures; LV1, LV2: Loma del Viento Fault ruptures. SD: seismogenic depth (upper-lower) from the QAFI (García-Mayordomo et al., 2012). HD: hypocentral depth.

4.2. Seismic scenarios

Seismic scenarios built for each of the candidate ruptures presented in Table 1 are shown in Figures 4 and 5. Overall, no scenario shows a perfect correlation with I_{obs} spatial distribution. Nevertheless, the intensity distribution patterns of scenarios A2, A3, AI, LV2 and B seem closer to I_{obs} distribution than the other scenarios.

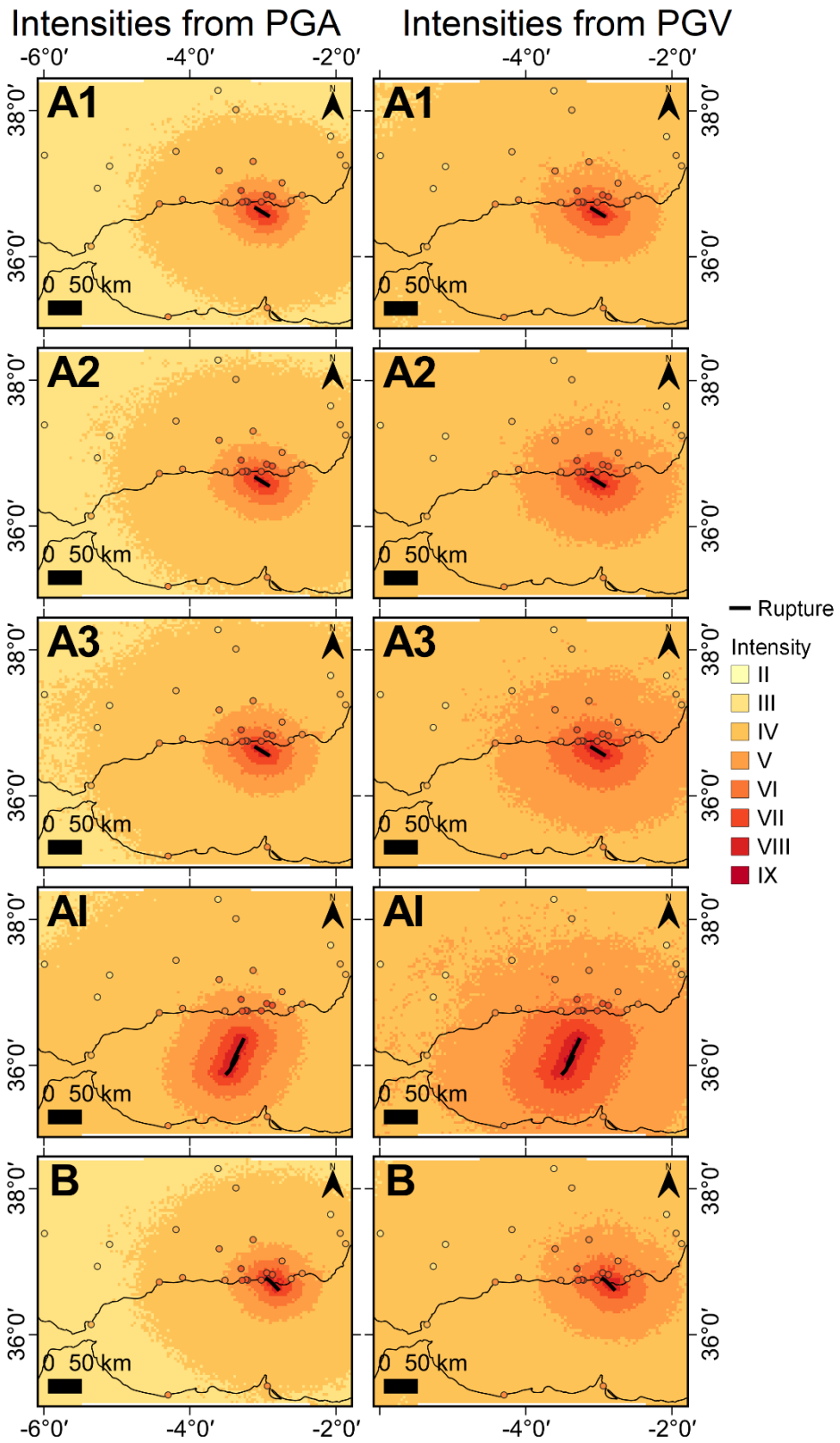

370 **Figure 4.** Seismic scenarios built for candidate ruptures A1 to A3 (Adra Fault), AI (Al-Idrissi Fault), and B (Balanegra Fault). The observed intensity field is superimposed in the same color palette.

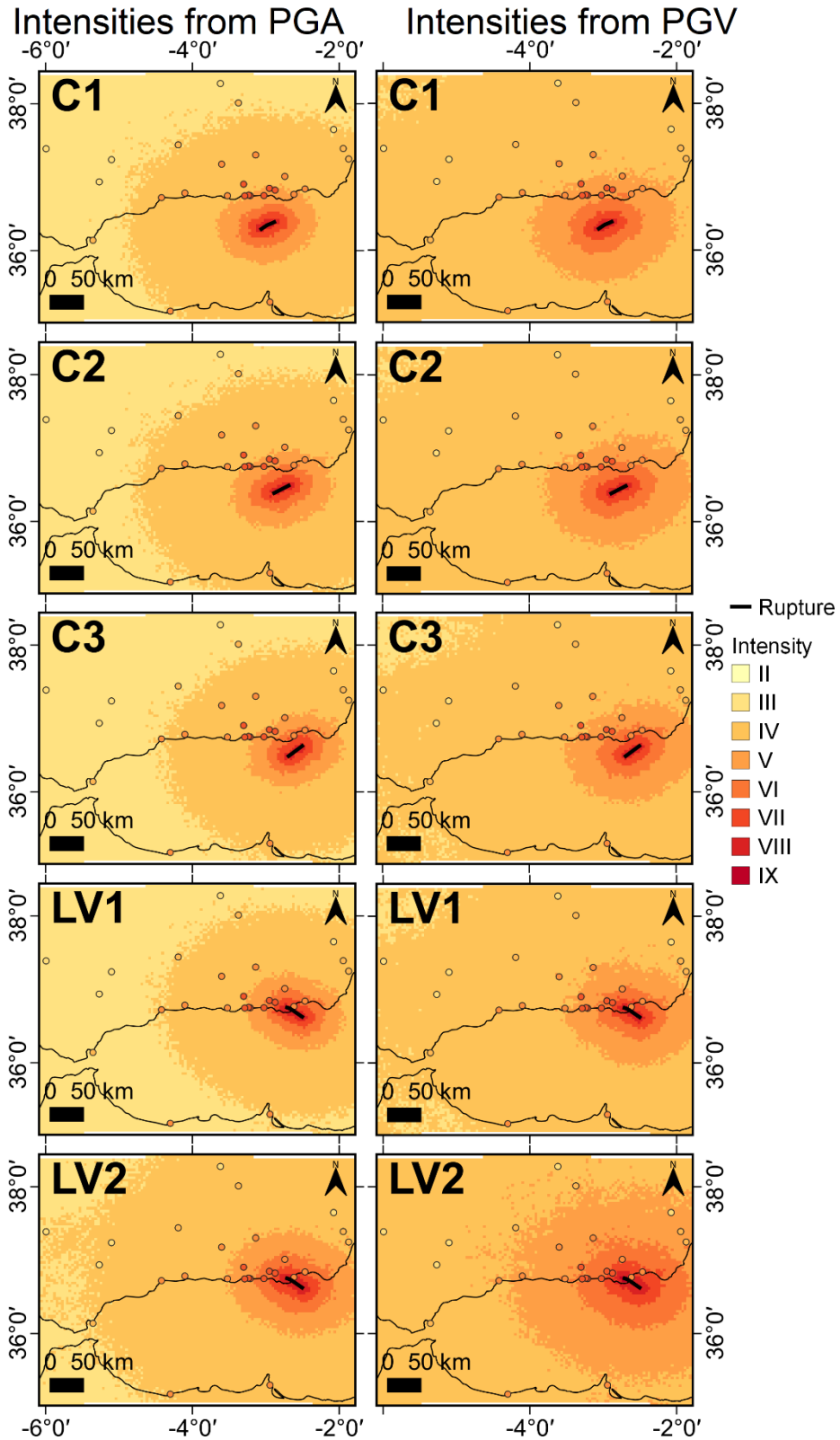

Figure 5. Seismic scenarios built for candidate ruptures C1 to C3 (Carboneras Fault) and LV1 to LV2 (Loma del Viento Fault). The observed intensity field is superimposed in the same color palette.

Figure 6 shows $R_{obs-rup}$ for the scenarios of the ten candidate ruptures. All scenarios seem to underestimate intensities, although some more than others. Scenarios A3, AI, LV2 and B predict intensities which are less than one degree lower than the observed values on average, so ruptures A3, AI, LV2 and B are considered as the best candidates in this step of the analysis. The rest of the scenarios underpredict intensities for more than one degree on average respect to the observed values, which marks their ruptures as worse candidates. We thus proceed to the next step of the analysis with A3, LV2 and B as competing scenarios.

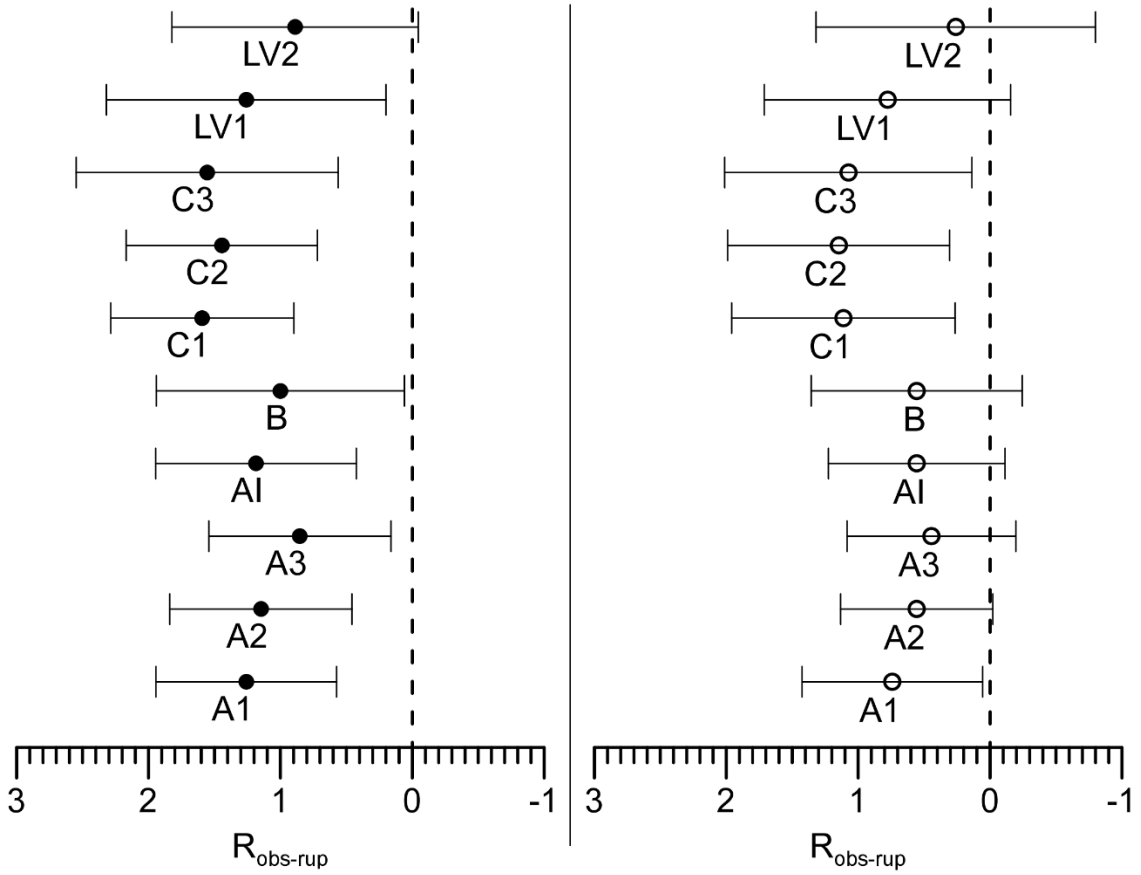

Figure 6. Residuals $R_{obs-rup}$ for each of the scenarios for the Alborán earthquake. The average residual is represented with a dot and the bars represent the standard deviation. Black dots correspond to results from scenarios with intensities calculated from PGA, and white dots correspond to results from scenarios with intensities calculated from PGV. Each scenario is labeled below the dot.

We initially built the scenarios using Campbell & Bozorgnia (2014)'s GMM, but all of the scenarios built with this GMM underpredicted the observed intensities by almost one degree or more. These scenarios are presented in Figures AP1 and AP2 of the *Appendix* of this work, and their $R_{obs-rup}$ are shown in Figure AP3, but they have not been used in the rest of the analysis. The scenarios presented in the current section are built with Akkar & Bommer (2010)'s GMM. This change of GMM will be further addressed in the *Discussion*.

4.3. Differential zones

We compare the competing scenarios selected in the previous step by analyzing their intensity values distribution inside the differential zones: the areas in which two competing scenarios show different intensity values. Because scenario LV2 seemed to perform slightly better than scenarios AI, B and A3 in the residuals step, we compare scenarios AI, B and A3 with scenario LV2.

Differential zones for scenarios B and LV2 are presented in Figure 7. There are two differential zones: a bigger, sort of ring-like outer zone where scenario LV2 shows higher intensities than B; and a smaller, inner zone where scenario B shows higher intensities than LV2. Histograms in Figure 7 represent the value distribution of the observed intensity (I_{obs}), scenario B (I_{rupB}) and scenario LV2 (I_{rupLV2}) inside the differential zones. I_{rupB}'s distributions seem to be slightly more similar to I_{obs} than I_{rupLV2} in the outer zone. However, there are only seven I_{obs} points inside the outer zone, and this amount is not enough to perform a robust statistical test. As for the inner zone, there is only one I_{obs} point inside it, so it is not suitable either for a statistic analysis. Because of this lack of

points inside the differential zones, this step of the analysis cannot be applied to this pair of competing scenarios.

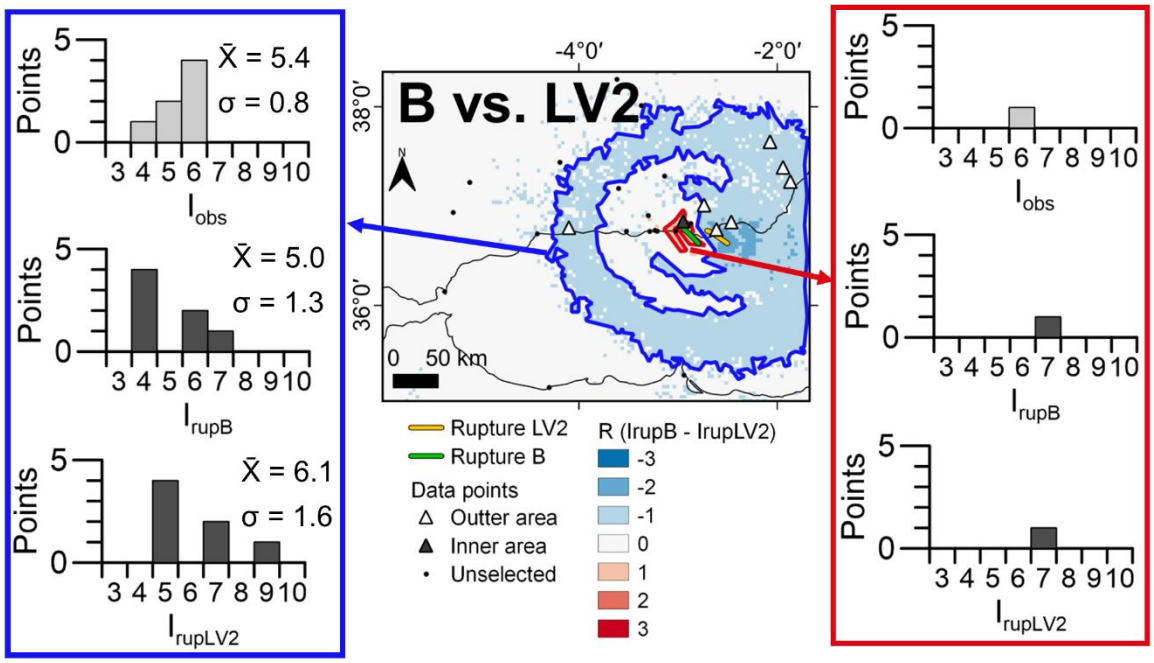

Figure 7. Differential zones for scenarios B and LV2. Histograms represent the distribution of the intensity values inside each differential zone for the observed intensity field (I_{obs}), scenario B (I_{rupB}) and scenario LV2 (I_{rupLV2}).

Differential zones for scenarios A3 and LV2 are presented in Figure 8. There are three differential zones, two to the northeast where scenario LV2 shows higher intensities than A3 (these two will be considered as the same zone for practical purposes), and the other to the southwest where it is the other way around. Histograms in Figure 8 represent the value distribution of the observed intensity (I_{obs}), scenario A3 (I_{rupA3}) and scenario LV2 (I_{rupLV2}) inside the differential zones. I_{rupA3}'s distributions seem to be slightly more similar to I_{obs} than I_{rupLV2}. However, there are only six I_{obs} points within the SW zone and seven within the NE zone, which again is not enough to perform a robust statistical test. Because of this, this step of the analysis cannot be applied to this pair of competing scenarios either.

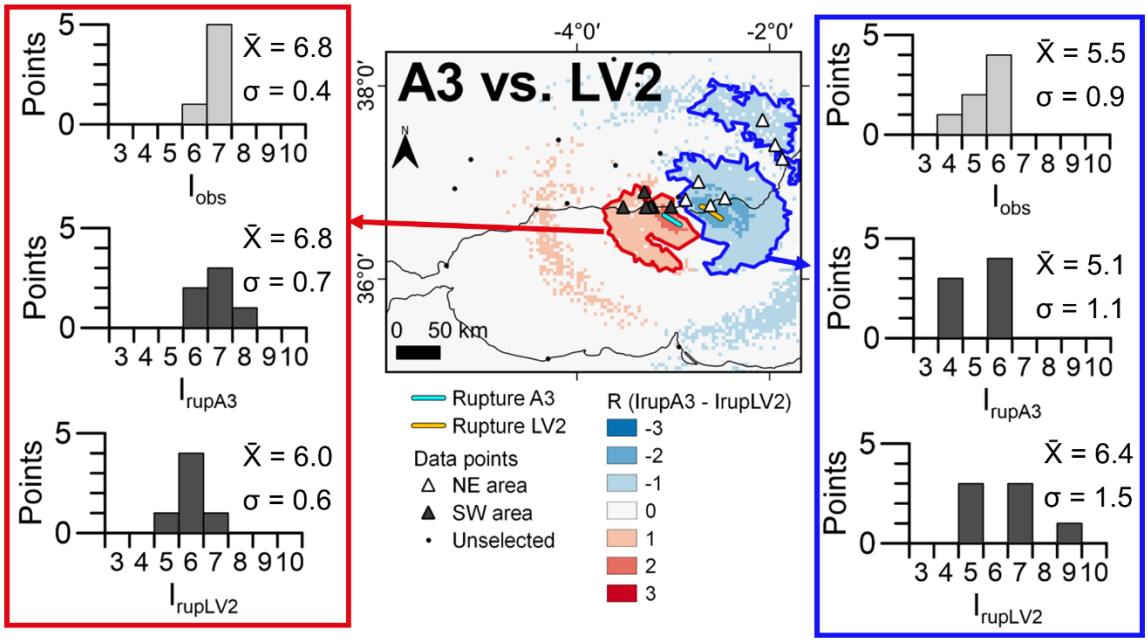

Figure 8. Differential zones for scenarios A3 and LV2. Histograms represent the distribution of the intensity values inside each differential zone for the observed intensity field (I_{obs}), scenario A3 (I_{rupA3}) and scenario LV2 (I_{rupLV2}).

Figure 9 shows the differential zones for scenarios AI and LV2. Again there are three differential zones: a bigger one to the SW where scenario AI shows higher intensity values, and two smaller ones to the NE where scenario LV2 shows higher values. As in the case of scenarios A3 and LV2, these two smaller zones will be considered as the same one for practical purposes. Histograms in Figure 9 represent the value distribution of the observed intensity (I_{obs}), scenario AI (I_{rupAI}) and scenario LV2 (I_{rupLV2}) inside the differential zones. I_{rupAI}'s distributions seem to be slightly more similar to I_{obs}, although once again the amount of I_{obs} points inside both areas is not enough to perform statistical analysis: six points in the SW zone, and eight in the NE zone. Thus we proceed on to step 4 of the methodology.

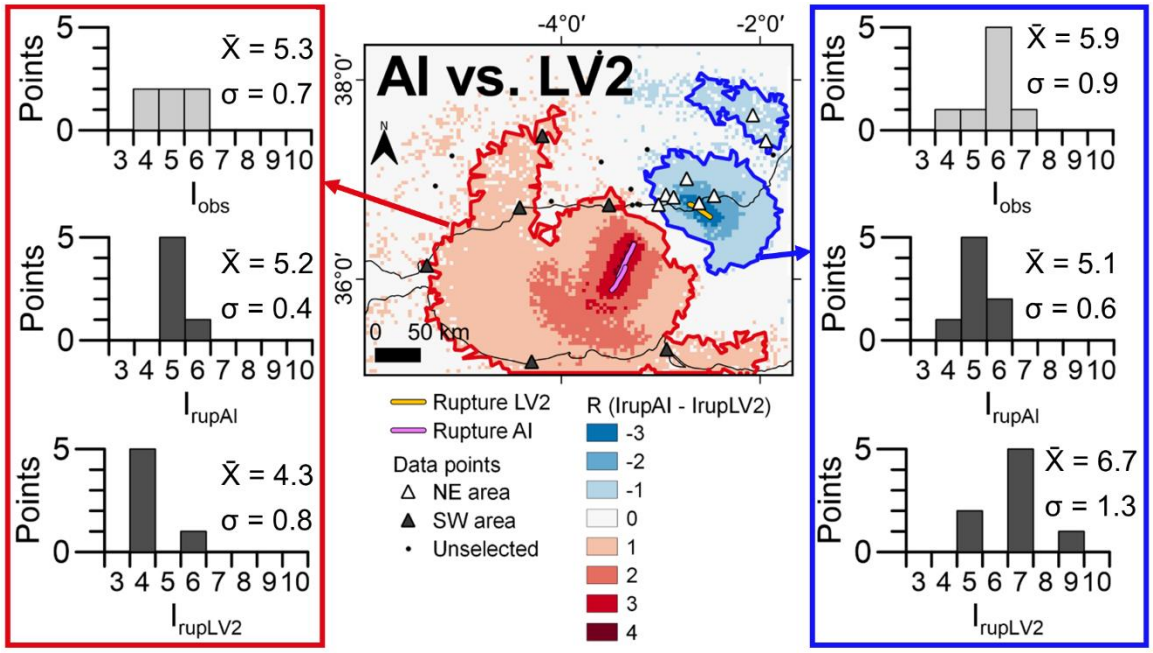

Figure 9. Differential zones for scenarios AI and LV2. Histograms represent the distribution of the intensity values inside each differential zone for the observed intensity field (I_{obs}), scenario AI (I_{rupAI}) and scenario LV2 (I_{rupLV2}).

4.4. Coulomb stress transfer

In this step, we model the static stress change (ΔCFS) produced by ruptures A3, AI, B and LV2 on the 25th August shock's rupture, which we call rupture D. Assuming from their closeness in time and space that the 13th January and the 25th August shocks are related by a triggering process, the rupture which causes ΔCFS > 0 on the most part of rupture D's surface would be the most likely source of the January shock. Rupture D has been tapered into 1 km^2 tiles in order to measure the "loaded" surface.

Figures 10, 11, 12 and 13 show the ΔCFS models from source rupture B to receiver rupture D, from source A3 to receiver D, from source LV2 to receiver D, and from source AI to receiver D, respectively. Rupture D involves the rupture of two faults: LVF and the nearby Llano del Águila Fault (LLAF). Two different views are presented in each figure in order to show both rupture surfaces. Rupture B caused ΔCFS > 0 in a total of 83 tiles of rupture D, which is a 15 % of rupture D's surface. Rupture A3 on the other hand

caused ΔCFS > 0 in 353 tiles, which is a 65 % of rupture D's surface. Rupture LV2 caused ΔCFS > 0 in the largest area: 394 tiles, which is a 73 % of rupture D's surface. Finally, rupture AI caused ΔCFS > 0 in 242 tiles, a 45 % of rupture D's surface.

460 Assuming the Alborán shock triggered the Dalías shock, this could point to rupture LV2 as the best candidate, although rupture A3 could also be a possible source of the Alborán earthquake.

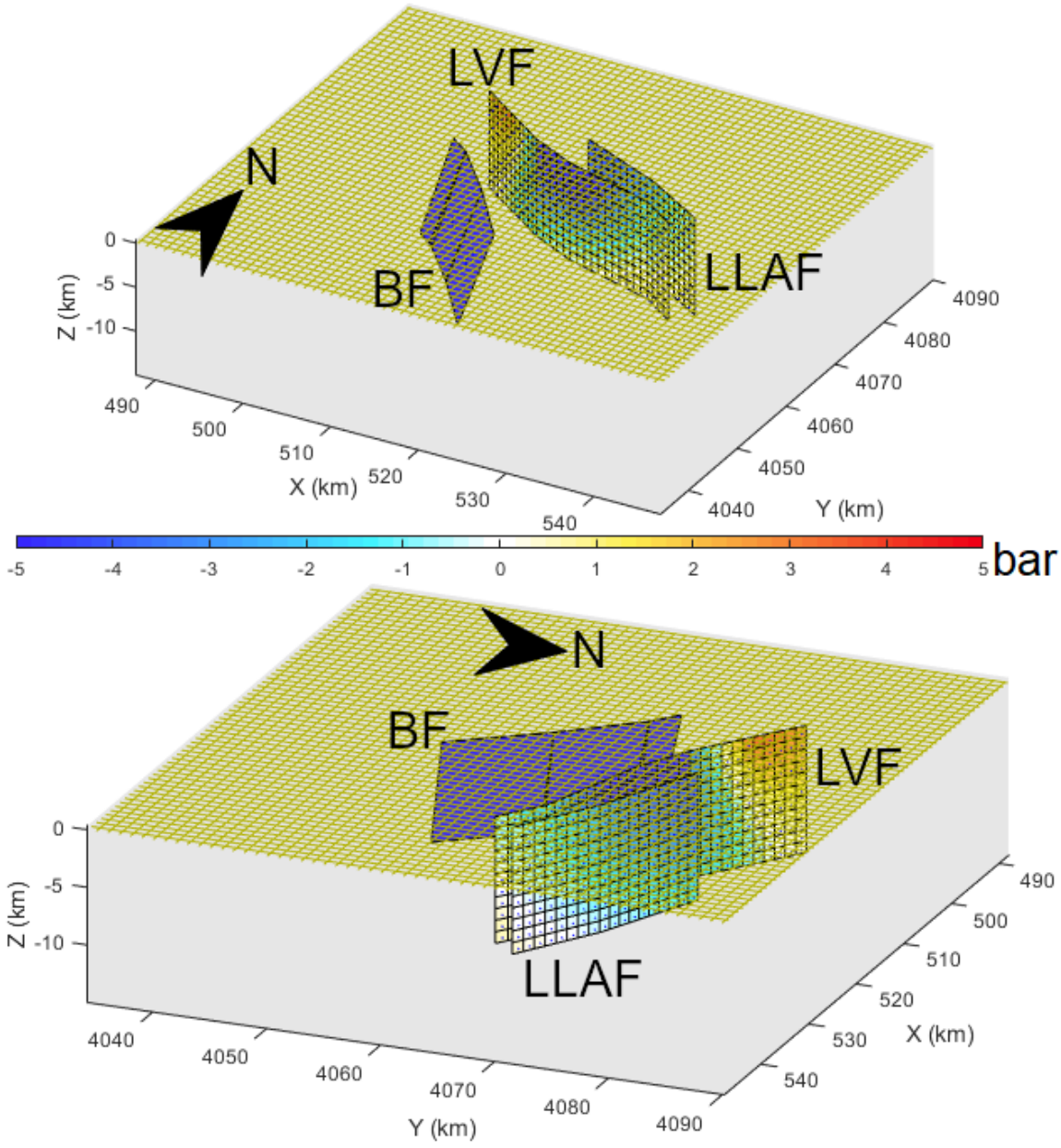

Figure 10. Coulomb static stress change model in rupture D (LVF+LLAF) caused by rupture B (BF).
465 BF: Balanegra Fault. LVF: Loma del Viento Fault. LLAF: Llano del Águila Fault.

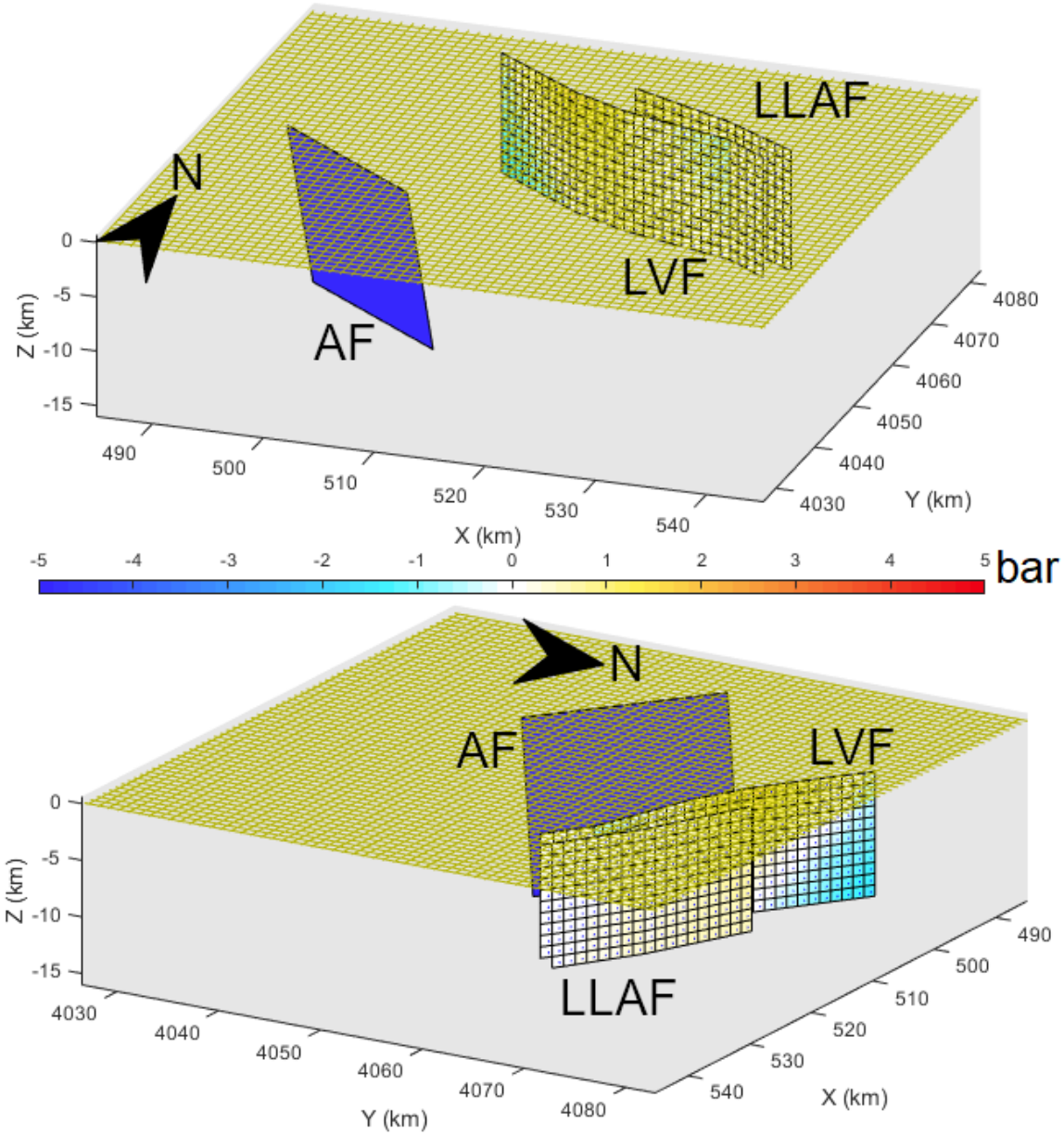

Figure 11. Coulomb static stress change model in rupture D (LVF+LLAF) caused by rupture A3 (AF).
AF: Adra Fault. LVF: Loma del Viento Fault. LLAF: Llano del Águila Fault.

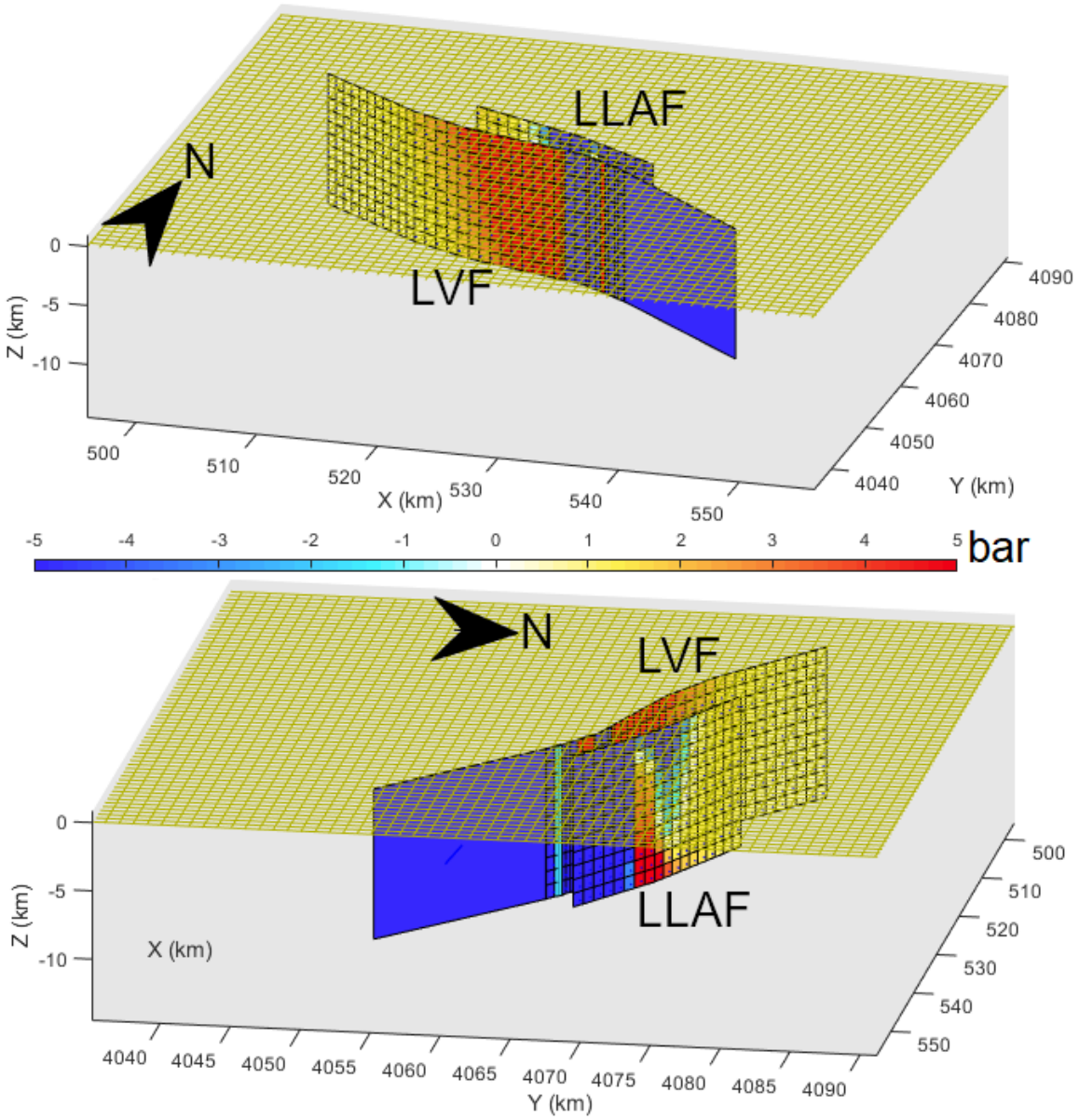

Figure 12. Coulomb static stress change model in rupture D (LVF+LLAF) caused by rupture LV2 (LVF's sea extension). LVF: Loma del Viento Fault. LLAF: Llano del Águila Fault.

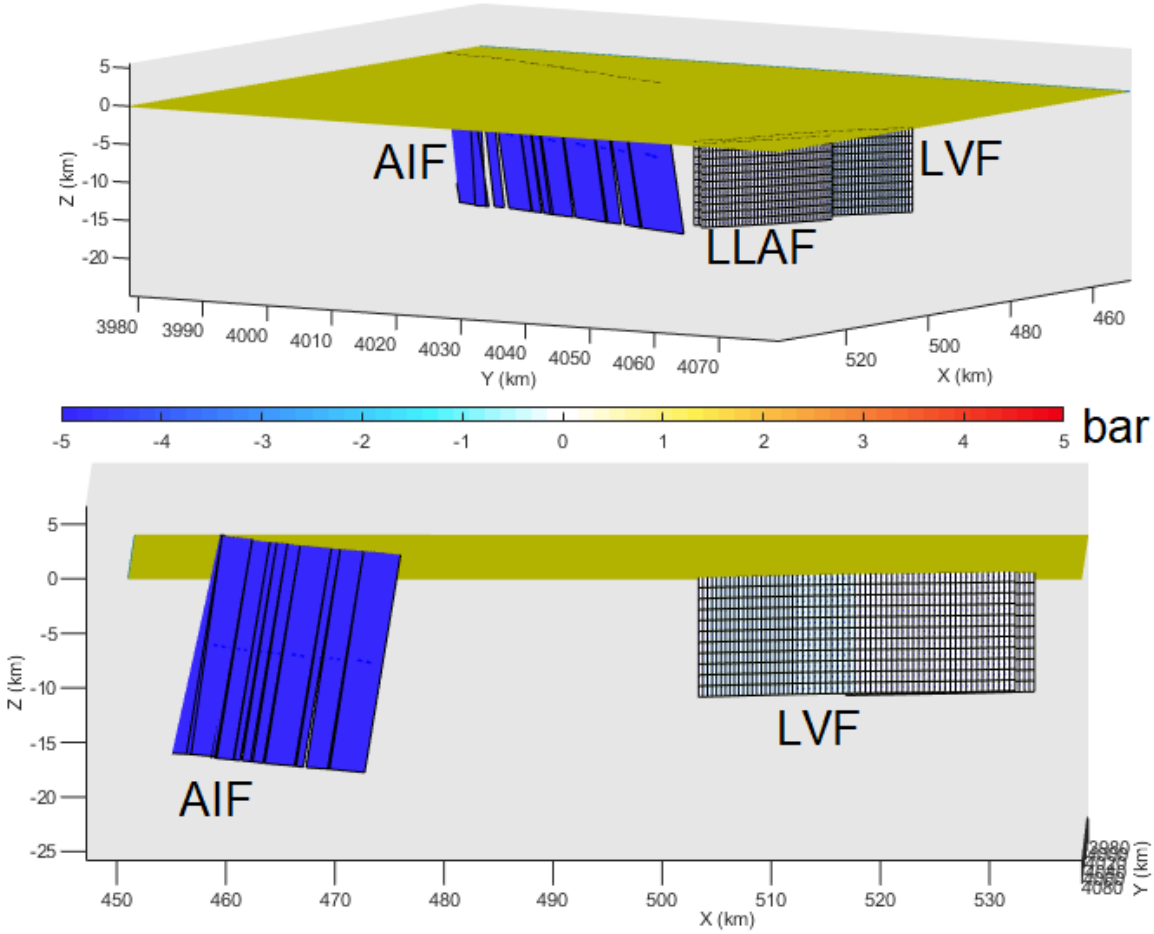

Figure 13. Coulomb static stress change model in rupture D (LVF+LLAF) caused by rupture AI (northern and central segments of Al-Idrissi Fault). LVF: Loma del Viento Fault. LLAF: Llano del Águila Fault. AIF: Al-Idrissi Fault.

4.5. ΔCFS of the 25th August earthquake

After calculating the local ΔCFS caused by rupture D on ideally oriented fault planes, we automatically detected the areas with ΔCFS > 0 bar, which are considered loaded zones, and those with ΔCFS < 0 bar, which are considered shadow zones. We then counted the number of located hypocenters in Instituto Geográfico Nacional (IGN)'s seismic catalogue inside loaded zones and shadow zones. If there is a significantly higher percentage of epicenters inside the loaded zones, it could point to an influence of the ΔCFS generated by the 25th August shock on the posterior seismicity.

IGN's seismic catalog includes a total of 251 events with $M_w > 3$ and hypocentral depth < 20 km in the study area since 25th August 1804 up to present times. Because hypocenter depth in the IGN's catalog can have uncertainties of several kilometers (especially for pre-instrumental earthquakes), we did the ΔCFS calculation for rupture D from 2 to 10 km deep. Figure 14 shows the ΔCFS induced by this earthquake on ideally oriented fault planes at three depths: 2 km, 5 km and 10 km. Epicenters for the 251 events are plotted as well in Figure 14. We found a total of 152 epicenters inside loaded zones (ΔCFS > 0 bar), and 34 events inside shadow zones (ΔCFS < 0 bar). This means that 61 % of the shallow main events in the catalog since 1804 are located inside areas that could have been loaded after the Dalías earthquake of 1804, while only a 13 % of the events after the earthquake occurred inside shadow zones, where we can expect a lesser seismicity rate. This could point to an influence of this region's last great earthquake of $M_w > 6.4$ in the posterior seismicity distribution, including earthquakes occurred during the time of instrumental records.

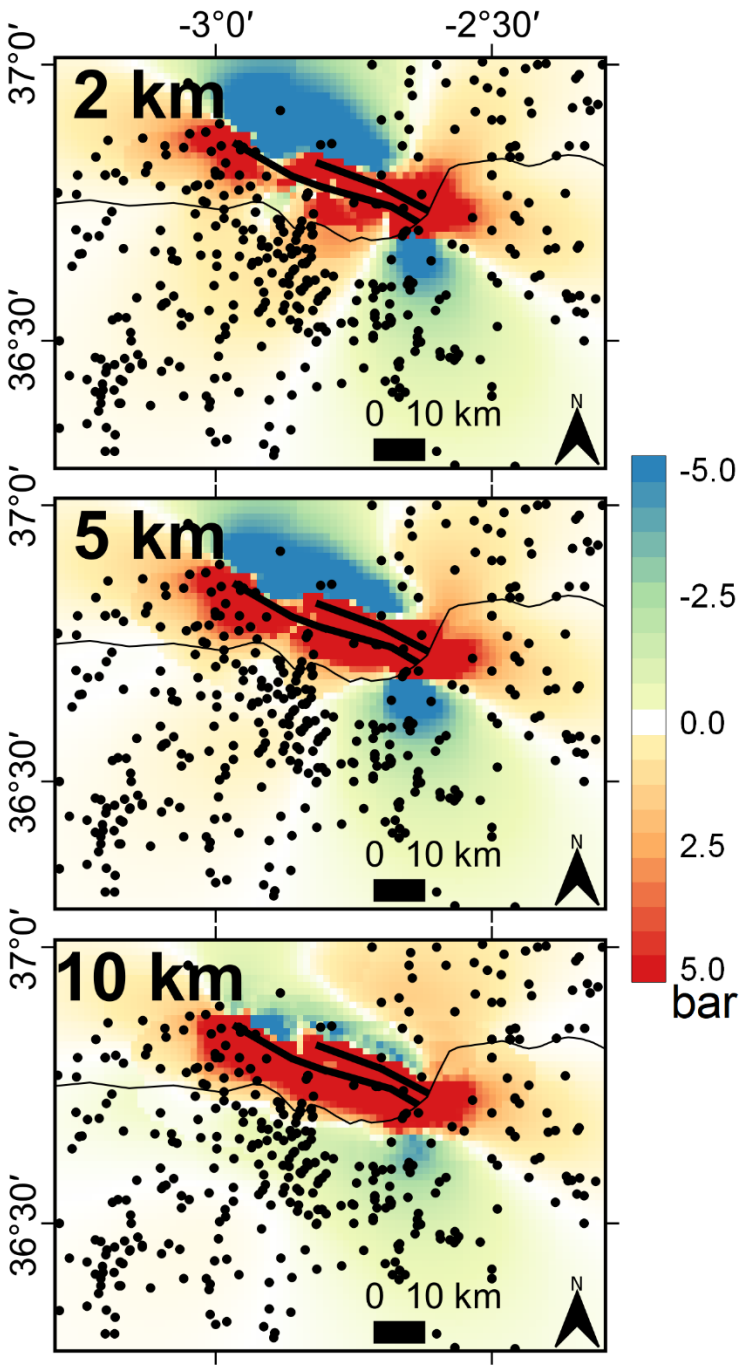

Figure 14. Coulomb static stress change model for rupture D of the Dalías earthquake (25th August 1804) at 2 km, 5 km and 10 km deep. Black dots correspond to epicenters of earthquakes recorded in IGN's seismic catalog of Mw > 3 and hypocentral depth < 20 km occurred from 1804 to 2013. σ_1 00º//158º, σ_3 00º//068º.

5. Discussion

In this work, we have searched for the most likely source of the 13th January 1804 Alborán earthquake combining different methodologies. First, we try to use Gasperini et

al. (1999, 2010)'s method to identify the most likely strike and area where the responsible source might be located. Then, we build intensity scenarios for several possible candidates to be the earthquake source and compare each of them with the observed intensity field, searching for the scenario that best fits the actual earthquake effects, following de Pro-Díaz et al. (2022, 2023)'s method. Finally, we use static Coulomb stress change calculations to refine the results.

The boxer calculated with Gasperini et al. (1999, 2010)'s method for the Alborán earthquake did not match any known active fault. Considering the amount of active tectonics studies conducted in the past in this area, most of which are referenced in the geological context of this work, the possibility of an unknown and unmapped active fault which would match the boxer in position and strike is highly unlikely. A more likely occurrence is a deviation of the boxer due to the intensity data points distribution over the study area: Boxer is known to show a geographical bias towards areas with a more dense population of intensity data points (de Pro-Díaz et al., 2023). As there are no data points offshore, the boxer has clearly been biased towards the Iberian coast, on which there are significantly more points than on the African coast. But this spatial bias is not the only issue with Gasperini et al. (1999, 2010)'s method detected in this work: Boxer also greatly underestimated the magnitude of the Alborán earthquake. This underestimation has been observed before in the Betics in the 1804 Dalías, the 2011 Lorca and the 1680 Málaga earthquakes (de Pro-Díaz et al., 2023) and is probably also related to the intensity data points distribution, or more precisely, to the absence of intensity data offshore, where the seismic source was most likely located. From these results, we suggest it is not possible to obtain valid results using Gasperini et al. (1999, 2010)'s method to study

earthquakes with intensity fields showing such poor azimuthal coverage as this one. Because of this, we did not take into account Boxer's results for the selection of candidate ruptures, and instead searched among the Quaternary active known faults for the ones which might match other authors' proposed sources.

None of the scenarios built for the Alborán earthquake show a perfect correlation with the intensity field's distribution when using the seismic scenario method, as seen in earlier works (de Pro-Díaz et al., 2022, 2023). During our first try building the scenarios with Campbell & Bozorgnia (2014)'s GMM, none of the candidate ruptures generated intensities high enough to match the observed earthquake effects, not even with M_w higher than those proposed by other authors (Figure AP3). We considered three possible explanations to this underprediction of the scenarios: a) the earthquake rupture might be longer than the ones we were using, which would also increase the magnitude; b) this earthquake could be a case in which complex ruptures involving several faults or fault segments lead to a higher energy release, and thus to heavier damage than expected, as it happened in the Kaikoura earthquake of 2016 (e. g. Goded et al., 2017; Kaiser et al., 2017; Stirling et al., 2017; Hamling, 2019); c) the best candidate was another, unknown fault we were not trying; and d) the GMM was underpredicting the ground motion, which in turn led to an underprediction of the intensity. We cast away option *a* because there was no geomorphologic evidence to further extend the fault traces of the BF, AF or LVF, and extending rupture AI further down the south of the AIF did not affect the predicted intensity distribution in the Iberian Peninsula, only in the African coast. Exploring option *b* would require another separate study on its own, so we will not address this option in this work. As for option *c*, the aforementioned absence of evidence for this hypothetical

unknown fault's existence despite intense active tectonics study in the area made this option highly unlikely. We were then down to option *d*: the GMM being the source of the issue. To address this possibility we rebuilt the scenarios using another GMM, Akkar & Bommer (2010), and the predicted intensities increased significantly in all of the scenarios, with some of them showing a rather good match (although not perfect) with the observed intensity distribution. We chose Akkar & Bommer (2010)'s GMM because it was built using data from the study area, as well as the rest of the Mediterranean.

It is noteworthy, though, how even with the GMM change, every scenario using a M_w equal to the ones calculated by other authors seems to significantly underestimate the intensity values. Both Molina et al. (2018) and Martínez Solares & Mezcua Rodríguez (2002) estimated this earthquake's magnitude using mainly intensity data and methodologies similar to that of Gasperini et al. (1999, 2010). The unreliability of this kind of calculation when intensity data are scarce and so heterogeneously distributed over the study area as in this case has been shown before in this work and earlier ones (de Pro-Díaz et al., 2023), so it is possible that Molina et al. (2018) and Martínez Solares & Mezcua Rodríguez (2002) underestimated this earthquake's magnitude. In addition to this, according to the equations of Stirling et al. (2002) and Wells & Coppersmith (1994), $M_w \geq 6.9$ is plausible for the considered rupture areas in the best performing scenarios in this work, and in the case of the AIF, also highlight this fault's potential to generate $M_w \geq 7$ earthquakes. Whether the real M_w was 6.9, or 7.0, or another number altogether, is something we may never know with precision, considering this is a pre-instrumental earthquake. However, our results show that $M_w < 6.9$ does not explain the observed

damage distribution, but higher magnitudes in any of the nearby faults do. This should be considered in future seismic hazards assessments in this area.

The statistical tests could not be applied in the differential zones step for any of the competing scenarios for this earthquake. This is due to the reduced amount of intensity data points inside the differential areas (less than 10 in all cases), which has proven to be the main limitation of the seismic scenario methodology. A similar issue appeared while studying the 1680 Málaga earthquake (de Pro-Díaz et al., 2023), another earthquake which showed an azimuthal coverage of 180º or less on its intensity field and a high dispersion of the data points over a wide area. Poor azimuthal coverage combined with high point dispersion of the intensity field are clearly the main limitations of this methodology. These characteristics are typically present in offshore earthquakes, due to the spatial bias of intensity data; although some earthquakes of $M_w > 7$ may cause such shaking that even if the seismic source is located offshore, there could be enough intensity points inland to apply this methodology. This was the case of the 1755 Lisbon earthquake, which was studied by Silva et al. (2023) using a methodology slightly different to the one used here but also based on building seismic scenarios and comparing them with the observed effects of the earthquake.

The implementation of the Coulomb stress transfer analysis step into the methodology is a parallel approach to strengthen the results and try to discern the best candidate rupture when the intensity data's azimuthal coverage is too poor. In this case study, if we assume, considering their closeness in both space and time, that there was a triggering effect between the Alborán earthquake of January and the Dalías earthquake of August, based solely on our results with the Coulomb stress transfer, the sea extension of the LVF would

be the most likely source for the January shock. The AF would also be a plausible source nonetheless, since it also charged a significant percentage of the Dalías rupture's plane. However, we must bear in mind that this triggering is an assumption, and its occurrence has not been proved. We must also remember that despite none of the scenarios tried in this work shows a perfect match with the intensity field, the intensity spatial distribution of scenarios from the AF and the AIF seem to be more similar to the observed intensity distribution than the scenario from the LVF is.

Our results do not allow us to tell apart one best candidate for the Alborán earthquake, despite the different approaches that have been tried. Nevertheless, we were able to discard six out of ten possible candidates. Based on our results, either one of the AF, the LVF, the BF or the AIF are plausible sources for this earthquake. However, if we had to decide for one of them, our preferred candidate would be the AF, because scenario A3 strikes a balance between the triggering hypothesis and a somewhat good match with the observed intensity's spatial distribution. Until more data is available for this earthquake and based on our results, we propose the Adra Fault as the most likely source for the Alborán earthquake of 13th January 1804, although bearing in mind that the Al-Idrissi, Balanegra and Loma del Viento Faults cannot be cast aside as possible sources.

In this work we have also performed a simple analysis to check for initial evidence of a possible influence of the Coulomb stress transfer caused by the Dalías shock of August on the posterior local seismicity. Our results show a correlation between positive stress change and the post-1804 seismicity rate. This correlation could persist at the present day, especially considering the low tectonic rate of this region that favors a longer-term influence of dynamic changes.

6. Conclusions

We have applied the Gasperini method, the seismic scenario method and Coulomb stress transfer analysis to investigate the most likely source of the Alborán earthquake from 1804. The Gasperini method produced results which were incompatible with the consensus of an offshore source accepted by all independent authors in the bibliography, so we decided against taking those results into account for this work. The seismic scenario method allowed us to discard six out of ten possible candidate ruptures, but the observed intensity field was too scarce and lacked the azimuthal coverage needed to discern the best candidate among the remaining four. The results of the Coulomb stress transfer analysis allowed us to rank these four candidates, but only with the assumption of a triggering effect between the Alborán shock of 13th January and the Dalías shock of 25th August. In the end, we lack enough data to select one best candidate among the Al-Idrissi, Adra, Balanegra and Loma del Viento Faults. The Adra Fault is the one which strikes the best balance between all the proposed hypothesis, but the other three are also plausible candidates to be the source of this earthquake.

We also investigated the possible influence of the stress transfer caused by the Dalías earthquake of 1804 on the local seismicity rate. This influence might still prevail in the present day, although more research is needed on this subject.

Acknowledgements

This work has been funded thanks to a predoctoral research contract from Universidad Complutense de Madrid (2019) and its following Postdoctoral Orientation Period (POP), as well as the research project “Análisis del ciclo sísmico a largo plazo a partir de datos geológicos y modelado” with reference number PID2021-124155NB-C31.

Data and code availability

Data used in this work was not compiled by the authors. The authors used data from Murphy Corella (2019), which is an open-access book available in the digital archive of the Instituto Geográfico Nacional (https://www.ign.es/web/libros-digitales/terremotos-almeria-1804).

Competing interests

The authors have no competing interests.

References

Abrahamson, N. A., Silva, W. J., & Kamai, R. (2014). Update of the AS08 Ground-Motion Prediction equations based on the NGA-west2 data set. *Pacific Engineering Research Center Report*, *May*, 174. http://scholar.google.com/scholar?hl=en&btnG=Search&q=intitle:Update+of+the+AS08+Ground-Motion+Prediction+Equations+Based+on+the+NGA-West2+Data+Set#0

Akkar, S., Sandıkkaya, M. A., & Bommer, J. J. (2014). Empirical ground-motion models for point- and extended-source crustal earthquake scenarios in Europe and the Middle East. *Bulletin of Earthquake Engineering*, *12*(1), 359–387. https://doi.org/10.1007/s10518-013-9461-4

Akkar, Sinan, & Bommer, J. J. (2010). Empirical equations for the prediction of PGA, PGV, and spectral accelerations in Europe, the mediterranean region, and the Middle East. *Seismological Research Letters*, *81*(2), 195–206. https://doi.org/10.1785/gssrl.81.2.195

Álvarez-Gómez, José A., Herrero-Barbero, P., & Martínez-Díaz, J. J. (2023). Seismogenic potential and tsunami threat of the strike-slip Carboneras fault in the western Mediterranean from physics-based earthquake simulations. *Natural Hazards and Earth System Sciences*, *23*(6), 2031–2052. https://doi.org/10.5194/nhess-23-2031-2023

Álvarez-Gómez, Jose Antonio, Martín, R., Pérez-López, R., Stich, D., Cantavella, J. V., Martínez-Díaz, J. J., Morales Soto, J., Martínez-García, P., Soto, J. I., & Carreño, E. (2016). La serie sísmica de Alhucemas 2016. Partición de la deformación e interacción de estructuras en un límite de placas difuso. *Geo-Temas*, *16*(2), 491–494.

Ambraseys, N. N., Douglas, J., Sarma, S. K., & Smit, P. M. (2005). Equations for the estimation of strong ground motions from shallow crustal earthquakes using data from Europe and the middle east: Horizontal peak ground acceleration and spectral acceleration. *Bulletin of Earthquake Engineering*, *3*(1), 1–53. https://doi.org/10.1007/s10518-005-0183-0

Ambraseys, N. N., & Jackson, J. A. (1998). Faulting associated with historical and recent earthquakes in the Eastern Mediterranean region. *Geophysical Journal International*, *133*(2), 390–406. https://doi.org/10.1046/j.1365-246X.1998.00508.x

Ammar, A., Mauffret, A., Gorini, C., & Jabour, H. (2007). The Tectonic Structure Of The Alboran Margin Of Morocco. *Revista de La Sociedad Geológica de España*, *20*(3–4), 247–271.

Atkinson, G. M., & Kaka, S. L. I. (2007). Relationships between felt intensity and

instrumental ground motion in the Central United States and California. *Bulletin of the Seismological Society of America*, *97*(2), 497–510. https://doi.org/10.1785/0120060154

Atkinson, G. M., & Wald, D. J. (2007). “Did You Feel It?” intensity data: a surprisingly good measure of earthquake ground motion. *Seismological Research Letters*, *78*(3), 362–368.

Basili, R., Valensise, G., Vannoli, P., Burrato, P., Fracassi, U., Mariano, S., Tiberti, M. M., & Boschi, E. (2008). The Database of Individual Seismogenic Sources (DISS), version 3: Summarizing 20 years of research on Italy’s earthquake geology. *Tectonophysics*, *453*(1–4), 20–43. https://doi.org/10.1016/j.tecto.2007.04.014

Campbell, K. W. (2003). Prediction of strong ground motion using the hybrid empirical method and its use in the development of ground-motion (attenuation) relations in Eastern North America. *Bulletin of the Seismological Society of America*, *93*(3), 1012–1033. https://doi.org/10.1785/0120020002

Campbell, K. W., & Bozorgnia, Y. (2014). NGA-West2 ground motion model for the average horizontal components of PGA, PGV, and 5% damped linear acceleration response spectra. *Earthquake Spectra*, *30*(3), 1087–1114. https://doi.org/10.1193/062913EQS175M

Canora, C., Martínez-Díaz, J. J., Villamor, P., Berryman, K., Álvarez-Gómez, J. A., Pullinger, C., & Capote, R. (2010). Geological and seismological analysis of the 13 february 2001 Mw 6.6 el salvador earthquake: Evidence for surface rupture and

implications for seismic hazard. *Bulletin of the Seismological Society of America*, *100*(6), 2873–2890. https://doi.org/10.1785/0120090377

Canora, C., Vilanova, S. P., de Pro-Díaz, Y., Pina, P., & Heleno, S. (2021). Evidence of surface rupture associated with historical earthquakes in the Lower Tagus Valley, Portugal. Implications for seismic hazard in the Greater Lisbon Area. *Frontiers in Earth Science, 9:620778*. https://doi.org/10.3389/feart.2021.620778

Caprio, M., Tarigan, B., Bruce Worden, C., Wiemer, S., & Wald, D. J. (2015). Ground motion to intensity conversion equations (GMICEs): A global relationship and evaluation of regional dependency. *Bulletin of the Seismological Society of America*, *105*(3), 1476–1490. https://doi.org/10.1785/0120140286

Caputo, R., Sboras, S., Pavlides, S., & Chatzipetros, A. (2015). Comparison between single-event effects and cumulative effects for the purpose of seismic hazard assessment. A review from Greece. *Earth-Science Reviews, 148*, 94–120. https://doi.org/10.1016/j.earscirev.2015.05.004

d'Acremont, E., Gutscher, M. A., Rabaute, A., Mercier de Lépinay, B., Lafosse, M., Poort, J., Ammar, A., Tahayt, A., Le Roy, P., Smit, J., Do Couto, D., Cancouët, R., Prunier, C., Ercilla, G., & Gorini, C. (2014). High-resolution imagery of active faulting offshore Al Hoceima, Northern Morocco. *Tectonophysics, 632*(C), 160–166. https://doi.org/10.1016/j.tecto.2014.06.008

De Larouzière, F. D., Bolze, J., Bordet, P., Hernandez, J., Montenat, C., & Ott d'Estevou, P. (1988). The Betic segment of the lithospheric Trans-Alboran shear zone during

the Late Miocene. *Tectonophysics*, *152*(1–2), 41–52. https://doi.org/10.1016/0040-1951(88)90028-5

de Pro-Díaz, Y., Perea, H., Insua-Arévalo, J. M., Martínez-Díaz, J. J., & Canora, C. (2023). Constraining earthquake fault sources through the use of intensity data and seismic scenarios: application to the Betic Cordillera (South Spain). *Frontiers in Earth Science, 11:1214836*. https://doi.org/10.3389/feart.2023.1214836

de Pro-Díaz, Y., Vilanova, S., & Canora, C. (2022). Ranking Earthquake Sources Using Spatial Residuals of Seismic Scenarios: Methodology Application to the 1909 Benavente Earthquake. *Bulletin of the Seismological Society of America*, *113*(2), 710–731. https://doi.org/10.1785/0120220067

Delavaud, E., Scherbaum, F., Kuehn, N., & Riggelsen, C. (2009). Information-theoretic selection of ground-motion prediction equations for seismic hazard analysis: An applicability study using californian data. *Bulletin of the Seismological Society of America*, *99*(6), 3248–3263. https://doi.org/10.1785/0120090055

DeMets, C., Gordon, R. G., & Argus, D. F. (2010). Geologically current plate motions. *Geophysical Journal International*, *181*(1), 1–80. https://doi.org/10.1111/j.1365-246X.2009.04491.x

Echeverria, A., Khazaradze, G., Asensio, E., & Masana, E. (2015). Geodetic evidence for continuing tectonic activity of the Carboneras fault (SE Spain). *Tectonophysics*, *663*, 302–309. https://doi.org/10.1016/j.tecto.2015.08.009

Espinar Moreno, M. (1994). Los estudios de sismicidad histórica en Andalucía: los

terremotos históricos de la provincia de Almería. In *El estudio de los terremotos en Almería* (pp. 115–180). Instituto de EStudios Almerienses. https://dialnet.unirioja.es/servlet/articulo?codigo=2767758

Ferrater, M., Ortuño, M., Masana, E., Martínez-Díaz, J. J., Pallàs, R., Perea, H., Baize, S., García-Meléndez, E., Echeverria, A., Rockwell, T., Sharp, W. D., & Arrowsmith, R. (2017). Lateral slip rate of Alhama de Murcia fault (SE Iberian Peninsula) based on a morphotectonic analysis: Comparison with paleoseismological data. *Quaternary International*, *451*, 87–100. https://doi.org/10.1016/j.quaint.2017.02.018

Ferrater, M., Ortuño, M., Masana, E., Pallàs, R., Perea, H., Baize, S., García-Meléndez, E., Martínez-Díaz, J. J., Echeverria, A., Rockwell, T. K., Sharp, W. D., Medialdea, A., & Rhodes, E. J. (2016). Refining seismic parameters in low seismicity areas by 3D trenching: The Alhama de Murcia fault, SE Iberia. *Tectonophysics*, *680*, 122–128. https://doi.org/10.1016/j.tecto.2016.05.020

Fracassi, U., & Valensise, G. (2007). Unveiling the sources of the catastrophic 1456 multiple earthquake: Hints to an unexplored tectonic mechanism in southern Italy. *Bulletin of the Seismological Society of America*, *97*(3), 725–748. https://doi.org/10.1785/0120050250

García-Mayordomo, J., Insua-Arévalo, J. M., Martínez-Díaz, J. J., Jiménez-Díaz, A., Martín-Banda, R., Martín-Alfageme, S., Álvarez-Gómez, J. A., Rodríguez-Peces, M., Pérez-López, R., Rodríguez-Pascua, M. A., Masana, E., Perea, H., Martín-González, F., Giner-Robles, J., Nemser, E. S., Cabral, J., & The_QAFI_Compilers_Working_Group. (2012). The Quaternary Faults Database of

Iberia (QAFI v.2.0). *Journal of Iberian Geology*, *38*(1), 285–302.

Gasperini, P., Bernardini, F., Valensise, G., & Boschi, E. (1999). Defining seismogenic sources from historical earthquake felt reports. *Bulletin of the Seismological Society of America*, *89*(1), 94–110.

Gasperini, P., Vannucci, G., Tripone, D., & Boschi, E. (2010). The location and sizing of historical earthquakes using the attenuation of macroseismic intensity with distance. *Bulletin of the Seismological Society of America*, *100*(5 A), 2035–2066. https://doi.org/10.1785/0120090330

Goded, T., Horspool, N., Canessa, S., & Gerstenberger, M. (2017). Modified Mercalli intensities for the M7.8 Kaikōura (New Zealand) 14 November 2016 earthquake derived from "felt detailed" and "felt rapid" online questionnaires. *Bulletin of the New Zealand Society for Earthquake Engineering*, *50*(2), 352–362. https://doi.org/10.5459/bnzsee.50.2.352-362

Gómez-Novell, O., García-Mayordomo, J., Ortuño, M., Masana, E., & Chartier, T. (2020). Fault System-Based Probabilistic Seismic Hazard Assessment of a Moderate Seismicity Region: The Eastern Betics Shear Zone (SE Spain). *Frontiers in Earth Science*, *8*(December). https://doi.org/10.3389/feart.2020.579398

Gómez de la Peña, L., Gràcia, E., Maesano, F. E., Basili, R., Kopp, H., Sánchez-Serra, C., Scala, A., Romano, F., Volpe, M., Piatanesi, A., & R. Ranero, C. (2022). A first appraisal of the seismogenic and tsunamigenic potential of the largest fault systems in the westernmost Mediterranean. *Marine Geology*, *445*(February).

https://doi.org/10.1016/j.margeo.2022.106749

Gràcia, E., Bartolome, R., Lo Iacono, C., Moreno, X., Stich, D., Martínez-Diaz, J. J., Bozzano, G., Martínez-Loriente, S., Perea, H., Diez, S., Masana, E., Dañobeitia, J. J., Tello, O., Sanz, J. L., & Carreño, E. (2012). Acoustic and seismic imaging of the Adra Fault (NE Alboran Sea): In search of the source of the 1910 Adra earthquake. *Natural Hazards and Earth System Sciences*, *12*(11), 3255–3267. https://doi.org/10.5194/nhess-12-3255-2012

Gràcia, E., Grevemeyer, I., Bartolomé, R., Perea, H., Martínez-Loriente, S., Gómez de la Peña, L., Villaseñor, A., Klinger, Y., Lo Iacono, C., Diez, S., Calahorrano, A., Camafort, M., Costa, S., d'Acremont, E., Rabaute, A., & Ranero, C. R. (2019). Earthquake crisis unveils the growth of an incipient continental fault system. *Nature Communications*, *10*(1), 1–12. https://doi.org/10.1038/s41467-019-11064-5

Gràcia, E., Pallàs, R., Soto, J. I., Comas, M., Moreno, X., Masana, E., Santanach, P., Diez, S., García, M., Dañobeitia, J., Bartolomé, R., Farrán, M., Gómez, M., Alpiste, M. J. R., Lastras, G., Wilmott, V., Perea, H., Blondel, P., Gómez, O., … Roque, C. (2006). Active faulting offshore SE Spain (Alboran Sea): Implications for earthquake hazard assessment in the Southern Iberian Margin. *Earth and Planetary Science Letters*, *241*(3–4), 734–749. https://doi.org/10.1016/j.epsl.2005.11.009

Griffin, J., Nguyen, N., Cummins, P., & Cipta, A. (2019). Historical earthquakes of the eastern sunda arc: Source mechanisms and intensity-based testing of Indonesia's national seismic hazard assessment. *Bulletin of the Seismological Society of America*, *109*(1), 43–65. https://doi.org/10.1785/0120180085

Grünthal, G. (1998). *European Macroseismic Scale 1998* (Vol. 15). European Seismological Commission (ESC). http://lib.riskreductionafrica.org/bitstream/handle/123456789/1193/1281.European Macroseismic Scale 1998.pdf?sequence=1

Hamling, I. J. (2019). A review of the 2016 Kaikōura earthquake: insights from the first 3 years. *Journal of the Royal Society of New Zealand*, *50*(2), 226–244. https://doi.org/10.1080/03036758.2019.1701048

Harris, R. A. (1998). Introduction to special section: Stress triggers, stress shadows, and implications for seismic hazard. *Journal of Geophysical Research: Solid Earth*, *103*(B10), 24347–24358. https://doi.org/10.1029/98jb01576

Herrero-Barbero, P., Álvarez-Gómez, J. A., Williams, C., Villamor, P., Insua-Arévalo, J. M., Alonso-Henar, J., & Martínez-Díaz, J. J. (2021). Physics-based earthquake simulations in slow-moving faults: a case study from the Eastern Betic Shear Zone (SE Iberian Peninsula). *Journal of Geophysical Research: Solid Earth*, *126*(5), 1–25. https://doi.org/10.1029/2020JB021133

Herrero Barbero, P. (2021). *Modelización 3D de la estructura, la cinemática y el comportamiento sismogénico del sistema de fallas de las Béticas Orientales. Aplicación a la amenaza sísmica*. Universidad Complutense de Madrid.

Hough, S. E., & Graves, R. W. (2020). The 1933 Long Beach Earthquake (California, USA): Ground Motions and Rupture Scenario. *Scientific Reports*, *10*(1), 1–10. https://doi.org/10.1038/s41598-020-66299-w

Huerta, P., Silva, P. G., Giner-Robles, J. L., Rodríguez-Pascua, M. A., & Bautista Davila, M. B. (2015). Efectos geológicos del terremoto de Dalías-Berja 1804 AD. (Almería, SE España). *XIV Reunión Nacional de Cuaternario*, *1*, 194–197.

IGN-UCM. (2013). *Actualización de mapas de peligrosidad sísmica de España 2012 (Vol. 267)* (p. 272). Centro Nacional de Información Geográfica (CNIG). https://doi.org/10.7419/162.05.2017

Insua-Arévalo, J. M., García-Mayordomo, J., Salazar, A., Rodríguez-Escudero, E., Martín-Banda, R., Álvarez-Gómez, J. A., Canora, C., & Martínez-Díaz, J. J. (2015). Paleoseismological evidence of holocene activity of the los tollos fault (Murcia, se Spain): A lately formed quaternary tectonic feature of the eastern betic shear zone. *Journal of Iberian Geology*, *41*(3), 333–350. https://doi.org/10.5209/rev_JIGE.2015.v41.n3.49948

Kaiser, A., Balfour, N., Fry, B., Holden, C., Litchfield, N., Gerstenberger, M., D'Anastasio, E., Horspool, N., McVerry, G., Ristau, J., Bannister, S., Christophersen, A., Clark, K., Power, W., Rhoades, D., Massey, C., Hamling, I., Wallace, L., Mountjoy, J., … Gledhill, K. (2017). The 2016 Kaikōura, New Zealand, earthquake: Preliminary seismological report. *Seismological Research Letters*, *88*(3), 727–739. https://doi.org/10.1785/0220170018

Kaka, S. L. I., & Atkinson, G. M. (2004). Relationships between instrumental ground-motion parameters and modified Mercalli intensity in eastern North America. *Bulletin of the Seismological Society of America*, *94*(5), 1728–1736. https://doi.org/10.1785/012003228

King, G. C. P., Stein, R. S., & Jian Lin. (1994). Static stress changes and the triggering of earthquakes. *Bulletin - Seismological Society of America*, *84*(3), 935–953. https://doi.org/10.1016/0148-9062(95)94484-2

Lafosse, M., D'Acremont, E., Rabaute, A., Estrada, F., Jollivet-Castelot, M., Vázquez, J. T., Galindo-Zaldivar, J., Ercilla, G., Alonso, B., Smit, J., Ammar, A., & Gorini, C. (2020). Plio-Quaternary tectonic evolution of the southern margin of the Alboran Basin (Western Mediterranean). *Solid Earth*, *11*(2), 741–765. https://doi.org/10.5194/se-11-741-2020

Lozos, J. C. (2016). A case for historic joint rupture of the San Andreas and San Jacinto faults. *Science Advances*, *2*(3), 1–8. https://doi.org/10.1126/sciadv.1500621

Marín-Lechado, C., Galindo-Zaldívar, J., Gil, A. J., Borque, M. J., de Lacy, M. C., Pedrera, A., López-Garrido, A. C., Alfaro, P., García-Tortosa, F., Ramos, M. I., Rodríguez-Caderot, G., Rodríguez-Fernández, J., Ruiz-Constán, A., & de Galdeano-Equiza, C. S. (2010). Levelling profiles and a GPS network to monitor the active folding and faulting deformation in the campo de dalias (Betic Cordillera, Southeastern Spain). *Sensors*, *10*(4), 3504–3518. https://doi.org/10.3390/s100403504

Marín-Lechado, C., Galindo-Zaldívar, J., Rodríguez-Fernández, L. R., Serrano, I., & Pedrera, A. (2005). Active faults, seismicity and stresses in an internal boundary of a tectonic arc (Campo de Dalías and Níjar, southeastern Betic Cordilleras, Spain). *Tectonophysics*, *396*(1–2), 81–96. https://doi.org/10.1016/j.tecto.2004.11.001

Martín-Banda, R., García-Mayordomo, J., Insua-Arévalo, J. M., Salazar, Á. E., Rodríguez-Escudero, E., Álvarez-Gõmez, J. A., Medialdea, A., & Herrero, M. J. (2016). New insights on the seismogenic potential of the Eastern Betic Shear Zone (SE Iberia): Quaternary activity and paleoseismicity of the SW segment of the Carrascoy Fault Zone. *Tectonics*, *35*(1), 55–75. https://doi.org/10.1002/2015TC003997

Martínez-Díaz, J. J. (1999). *Neotectónica y Tectónica Activa del Sector Centro-Occidental de la Región de Murcia y Sur de Almería (Cordillera Bética - España)*. Universidad Complutense de Madrid.

Martínez-Díaz, J. J., & Hernández-Enrile, J. L. (2004). Neotectonics and morphotectonics of the southern Almería region (Betic Cordillera-Spain) kinematic implications. *International Journal of Earth Sciences*, *93*(2), 189–206. https://doi.org/10.1007/s00531-003-0379-y

Martínez-Díaz, J. J., Masana, E., & Ortuño, M. (2012). Active tectonics of the Alhama de Murcia fault, Betic Cordillera, Spain. *Journal of Iberian Geology*, *38*(1), 253–270. https://doi.org/10.5209/rev_jige.2012.v38.n1.39218

Martínez-García, P., Comas, M., Soto, J. I., Lonergan, L., & Watts, A. B. (2013). Strike-slip tectonics and basin inversion in the Western Mediterranean: The Post-Messinian evolution of the Alboran Sea. *Basin Research*, *25*(4), 361–387. https://doi.org/10.1111/bre.12005

Martínez-García, P., Soto, J. I., & Comas, M. (2011). Recent structures in the Alboran

Ridge and Yusuf fault zones based on swath bathymetry and sub-bottom profiling: Evidence of active tectonics. *Geo-Marine Letters*, *31*(1), 19–36. https://doi.org/10.1007/s00367-010-0212-0

Martínez-Martínez, J. M. (2006). Lateral interaction between metamorphic core complexes and less-extended, tilt-block domains: the Alpujarras strike-slip transfer fault zone (Betics, SE Spain). *Journal of Structural Geology*, *28*(4), 602–620. https://doi.org/10.1016/j.jsg.2006.01.012

Martínez Solares, J. M., & Mezcua Rodríguez, J. (2002). *Catálogo sísmico de la Península Ibérica (880 a. C. - 1900)*. Instituto Geográfico Nacional.

McCalpin, J. P., & Nelson, A. S. (1996). *Paleoseismology* (J. P. McCalpin (ed.)). Academic Press.

Mezcua, J., Rueda, J., & García Blanco, R. M. (2013). Iberian peninsula historical seismicity revisited: An intensity data bank. *Seismological Research Letters*, *84*(1), 9–18. https://doi.org/10.1785/0220120097

Michetti, A. M., Esposito, E., Guerrieri, L., Porfido, S., Serva, L., Tatevossian, R., Vittori, E., Audemard, F., Azuma, T., Clague, J., Comerci, V., Gürpinar, A., McCalpin, J., Mohammadioun, B., Mörner, N. A., Ota, Y., & Roghozin, E. (2007). *INQUA Environmental Seismic Intensity Scale 2007 (ESI-2007)* (L. Guerrieri & E. Vittori (eds.)). Servizio Geológico d'Italia - Dipartamento Difensa del Suolo.

Molina, S., Navarro, M., Martínez-Pagan, P., Pérez-Cuevas, J., Vidal, F., Navarro, D., & Agea-Medina, N. (2018). Potential damage and losses in a repeat of the 1910 Adra

(Southern Spain) earthquake. *Natural Hazards*, *92*(3), 1547–1571. https://doi.org/10.1007/s11069-018-3263-6

Molins-Vigatà, J., García-Mayordomo, J., Ortuño, M., García-Sellés, D., & Gómez-Novell, O. (2022). Caracterización geológica de la falla del Llano del Águila en Campo Dalías (Almería): posible fuente sismogénica del terremoto de 1804. *Revista de La Sociedad Geológica de España*, *35*(1), 71–83. https://doi.org/10.55407/rsge.94908

Moreno Mota, X. (2011). *Neotectonic and Paleoseismic onshore-offshore integrated study of the Carboneras Fault (Eastern Betics, SE Iberia)*. Universitat de Barcelona.

Moreno, X., Gràcia, E., Bartolomé, R., Martínez-Loriente, S., Perea, H., de la Peña, L. G., Iacono, C. Lo, Piñero, E., Pallàs, R., Masana, E., & Dañobeitia, J. J. (2016). Seismostratigraphy and tectonic architecture of the Carboneras Fault offshore based on multiscale seismic imaging: Implications for the Neogene evolution of the NE Alboran Sea. *Tectonophysics*, *689*, 115–132. https://doi.org/10.1016/j.tecto.2016.02.018

Moreno, X., Masana, E., Pallàs, R., Gràcia, E., Rodés, Á., & Bordonau, J. (2015). Quaternary tectonic activity of the Carboneras Fault in the La Serrata range (SE Iberia): Geomorphological and chronological constraints. *Tectonophysics*, *663*, 78–94. https://doi.org/10.1016/j.tecto.2015.08.016

Muñoz Clares, M., Fernández Carrascosa, M., Alcolea López, M. O., Arcas Navarro, M. C., Arcas Ruiz, N., Caro del Vas, P., Cruz López, M. T., García Poveda, M., García

Valera, M. A., Llamas Martínez, B., & Ruiz Llanes, A. E. (2012). Sismicidad histórica y documentación municipal: El caso de Lorca. *Boletin Geologico y Minero*, *123*(4), 415–429.

Murphy Corella, P. (2019). *Los terremotos de Almería de 1804 en el archivo histórico nacional*. Instituto Geográfico Nacional. https://www.ign.es/web/libros-digitales/terremotos-almeria-1804

Nocquet, J. M., & Calais, E. (2004). Geodetic measurements of crustal deformation in the Western Mediterranean and Europe. *Pure and Applied Geophysics*, *161*(3), 661–681. https://doi.org/10.1007/s00024-003-2468-z

Okada, Y. (1992). Internal deformation due to shear and tensile faults in a half-space. *Bulletin - Seismological Society of America*, *82*(2), 1018–1040. https://doi.org/10.1785/bssa0820021018

Ortuño, M., Masana, E., García-Meléndez, E., Martínez-Díaz, J., Štěpančíková, P., Cunha, P. P., Sohbati, R., Canora, C., Buylaert, J. P., & Murray, A. S. (2012). An exceptionally long paleoseismic record of a slow-moving fault: The Alhama de Murcia fault (Eastern Betic shear zone, Spain). *Bulletin of the Geological Society of America*, *124*(9–10), 1474–1494. https://doi.org/10.1130/B30558.1

Pagani, M., Monelli, D., Weatherill, G., Danciu, L., Crowley, H., Silva, V., Henshaw, P., Butler, L., Nastasi, M., Panzeri, L., Simionato, M., & Vigano, D. (2014). Openquake engine: An open hazard (and risk) software for the global earthquake model. *Seismological Research Letters*, *85*(3), 692–702.

https://doi.org/10.1785/0220130087

Palano, M., González, P. J., & Fernández, J. (2015). The Diffuse Plate boundary of Nubia and Iberia in the Western Mediterranean: Crustal deformation evidence for viscous coupling and fragmented lithosphere. *Earth and Planetary Science Letters*, *430*, 439–447. https://doi.org/10.1016/j.epsl.2015.08.040

Pedrera, A., Marín-Lechado, C., Stich, D., Ruiz-Constán, A., Galindo-Zaldívar, J., Rey-Moral, C., & de Lis Mancilla, F. (2012). Nucleation, linkage and active propagation of a segmented Quaternary normal-dextral fault: The Loma del Viento fault (Campo de Dalías, Eastern Betic Cordillera, SE Spain). *Tectonophysics*, *522–523*, 208–217. https://doi.org/10.1016/j.tecto.2011.12.001

Perea, H, Roldán, J. L., Sánchez-Lozano, L., Álvarez-Gómez, J. A., & P. Herrero-Barbero1, M.J. Jiménez4, S. Martínez-Loriente2, A. C. y J. L. (2022). Serie sísmica del sur del Mar de Alborán del 2021-2022: relocalización de los eventos e implicaciones sismotectónicas. *IV Reunión Ibérica Sobre Fallas Activas y Paleosismología*, 141–144.

Perea, Hector. (2009). The Catalan seismic crisis (1427 and 1428; NE Iberian Peninsula): Geological sources and earthquake triggering. *Journal of Geodynamics*, *47*(5), 259–270. https://doi.org/10.1016/j.jog.2009.01.002

Pezeshk, S., Zandieh, A., Campbell, K. W., & Tavakoli, B. (2018). Ground-motion prediction equations for central and eastern north America using the hybrid empirical method and NGA-west2 empirical ground-motion models. *Bulletin of the*

Seismological Society of America, *108*(4), 2278–2304. https://doi.org/10.1785/0120170179

Posadas, A., Vidal, F., & Navarro, M. (2006). The M = 6.3 Earthquake of January 13 (1804) in Motril (Spain). *Proceedings of the First Europen Conference on Earthquake Engineering and Seismology*, *91*, 1–8.

Rodríguez-Pascua, M. A., Silva, P. G., Perucha, M. A., Robles, J. L. G., Elez, J., & Roquero, E. (2017). El escenario sísmico del terremoto de Arenas del Rey de 1884. *IX Reunião Do Quaternário Ibérico*, 49–52.

Sanz de Galdeano, C. (1983). Los accidentes y fracturas principales de las Cordilleras Béticas. *Estudios Geológicos*, *39*(3–4), 157–165.

Sanz de Galdeano, C., Azañón, J. M., Cabral, J., Ruano, P., Alfaro, P., Canora, C., Ferrater, M., García Tortosa, F. J., García-Mayordomo, J., Gràcia, E., Insua-Arévalo, J. M., Jiménez Bonilla, A., Lacan, P. G., Marín-Lechado, C., Martín-Banda, R., Martín González, F., Martínez-Díaz, J. J., Martín-Rojas, I., Masana, E., … Simón, J. L. (2020). Active faults in Iberia. In *The geology of Iberia: a geodynamic approach. Volume 5: Active Processes: seismicity, active faulting and relief* (pp. 33–75).

Sanz de Galdeano, C., Rodriguez-Fernandez, J., & Lopez-Garrido, A. C. (1985). A strike-slip fault corridor within the Alpujarra Mountains (Betic Cordilleras, Spain). *Geologische Rundschau*, *74*(3), 641–655. https://doi.org/10.1007/BF01821218

Serpelloni, E., Vannucci, G., Pondrelli, S., Argnani, A., Casula, G., Anzidei, M., Baldi,

P., & Gasperini, P. (2007). Kinematics of the Western Africa-Eurasia plate boundary from focal mechanisms and GPS data. *Geophysical Journal International*, *169*(3), 1180–1200. https://doi.org/10.1111/j.1365-246X.2007.03367.x

Silva, P.G., Goy, J. L., Somoza, L., Zazo, C., & Bardají, T. (1993). Landscape response to strike-slip faulting linked to collisional settings: Quaternary tectonics and basin formation in the Eastern Betics, southeastern Spain. *Tectonophysics*, *224*(4), 289–303. https://doi.org/10.1016/0040-1951(93)90034-H

Silva, Pablo G., Elez, J., Giner-Robles, J. L., Rodríguez-Pascua, M. A., Pérez-López, R., Roquero, E., Bardají, T., & Martínez-Graña, A. (2017). ESI-07 ShakeMaps for instrumental and historical events in the Betic Cordillera (SE Spain): An approach based on geological data and applied to seismic hazard. *Quaternary International*, *451*, 185–208. https://doi.org/10.1016/j.quaint.2016.10.020

Silva, Pablo G., Elez, J., Pérez-López, R., Giner-Robles, J. L., Gómez-Diego, P. V., Roquero, E., Rodríguez-Pascua, M. Á., & Bardají, T. (2023). The AD 1755 Lisbon Earthquake-Tsunami: Seismic source modelling from the analysis of ESI-07 environmental data. *Quaternary International*, *651*, 6–24. https://doi.org/10.1016/j.quaint.2021.11.006

Stein, R. S. (1999). The role of stress transfer in earthquake occurrence. *Nature*, *402*, 605–609.

Stein, R. S. (2003). Earthquake conversations. *Scientific American*, *288*(1), 72–79. https://doi.org/10.1038/scientificamerican0103-72

Stirling, Mark, Rhoades, D., & Berryman, K. (2002). Comparison of earthquake scaling relations derived from data of the instrumental and preinstrumental era. *Bulletin of the Seismological Society of America*, *92*(2), 812–830. https://doi.org/10.1785/0120000221

Stirling, MW, Litchfield, N. J., Villamor, P., Van Dissen, R. J., Nicol, A., Pettinga, J., Barnes, P., Langridge, R. M., Little, T., Barrell, D. J., Mountjoy, J., Ries, W. F., Rowland, J., Fenton, C., Hamling, I., Asher, C., Barrier, A., Benson, A., Bischoff, A., … Zinke, R. (2017). The M(w)7.8 2016 Kaikoura earthquake: sufrace fault rupture and seismic hazard context. *Bulletin of the New Zealand Society for Earthquake Engineering*, *50*(2), 73–84.

Teves-Costa, P., & Batlló, J. (2011). The 23 April 1909 Benavente earthquake (Portugal): Macroseismic field revision. *Journal of Seismology*, *15*(1), 59–70. https://doi.org/10.1007/s10950-010-9207-6

Toda, S., Stein, R. S., Sevilgen, V., & Lin, J. (2011). *Coulomb 3.3 Graphic-rich deformation and stress-change software for earthquake, tectonic, and volcano research and teaching-user guide: U.S. Geological Survey Open-File Report 2011-1060* (p. 63). http://pubs.usgs.gov/of/2011/1060/

Trifunac, M. D., & Brady, A. G. (1975). On the correlation of seismic intensity scales with the peaks of recorded strong ground motion. *Bulletin of the Seismological Society of America*, *65*(1), 139–162. https://doi.org/

Tselentis, G. A., & Danciu, L. (2008). Empirical relationships between modified Mercalli

intensity and engineering ground-motion parameters in Greece. *Bulletin of the Seismological Society of America*, *98*(4), 1863–1875. https://doi.org/10.1785/0120070172

Wald, D. J., Quitoriano, V., Heaton, T. H., & Kanamori, H. (1999). Relationships between peak ground acceleration, peak ground velocity, and modified mercalli intensity in California. In *Earthquake Spectra* (Vol. 15, Issue 3, pp. 557–564). https://doi.org/10.1193/1.1586058

Wells, D. L., & Coppersmith, K. J. (1994). New empirical relationships among magnitude, rupture length, rupture width, rupture area, and surface displacement. *Bulletin - Seismological Society of America*, *84*(4), 974–1002.

Worden, C. B., Gerstenberger, M. C., Rhoades, D. A., & Wald, D. J. (2012). Probabilistic relationships between ground-motion parameters and modified mercalli intensity in California. *Bulletin of the Seismological Society of America*, *102*(1), 204–221. https://doi.org/10.1785/0120110156

Yelles-Chaouche, A. K., Abacha, I., Boulahia, O., Aidi, C., Chami, A., Belheouane, A., Rahmani, S. T. E., & Roubeche, K. (2021). The 13 July 2019 Mw 5.0 Jijel Earthquake, northern Algeria: An indicator of active deformation along the eastern Algerian margin. *Journal of African Earth Sciences*, *177*, 104149. https://doi.org/10.1016/j.jafrearsci.2021.104149

Appendix

Site	I_{EMS-98}	Earthquake effects

Motril	VII-VIII	Part of the building stock was damaged and part was left in ruins. Two casualties. Sea withdrawal of 22 varas (~18 m). The population left their houses for the main square in fear. The different seismic phases are described as follows: first, a strong shaking with perpendicular movement; 14-16 seconds later, trepidation for 4-5 seconds; after that, a strong undulating movement for more than 20 seconds. Total shaking lasted for 40-42 seconds. 11 aftershocks are described in the following days.
Almegíjar	VII	Town hall was destroyed.
Dalías	VI+	Four churches and several private buildings were damaged, the population left their houses and camped outside town in fear. Shaking lasted for 50 seconds. Damage was repaired more than a month afterwards.
Berja		
Adra	VI+	Shaking lasted for 110 seconds. The population left their houses for the streets and squares in fear. Some buildings were damaged.
Roquetas	VI+	The ceiling of the lye storehouse was razed.
Almería	VI+	Generalized damage to the whole building stock.

		Shaking lasted for 30 seconds. No casualties.
Málaga	VI	Population left their houses for the streets and squares in fear.
Gibraltar	V	Shaken furniture inside the houses, loss of balance from standing people.

Table AP1. Translation of earthquake effects reports for different sites studied by Murphy Corella, (2019) and the intensity values he initially assigned to each site.

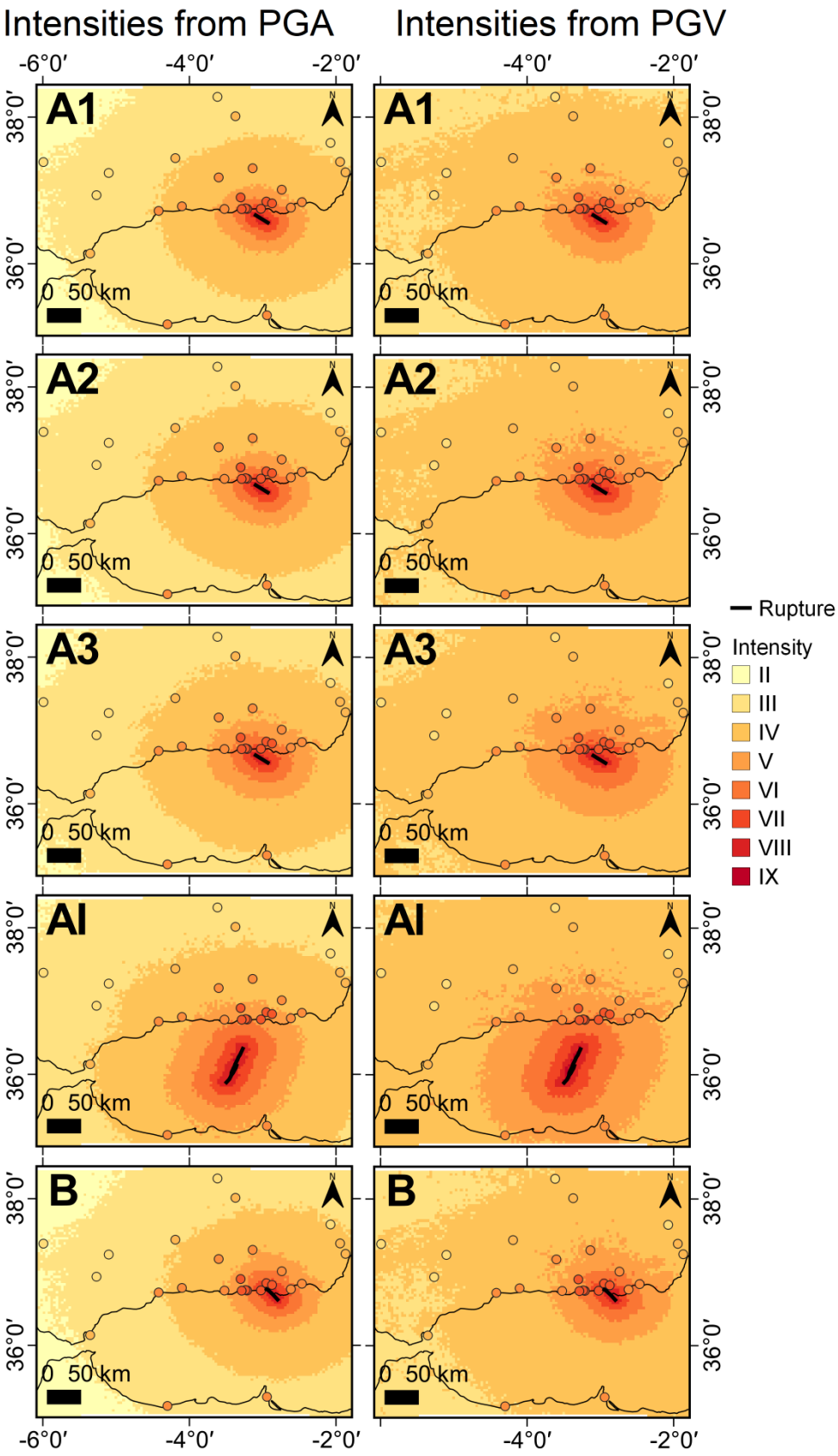

Figure AP1. Seismic scenarios built for candidate ruptures A1 to A3 (Adra Fault), AI (Al-Idrissi

Fault), and B (Balanegra Fault) with the Campbell & Bozorgnia (2014) GMM. The observed intensity field is superimposed in the same color palette.

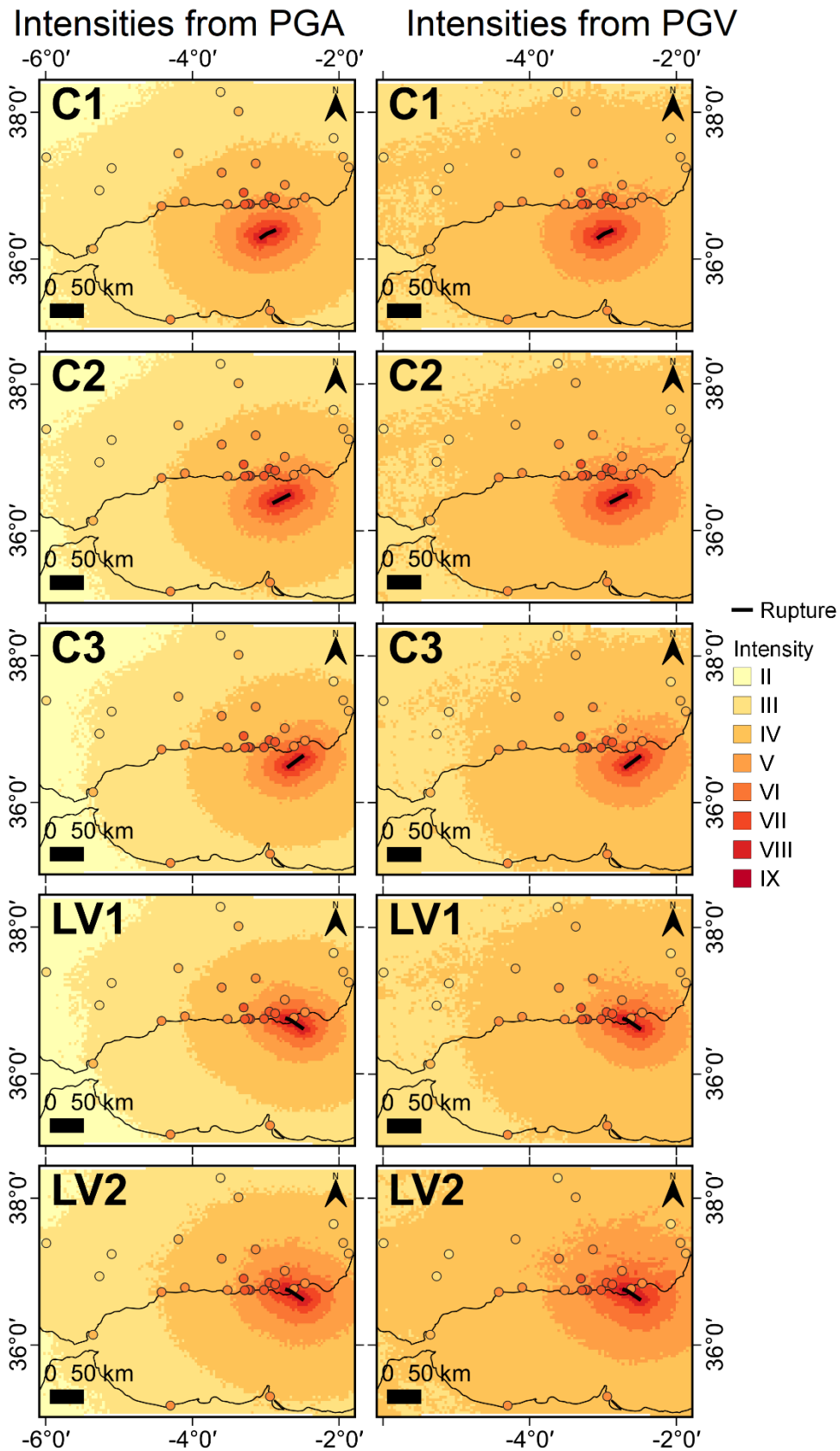

Figure AP2. Seismic scenarios built for candidate ruptures C1 to C3 (Carboneras Fault), and LV1 and

LV2 (Loma del Viento Fault) with the Campbell & Bozorgnia (2014) GMM. The observed intensity field is superimposed in the same color palette.

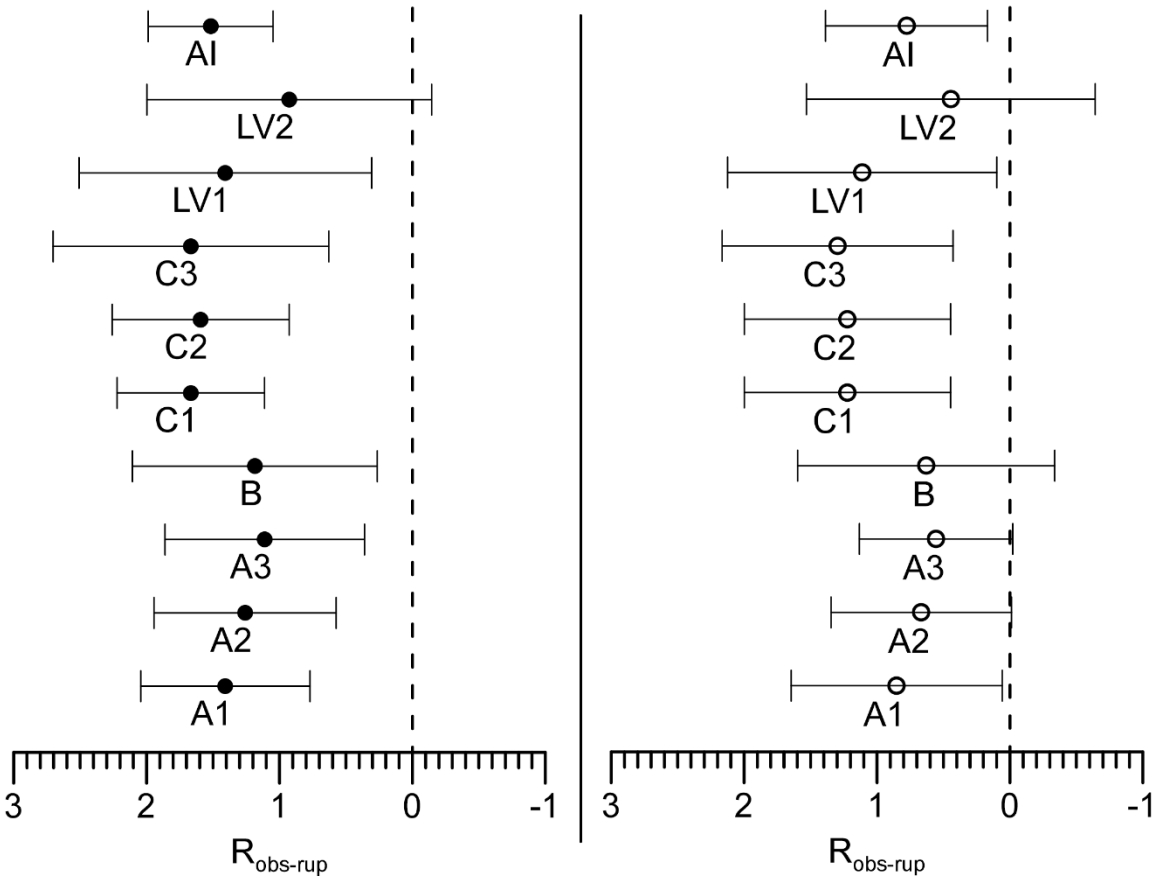

Figure AP3. Residuals $R_{obs-rup}$ for each of the scenarios for the Alborán earthquake built with the Campbell & Bozorgnia (2014) GMM. The average residual is represented with a dot and the bars represent the standard deviation. Black dots correspond to results from scenarios with intensities calculated from PGA, and white dots correspond to results from scenarios with intensities calculated from PGV. Each scenario is labeled below the dot.

The 1804 Alborán seismic series: search for the source using seismic scenarios and static stress interactions

Y. de Pro-Díaz[1,*], J. J. Martínez-Díaz[1-2], and C. Canora-Catalán[3]

[1]Department of Geodynamics, Stratigraphy and Paleontology, Universidad Complutense de Madrid, Madrid, Spain
[2]Instituto de Geociencias (CSIC, UCM)
[3]Department of Geology and Geochemistry, Universidad Autónoma de Madrid, Cantoblanco, Spain
[*]Corresponding author: ypro@ucm.es

Author ORCIDs

Y. de Pro-Díaz: 0000-0001-9807-3627
J. J. Martínez-Díaz: 0000-0003-4846-0279
C. Canora-Catalán: 0000-0003-2480-3679

Author contributions

Conceptualization: Y. de Pro-Díaz
Data Curation: Y. de Pro-Díaz
Formal Analysis: Y. de Pro-Díaz
Funding Acquisition: Y. de Pro-Díaz, J. J. Martínez-Díaz, C. Canora-Catalán
Investigation: Y. de Pro-Díaz, J. J. Martínez-Díaz, C. Canora-Catalán
Methodology: Y. de Pro-Díaz
Project Administration: J. J. Martínez-Díaz
Supervision: J. J. Martínez-Díaz, C. Canora-Catalán
Validation: J. J. Martínez-Díaz, C. Canora-Catalán
Visualization: Y. de Pro-Díaz
Writing – original draft: Y. de Pro-Díaz
Writing – review & editing: Y. de Pro-Díaz, J. J. Martínez-Díaz, C. Canora-Catalán

Abstract

Linking historical earthquakes with the faults that caused them is crucial for seismic hazard assessment. Historical documentation describing the effects of an earthquake is a useful information source, from which we can compile the observed intensity field of the earthquake. In this work we use intensity data from the catastrophic 1804 Alborán earthquake (south of Iberia) along with intensity simulations and coseismic stress transfer analysis to search for this earthquake's seismic source. We build intensity simulations for each "candidate" fault to be the source, and compare these simulations with the intensity field. We also propose a possible triggering between the Alborán 1804 earthquake and the Dalías earthquake (I_{EMS-98} IX) occurred seven months after, and analyze stress transfer between the two faults. Finally, we investigate the possible influence of the coseismic stress transfer caused by the Dalías earthquake in the subsequent local seismicity.

The Alborán earthquake could be linked to the Adra Fault, the Al-Idrissi Fault, the Balanegra Fault or the Loma del Viento Fault. The influence of the Dalías earthquake might still linger nowadays.

Second language abstract: Resumen (Español)

Relacionar los terremotos históricos con sus fallas responsables es crucial para las evaluaciones de peligrosidad sísmica. Una fuente de información sobre estos terremotos es la documentación histórica que describe sus efectos, a partir de la cual se puede recopilar el campo de intensidad observada del terremoto.

En este trabajo utilizamos los datos de intensidad del terremoto de Alborán de 1804 (al sur de Iberia) junto con simulaciones y análisis del cambio de esfuerzos cosísmico para buscar su falla responsable. Construimos simulaciones de intensidad para las distintas fallas "candidatas" a ser la fuente y las comparamos con el campo de intensidad. También proponemos un posible *triggering* entre el terremoto de Alborán y el terremoto de Dalías (I_{EMS-98} IX) ocurrido siete meses después, y analizamos la posible transferencia de esfuerzos entre ambas fallas. Finalmente, investigamos la influencia que el cambio de esfuerzos cosísmico del terremoto de Dalías haya podido tener en la sismicidad local posterior.

El terremoto de Alborán puede relacionarse con la Falla de Adra, la Falla de Al-Idrissi, la Falla de Balanegra o la Falla de Loma del Viento. La influencia del terremoto de Dalías en la tasa de sismicidad podría perdurar a día de hoy.

Non-technical summary

To avoid earthquake damage, we must first know as best as we can the faults that cause earthquakes and how they behave over time. Studying the effects caused by historical earthquakes is one way to achieve this.

We use data from effects of the 1804 Alborán earthquake (south of Spain) to search for the fault that most likely caused this earthquake. We recreate the earthquake effects trying out different possible faults as sources and compare the hypothetical effects caused by each one with the historically documented effects. The recreation which best fits the historical effects will also be the one built on a source which is the most similar to the actual earthquake source. We also propose the Alborán earthquake could have triggered another one which occurred nearby seven months later, the Dalías earthquake, and explore this possibility. Finally, we explore whether or not the Dalías earthquake could have boosted seismicity afterwards in the nearby region.

The faults that could have caused the Alborán earthquake are: Adra, Al-Idrissi, Balanegra and Loma del Viento. The influence of the Dalías earthquake might still linger nowadays.

1. Introduction

Linking historical earthquakes to their fault sources has become crucial in modern seismic hazard assessment (SHA) studies, particularly in regions with slow-to-moderate moving faults such as the Iberian Peninsula. In these regions, including accurate historical earthquake data in SHA studies can make a difference when considering whether or not a particular fault might rupture in the future. The importance of addressing faults as seismogenic sources in SHA studies and extend back their known seismic history beyond the instrumental record has been rising in the recent years (e. g. Ambraseys & Jackson, 1998; Basili et al., 2008; Caputo et al., 2015; Gómez-Novell et

al., 2020). Paleoseismology, which studies geological evidence of past earthquakes, is one way to achieve this; however, there are seismically active areas where paleoseismological analysis cannot be performed. This happens either because the structures ~~which~~ expose an earthquake occurrence never formed in the first place due to the site's geological conditions, or these structures did form but high erosion rates immediately dismantled them, or the human activity has destroyed these structures, or they are located in a not easily accessed area (McCalpin & Nelson, 1996). An alternative approach to paleoseismology in these cases can be the analysis of the effects caused by the earthquake on the human communities and their building stock. Documents such as personal diaries, letters to the authorities and reconstruction bills provide ~~present~~ researchers with a lot of information about earthquakes occurred in historical times (Teves-Costa & Batlló, 2011; Muñoz Clares et al., 2012; Murphy Corella, 2019). Sometimes, historical documents also preserve descriptions of geological evidence even after ~~the geological structure itself has been lost~~ due to erosion or anthropic activities (Huerta et al., 2015; Murphy Corella, 2019). Damage and effects reported on these documents can be addressed using modern intensity scales such as the EMS-98 (Grünthal, 1998) or the ESI-07 (Michetti et al., 2007) to assign each site a numeric value and compile the observed intensity field of historical earthquakes.

It has been noted in many studies how seismic intensity correlates quite well with strong ground motion parameters such as peak ground acceleration (PGA) and peak ground velocity (PGV) (Trifunac & Brady, 1975; Wald et al., 1999; Atkinson & Wald, 2007; Delavaud et al., 2009). Because of this correlation, several authors have developed ground-motion-to intensity-conversion equations (GMICE) which allow us to ~~"translate"~~

ground motion into intensity values and vice versa (e. g. Kaka & Atkinson, 2004; Atkinson & Kaka, 2007; Tselentis & Danciu, 2008; Worden et al., 2012; Caprio et al., 2015). Additionally, ~~plethora of~~ authors have also developed ground motion models (GMM), which calculate the ground motion on a certain point considering a certain seismic source (e. g. Campbell, 2003; Ambraseys et al., 2005; Akkar & Bommer, 2010; Abrahamson et al., 2014; Akkar et al., 2014; Campbell & Bozorgnia, 2014; Pezeshk et al., 2018). A lot of research has also been done on the effect that an earthquake causes in the local stress state and how it can influence the occurrence of future ~~shocks~~. One of the most successful approaches is the analysis of Coulomb failure static stress change (ΔCFS) (e. g. Okada, 1992; King et al., 1994; Harris, 1998; Stein, 1999, 2003).

Through the combined use of GMM, GMICE, and/or ΔCFS, we can build a simulation of the effects caused by any given earthquake on the building stock, on geological terrain and on the local stress field as long as we know the source parameters, so that we know what to expect of a well-known fault in the future. But we can also use this approach to look into the past and search for the source of historical earthquakes when the responsible fault is unclear and no other evidence is found. The premise is as follows: if we build a simulation ~~which~~ matches the observed effects, the seismic source on which we built that simulation will also match the actual source of the earthquake. Using this approach, the source of many historical earthquakes has been searched for before this work, for instance: the seismic crisis of 1456 on Italy (Fracassi & Valensise, 2007), the Catalan seismic series of 1427-1428 (Perea, 2009), the 2001 El Salvador earthquake (Canora et al., 2010), the California earthquake of 1812 (Lozos, 2016), the 1829, 1863 and 1755 earthquakes of Torrevieja, Huércal-Overa and Lisbon, respectively (Silva et al., 2017),

the Arenas del Rey earthquake of 1884 (Rodríguez-Pascua et al., 2017), several historical earthquakes east of the Sunda Arc (Griffin et al., 2019), the 1933 Long Beach earthquake (Hough & Graves, 2020), the 2019 Jijel and 2014 Ziama earthquakes (Yelles-Chaouche et al., 2021) or the 1531 Lisbon earthquake (Canora et al., 2021).

In this work, we search for the most likely source of the Almería earthquake of 13th January 1804, also known as the Alborán earthquake ~~of 1804~~, which caused significant damage at both the Spanish and Moroccan coasts as well as at several inland locations. The greatest damage occurred in the building stock from the provinces of Granada and especially Almería (Murphy Corella, 2019). This earthquake has been assigned M_w 6,3-6,7 by different authors, mostly based on the damage (Martínez Solares & Mezcua Rodríguez, 2002; Posadas et al., 2006; Mezcua et al., 2013). To investigate its source, we use a methodology based on simulations of earthquake effects caused by different possible seismic sources and comparing these simulations with the observed effects in search of the scenario that better fits reality. We use a methodology proposed by de Pro-Díaz et al. (2022, 2023) and incorporate a new extra step using ΔCFS analysis to better constrain the results.

2. Neotectonic and seismic context

2.1. The Betics and Alborán Sea area

The Betic Cordillera, also known as the Betics, is an ENE-WSW orogen located south of the Iberian Peninsula. During the neotectonic period (Late Miocene to Present), tectonic activity in the Eastern Betics is dominated by the convergence between Iberia and Nubia plates (DeMets et al., 2010; Serpelloni et al., 2007; Nocquet & Calais, 2004). The study area is located in the Eastern Betics where a compressional stress field with NNW-SSE

shortening has been dominant during the Quaternary (Echeverria et al., 2015). This strain regime is consistent with the kinematics of the largest active faults in this area (Martínez-Díaz et al., 2012).

Along the Eastern Betics, active faults show three main orientations: NE-SW, E-W and NW-SE (Sanz de Galdeano, 1983; Sanz de Galdeano et al., 2020). One of the most important fault systems is the Eastern Betics Shear Zone (EBSZ) (Silva et al., 1993), the continental part of the Trans-Alborán Shear Zone (TASZ) (De Larouzière et al., 1988), a sigmoidal, NE-SW, transpressive fault zone formed mainly by left-lateral strike-slip faults, and reverse faults on the northern sector (Silva et al., 1993). The EBSZ has been largely studied, ~~including plethora of paleoseismological work~~ (e. g. Ortuño et al., 2012; Insua-Arévalo et al., 2015; Martín-Banda et al., 2016; Ferrater et al., 2016, 2017; Herrero Barbero, 2021). The Carboneras Fault (CF) is one of the major faults of the TASZ, and part of its trace runs south of the epicentral area of the earthquakes addressed in this work (Figure 1) (Gràcia et al., 2006; Moreno Mota, 2011; Moreno et al., 2015, 2016; Álvarez-Gómez et al., 2023). Another major fault near the epicentral area is the Al-Idrissi Fault (AIF), a young, NE-SW oriented, subvertical, left-lateral strike-slip fault which has been related to three $M_w \geq 6$ earthquakes occurred near the African coast in 1994, 2004 and 2016 (Figure 1), as well as the seismic series of 2021-2022 near Al Hoceima (Ammar et al., 2007; Martínez-García et al., 2011, 2013; d'Acremont et al., 2014; Álvarez-Gómez et al., 2016; Gràcia et al., 2019; Lafosse et al., 2020; Perea et al., 2022). Both the CF and AIF are considered not only active and seismogenic, but also potentially tsunamigenic (Gómez de la Peña et al., 2022). The Alpujarras Fault Zone (AFZ) is also an important structure in this area: an E-W, strike-slip, right-lateral corridor composed of several

faults, some of which have been active in the Quaternary (Martínez-Martínez, 2006; Echeverria et al., 2015; Sanz de Galdeano et al., 1985, 2020). The AFZ and the CF are the northern and south-eastern limits of a complex crustal block which is divided in smaller, rotating blocks delimited by oblique (normal-strike-slip) faults trending NW-SE (Martínez-Díaz & Hernández-Enrile, 2004). The smaller NW-SE faults control several Neogene basins, such as the Campo de Dalías. Among these NW-SE faults are the Loma del Viento Fault (LVF) (Martínez-Díaz, 1999; Marín-Lechado et al., 2005; García-Mayordomo et al., 2012; Pedrera et al., 2012; Murphy Corella, 2019), the Llano del Águila Fault (LLAF) (Molins-Vigatà et al., 2022), the Adra Fault (AF), the Balanegra Fault (BF) (Martínez-Díaz & Hernández-Enrile, 2004; Gràcia et al., 2006, 2012; Marín-Lechado et al., 2010; Sanz de Galdeano et al., 2020) and the Punta Entinas Fault (PEF) (Gràcia et al., 2006, 2012; García-Mayordomo et al., 2012), which all share normal-dextral kinematics.

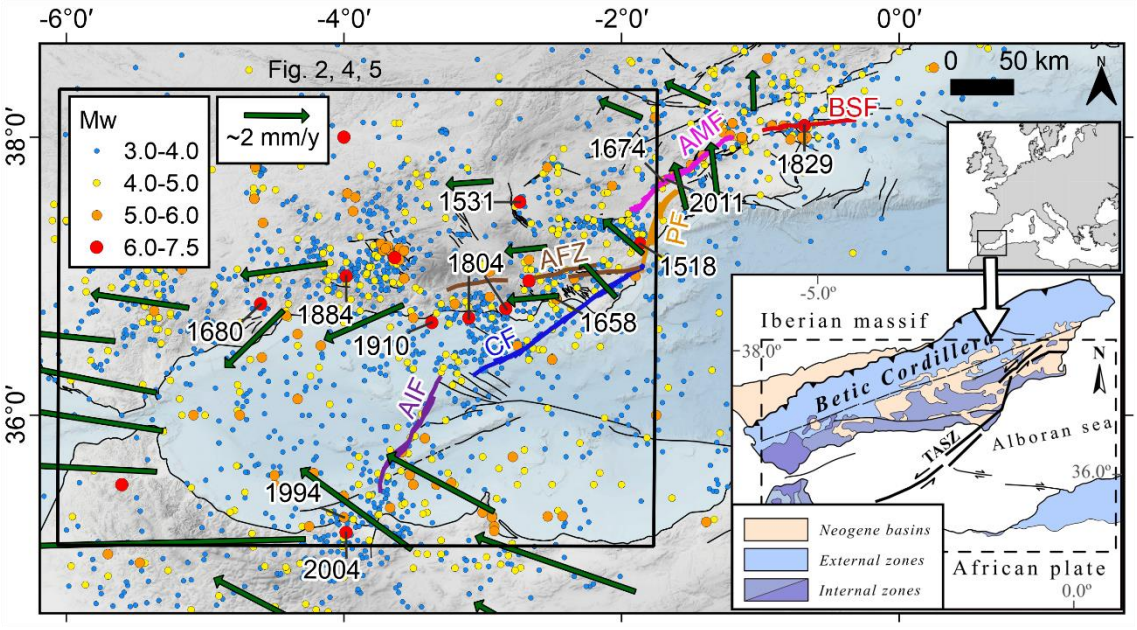

Figure 1. Seismotectonic context for the study region. Inset modified from Herrero-Barbero et al. (2021). Seismic catalog from IGN-UCM (2013), represented as dots with the dates of the main earthquakes. Geodetic velocity trends from GNSS networks are represented as green arrows, from

Palano et al. (2015). Fault traces from the QAFI database (García-Mayordomo et al., 2012) are represented as black lines, with the main faults of the EBSZ and TASZ highlighted in color. CF: Carboneras Fault. AFZ: Alpujarras Fault Zone. PF: Palomares Fault. AMF: Alhama de Murcia Fault. BSF: Bajo Segura Fault. AIF: Al-Idrissi Fault.

2.2. The 1804 Almería seismic series

In 1804, two seismic series occurred in the Campo de Dalías area, one in January and the other in August. The mainshock of the August series occurred on the 25th near the city of Dalías and its most likely source appears to be a conjunct rupture of the LVF and LLAF (de Pro-Díaz et al., 2023). The mainshock of the January series, which is the focus of this work, occurred on the 13th and was felt at several locations along both the south Iberian Peninsula's and north African coasts (Espinar Moreno, 1994; Murphy Corella, 2019).

The 1804 Almería seismic series was extensively researched by Murphy Corella (2019). This author recovered historical documents describing the effects of the earthquakes and their aftermath in the affected areas and analyzed these records in order to assign EMS-98 intensity values to each site. He also includes data from geological effects to assign ESI-07 intensity values. Although he focuses mainly on the 25th August shock, which was the most damaging of the series, he also addresses the 13th January shock in his analysis, as well as the strongest aftershocks in both the January and August series. In the following paragraph, we translate and resume some of Murphy Corella (2019)'s research regarding the 13th January shock.

In Berja and Dalías, historical records analyzed by Murphy Corella (2019) describe damage in several buildings after the January mainshock, including the four churches of these two towns. This earthquake and its subsequent aftershocks forced the people of these two localities to camp outside town for a whole month until the tremors stopped, and damage could be fixed during spring season. Records from the coastal town of Adra

describe how the earthquake was felt by the population, as well as a "disturbance in the sea, which was shaken with noisy movement, which completely ceased" after each shock of the series. The earthquake was also felt in Málaga, where "startled people occupied the streets and squares", as well as in several cities far from the epicentral area, like Sevilla, Melilla or even Madrid, more than 400 km north of the epicentral area. Certain buildings were also severely damaged in Roquetas. Records from the city of Almería's municipal archive report extensive damage to the whole building stock, although there were no casualties. In Motril, another coastal town, the sea was described to withdraw 22 varas (~18 m), and the earthquake caused "ruins and two deaths", being this the only site with confirmed casualties for the 13th January earthquake. Records addressing the effects in Motril also identify the different seismic phases, which is why this earthquake was known as the Motril earthquake for some time. As it happened in Berja and Dalías, Motril's citizens also camped outside town until the aftershocks stopped by the end of February (Murphy Corella, 2019).

These are the most known sites where the earthquake was felt, but its effects are reported in more localities ~~which were all addressed by Murphy Corella (2019) in his work.~~ A more detailed translation of the reported effects in these sites and some others can be found in Table AP1 of the *Appendix* of this article. From these records, he compiled an intensity field of 30 data points which is shown in Figure 2. This is the intensity field we will be using for our analysis of this earthquake.

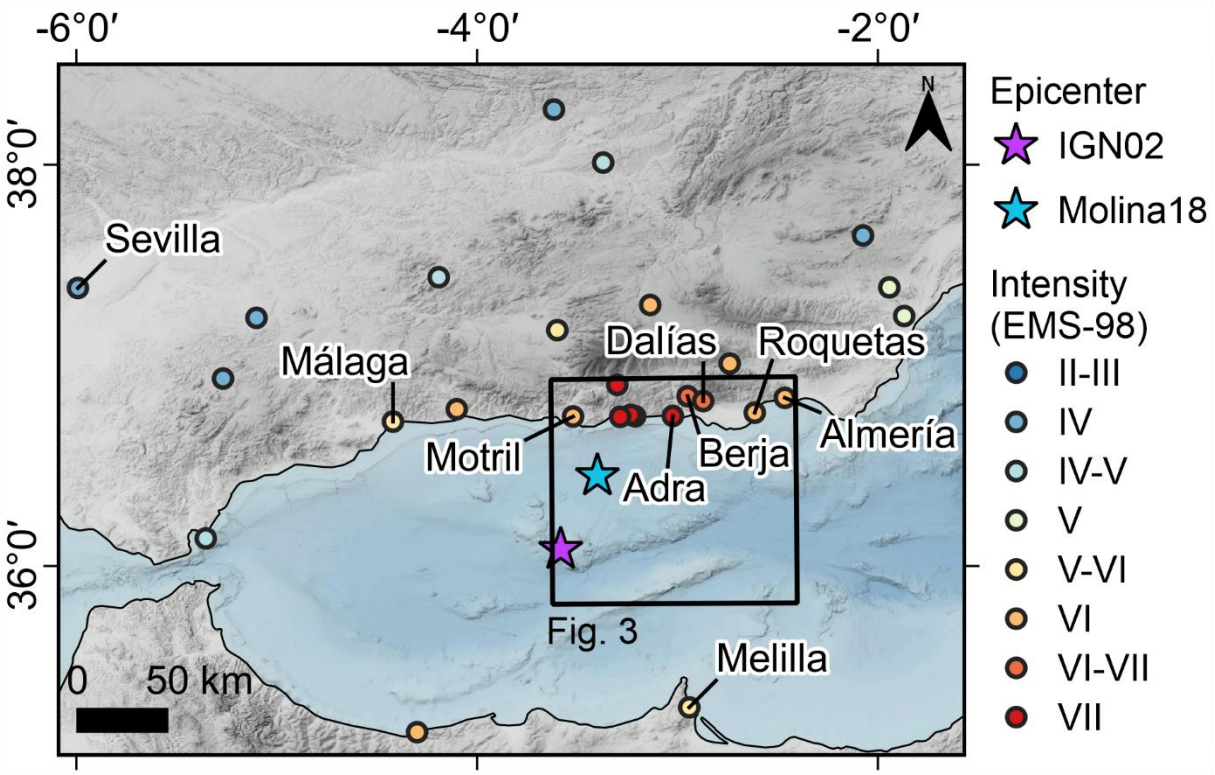

Figure 2. Intensity field of the Alborán earthquake of 13th January, 1804, compiled by Murphy Corella (2019). IGN02: epicenter estimated by Martínez Solares & Mezcua Rodríguez (2002). Molina18: epicenter estimated by Molina et al. (2018).

Two different locations have been proposed for the epicenter using intensity data: 36.083 ºN, 3.583 ºW by Martínez Solares & Mezcua Rodríguez (2002), estimated from the center of the highest intensity area with a previous and less rich dataset; and 36.45 ºN, 3.40 º W by Molina et al. (2018), who used Murphy Corella (2019)'s data and also considered the reported S-P arrival time difference from Motril (Figure 2). As stated before, different authors have proposed magnitudes of M_w 6,3-6,7 for this earthquake using also intensity data for their estimations (Martínez Solares & Mezcua Rodríguez, 2002; Posadas et al., 2006; Mezcua et al., 2013). As for the seismic source, Espinar Moreno (1994), Martínez Solares & Mezcua Rodríguez (2002), Molina et al. (2018) and Murphy Corella (2019) all agree on an offshore source based on the damage distribution at both the Spanish and Moroccan coasts, as well as the tsunami reports. Murphy Corella

(2019) proposed the offshore extension of the LVF as a possible source for this earthquake, although this is not the closest fault to the epicenters estimated by Martínez Solares & Mezcua Rodríguez (2002) and Molina et al. (2018) (Figures 2 and 3). No evidence of surface rupture has been found so far for this earthquake.

3. Methodology

In this work we have used the seismic scenario method proposed by de Pro-Díaz et al. (2022, 2023) for constraining the earthquake source through the use of seismic scenarios and the observed intensity field. We have also added an extra step using Coulomb stress transfer analysis to be used as an additional criterion to rank the preferred scenarios. Methodology is composed of four steps:

1. Boxer calculation. We use Gasperini et al. (1999, 2010)'s method and their Boxer software to calculate the most likely area of the surface where the seismic source might be located. This area is called "boxer". The boxer is then compared with the known seismogenic faults in the area. The faults which partially or totally overlap the boxer become possible candidates to be the source of the earthquake (from now on, "candidate ruptures"). If the boxer does not fit any known seismogenic fault and shows no overlap with any of the epicenters proposed by other authors, candidate ruptures are selected using sources proposed by other authors and the local known faults which are close to the epicenter.

2. Seismic scenarios. We build seismic scenarios for each one of the candidate ruptures using the OpenQuake software (Pagani et al., 2014). OpenQuake takes M_w, geometry and position of the rupture, as well as position of the hypocenter as input data, and

using a ~~ground-motion model (~~GMM~~)~~ produces a regular grid of points over the study area each containing values of ground motion – in this work, peak ground acceleration (PGA) and peak ground velocity (PGV). Then, using ~~ground-motion-to-intensity conversion equations (~~GMICE~~)~~ we translate the ground motion into ~~simulated~~ intensity values. In this work we initially used Campbell & Bozorgnia (2014)'s GMM and Worden et al. (2012)'s GMICE, following de Pro-Díaz et al. (2023), although we had to switch to Akkar & Bommer (2010)'s GMM ~~(this change will be addressed later on in the *Results* and *Discussion*)~~. Each scenario is then compared to the observed intensity field using this equation:

$$R_{obs\text{-}rup} = I_{obs} - I_{rup}$$

where I_{obs} is the observed intensity value and I_{rup} is the simulated intensity value sampled from the same location as I_{obs}. The scenario which shows $R_{obs\text{-}rup}$ closest to 0 is the one which better fits the observed effects of the earthquake. This means the candidate rupture upon which the best-performing scenario was built is the closest to the actual seismic source of the earthquake. If two or more scenarios show $R_{obs\text{-}rup}$ equally closer to 0, we proceed on to step 3 with those (~~from now on, "~~competing scenarios~~"~~).

3. Differential zones. We compare the competing scenarios to find the areas in which they differ from each other, or "differential zones". If there are enough I_{obs} data points inside the differential zones, we perform a statistical test to evaluate the likeness of the data distributions sampled inside these areas from I_{obs} and each seismic scenario. The aim is to find the scenario which is statistically similar to I_{obs}. If there are not enough

data points inside the differential areas, we proceed on to step 4 with the candidate ruptures for the competing scenarios.

4. Coulomb stress transfer. We model the static stress change (ΔCFS) associated with the ruptures selected as candidates using the Okada (1992) equations for dislocations in an elastic half-space following the methodology described by King et al. (1994) and Harris (1998) and the Coulomb 3.4 software (Toda et al., 2011). We also model the source for the 25th August earthquake proposed by de Pro-Díaz et al. (2023), which we call rupture D, and taper it into 539 tiles measuring 1 km^2 each. We then calculate the ΔCFS produced in rupture D by each of the modeled candidate ruptures. Based on their closeness in space and time, if we assume that the 13th January shock might have triggered the 25th August shock, the rupture which produces the largest area of positive ΔCFS in rupture D will be considered as the closest to the actual source of the 13th January shock.

Additionally, we model the local ΔCFS produced by rupture D after the 25th August shock on ideally oriented fault planes and compare it with the seismicity occurred in the study area after 1804. The aim is to tentatively search for a possible influence of the local ΔCFS caused by the 25th August shock on the spatial distribution of the seismicity afterwards in the area.

For the ΔCFS calculations, we use a 0.4 apparent friction coefficient (Harris, 1998) and a regional stress field with σ_1 00º//158º and σ_3 00º//068º.

4. Results

4.1. Boxer calculation

The boxer calculated with Gasperini's method is presented as a red rectangle in Figure 3. The boxer has an area of 81 km^2 and strikes N93ºE. The computed epicenter is located at 36.7499ºN, 3.2436ºW, which is 38 km away from the epicenter proposed by Molina et al. (2018) and 83 km away from the one proposed by Martínez Solares & Mezcua Rodríguez (2002). Magnitude estimated by Boxer is M_w 5.88±0.10, which is lower than both M_w 6.3 assigned by Molina et al. (2018) and M_w 6.7 calculated by Martínez Solares & Mezcua Rodríguez (2002).

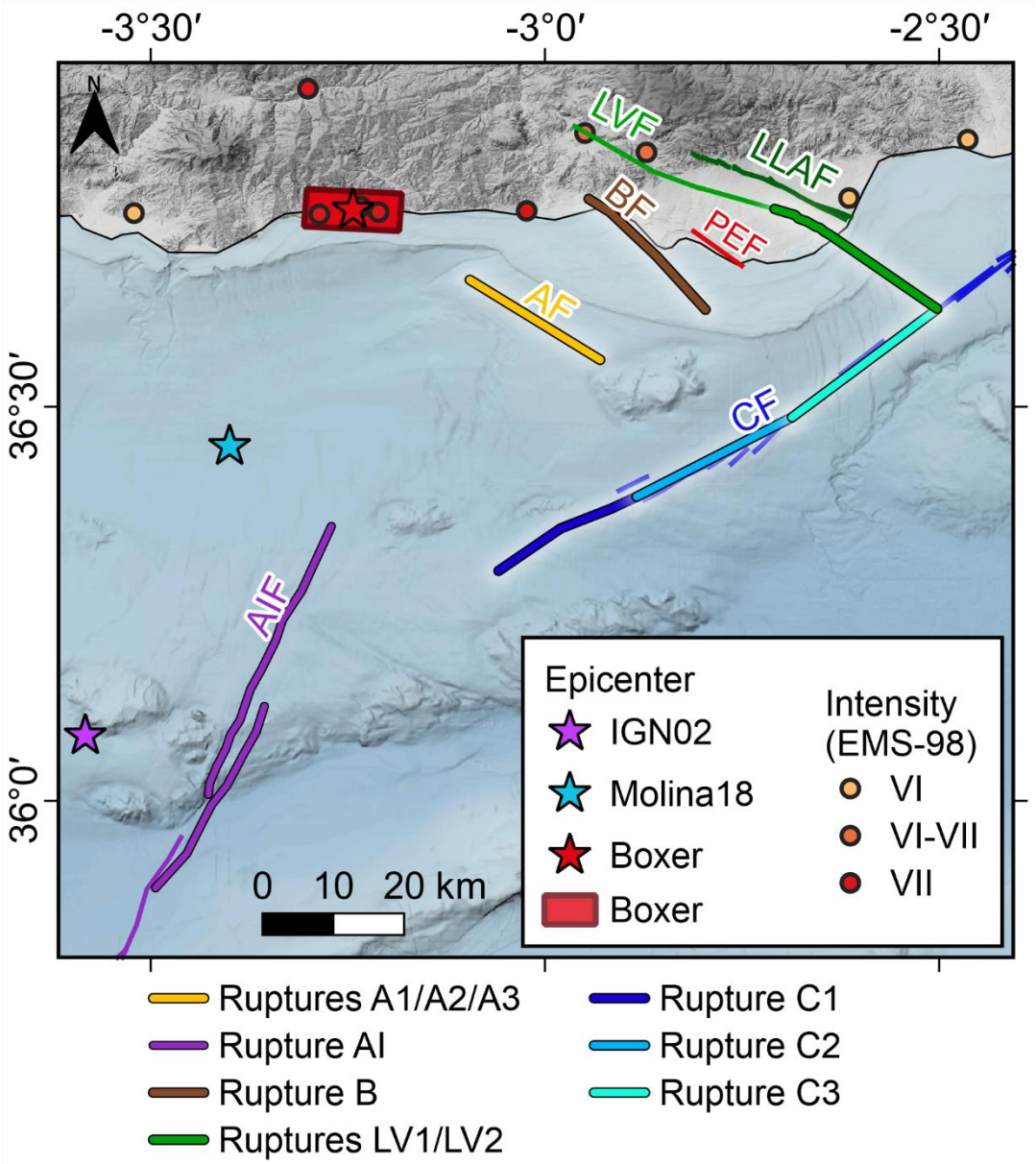

Figure 3. Boxer calculation result and known active faults in the area. Selected candidate ruptures for the Alborán earthquake are highlighted in thicker lines than the known active fault traces, and named with the fault's initial letter: A for Adra Fault, B for Balanegra Fault, C for Carboneras Fault and LV for Loma del Viento Fault. Parameters for the candidate ruptures are shown in Table 1. Molina18: Molina et al. (2018). IGN02: Martínez Solares & Mezcua Rodríguez (2002). LLAF: Llano del Águila Fault. LVF: Loma del Viento Fault. BF: Balanegra Fault. AF: Adra Fault. CF: Carboneras Fault. AIF: Al-Idrissi Fault. PEF: Punta Entinas Fault.

Despite intensive geomorphological and seismologic study in the past, no active fault has been described yet in the area around the boxer, not even smaller ones than the size required for an earthquake such as the one studied here (Figure 3). Additionally, Espinar Moreno (1994), Martínez Solares & Mezcua Rodríguez (2002), Molina et al. (2018) and

Murphy Corella (2019) all agree on an offshore source for this earthquake considering the damage distribution, yet the boxer is located mostly inland. Because of this discrepancy with the bibliography, we decided not to consider the boxer calculation result to select the candidate ruptures for the Alborán earthquake. This discrepancy will be further addressed later in the *Discussion*.

Following the hypothesis of the offshore source, candidate faults have been selected among faults with Quaternary activity evidence included in the QAFI database compiled by García-Mayordomo et al. (2012) which are also located less than 40 km away from either the highest intensity points or the epicenter proposed by Molina et al. (2018), since these authors consider the S-P arrival time in their calculations. The selected faults are the Balanegra Fault (BF), the Adra Fault (AF), the northern sector of the Al-Idrissi Fault (AIF), the sea extension of the Loma del Viento Fault (LVF), and three different sectors of the Carboneras Fault (CF). For the AF, BF and LVF we use the maximum mapped length for which geomorphological evidence has been found. For the CF, we select sectors with lengths according to the earthquake's magnitude using the empirical relations of Stirling et al. (2002) and Wells & Coppersmith (1994). For the AIF scenario, we selected a slightly bigger area comprising the north and central segments, with a higher magnitude (M_w 7.0) to compensate for the rupture being further from the coast and the subsequent intensity attenuation at the intensity field sites. Initially, for the other ruptures we tried magnitudes proposed by the already cited authors, but some ruptures had areas which could generate higher M_w according to Stirling et al. (2002)'s and Wells & Coppersmith (1994)'s empirical relationships. For these ruptures, we also try these higher magnitudes. All of this results in a total of ten different candidate ruptures which

are presented in Figure 3. Each candidate's fault parameters are presented in Table 1. Ruptures have been named using the initial letters of the rupturing fault, so rupture AI for instance corresponds to the Al-Idrissi Fault. In the case of the Adra Fault, ruptures A1, A2 and A3 correspond to the same area with different possible magnitudes. The same applies for the Loma del Viento Fault and ruptures LV1 and LV2. As for the Carboneras Fault, ruptures C1, C2 and C3 correspond to three consecutive sectors of the fault with similar areas and thus similar magnitudes.

Rupture	Strike (º)	Dip (º)	Rake (º)	Area (km^2)	Length (km)	Coordinates	SD (km)	Epicenter	M_w
A1	122	80	-135	285	19	36.6613ºN 3.0956ºW	0-15	36.6613ºN 3.0956ºW	6.5
A2	122	80	-135	285	19	36.6613ºN 3.0956ºW	0-15	36.6613ºN 3.0956ºW	6.7
A3	122	80	-135	285	19	36.6613ºN 3.0956ºW	0-15	36.6613ºN 3.0956ºW	6.9
AI	205	80	5	1100	55	36.348ºN 3.271ºW	0-20	36.348ºN 3.271ºW	7.0
B	134	70	-135	240	20	36.6233ºN 2.7967ºW	0-12	36.6233ºN 2.7967ºW	6.6

C1	62	90	0	228	19	36.292ºN 3.059ºW	0-12	36.346º N 2.98ºW	6.5
C2	63	90	0	240	21	36.387ºN 2.885ºW	0-12	36.387ºN 2.885ºW	6.5
C3	53	90	0	264	22	36.4868º N 2.6869ºW	0-12	36.4868ºN 2.6869ºW	6.4
LV1	121	80	35	297	27	36.7511ºN 2.7089ºW	0-12	36.7511ºN 2.7089ºW	6.4
LV2	121	80	35	297	27	36.7511ºN 2.7089ºW	0-12	36.751ºN 2.7089ºW	6.9

Table 1. Fault parameters for the eight proposed candidate ruptures considered as possible sources for the Alborán earthquake. The fault traces are presented in Figure 3, and named as follows: A1, A2, A3: Adra Fault ruptures; B: Balanegra Fault rupture; C1, C2, C3: Carboneras Fault ruptures; LV1, LV2: Loma del Viento Fault ruptures. SD: seismogenic depth (upper-lower) from the QAFI (García-Mayordomo et al., 2012). HD: hypocentral depth.

4.2. Seismic scenarios

Seismic scenarios built for each of the candidate ruptures presented in Table 1 are shown in Figures 4 and 5. Overall, no scenario shows a perfect correlation with I_{obs} spatial distribution. Nevertheless, the intensity distribution patterns of scenarios A2, A3, AI, LV2 and B seem closer to I_{obs} distribution than the other scenarios.

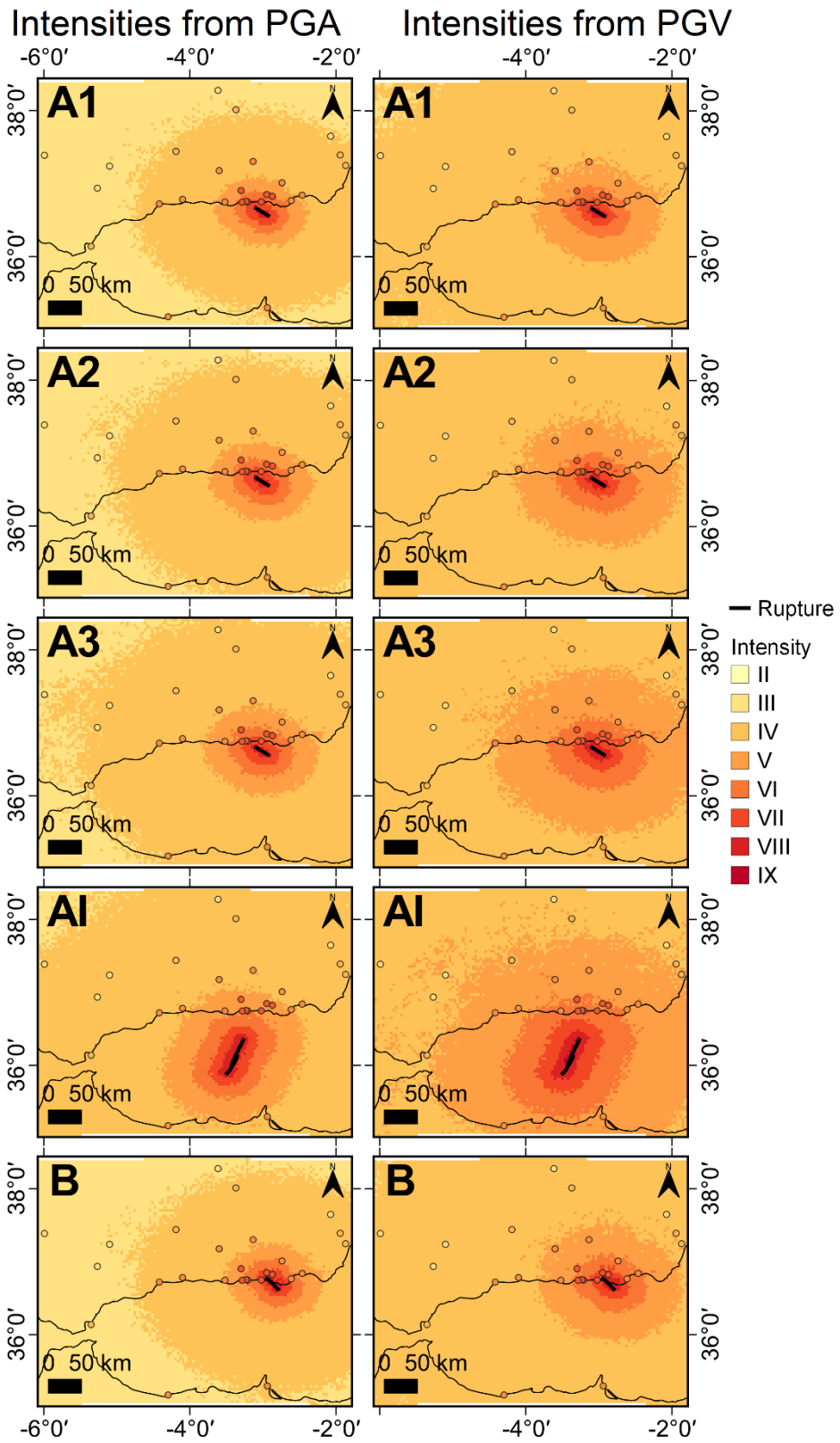

370 **Figure 4.** Seismic scenarios built for candidate ruptures A1 to A3 (Adra Fault), AI (Al-Idrissi Fault), and B (Balanegra Fault). The observed intensity field is superimposed in the same color palette.

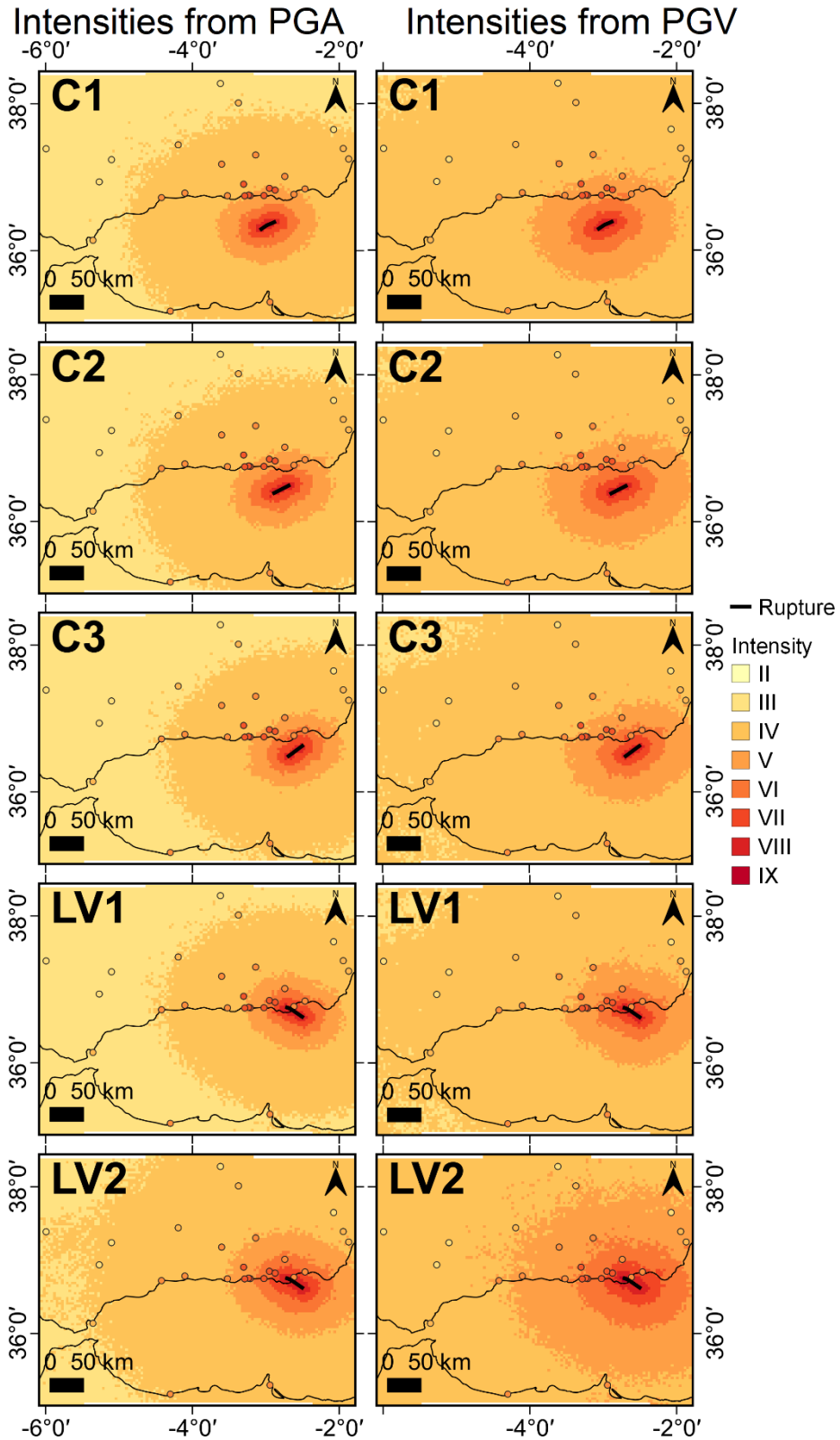

Figure 5. Seismic scenarios built for candidate ruptures C1 to C3 (Carboneras Fault) and LV1 to LV2 (Loma del Viento Fault). The observed intensity field is superimposed in the same color palette.

Figure 6 shows $R_{obs-rup}$ for the scenarios of the ten candidate ruptures. All scenarios seem to underestimate intensities, although some more than others. Scenarios A3, AI, LV2 and B predict intensities which are less than one degree lower than the observed values on average, so ruptures A3, AI, LV2 and B are considered as the best candidates in this step of the analysis. The rest of the scenarios underpredict intensities for more than one degree on average respect to the observed values, which marks their ruptures as worse candidates. We thus proceed to the next step of the analysis with A3, LV2 and B as competing scenarios.

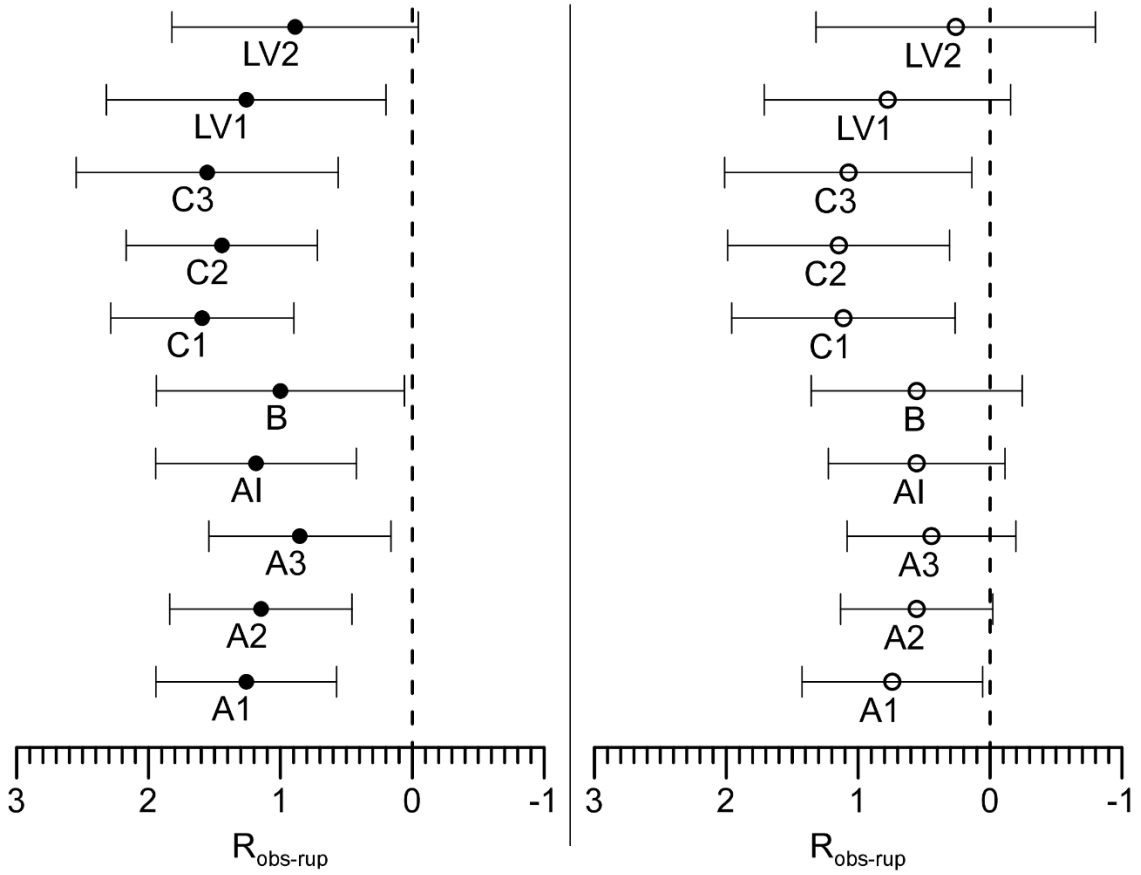

Figure 6. Residuals $R_{obs-rup}$ for each of the scenarios for the Alborán earthquake. The average residual is represented with a dot and the bars represent the standard deviation. Black dots correspond to results from scenarios with intensities calculated from PGA, and white dots correspond to results from scenarios with intensities calculated from PGV. Each scenario is labeled below the dot.

We initially built the scenarios using Campbell & Bozorgnia (2014)'s GMM, but all of the scenarios built with this GMM underpredicted the observed intensities by almost one degree or more. These scenarios are presented in Figures AP1 and AP2 of the *Appendix* of this work, and their $R_{obs\text{-}rup}$ are shown in Figure AP3, but they have not been used in the rest of the analysis. The scenarios presented in the current section are built with Akkar & Bommer (2010)'s GMM. ~~This change of GMM will be further addressed in the *Discussion*~~.

4.3. Differential zones

We compare the competing scenarios selected in the previous step by analyzing their intensity values distribution inside the differential zones: the areas in which two competing scenarios show different intensity values. Because scenario LV2 seemed to perform slightly better than scenarios AI, B and A3 in the residuals step, we compare scenarios AI, B and A3 with scenario LV2.

Differential zones for scenarios B and LV2 are presented in Figure 7. There are two differential zones: a bigger, sort of ring-like outer zone where scenario LV2 shows higher intensities than B; and a smaller, inner zone where scenario B shows higher intensities than LV2. Histograms in Figure 7 represent the value distribution of the observed intensity (I_{obs}), scenario B (I_{rupB}) and scenario LV2 (I_{rupLV2}) inside the differential zones. I_{rupB}'s distributions seem to be slightly more similar to I_{obs} than I_{rupLV2} in the outer zone. However, there are only seven I_{obs} points inside the outer zone, and this amount is not enough to perform a robust statistical test. As for the inner zone, there is only one I_{obs} point inside it, so it is not suitable either for a statistic analysis. Because of this lack of

points inside the differential zones, this step of the analysis cannot be applied to this pair of competing scenarios.

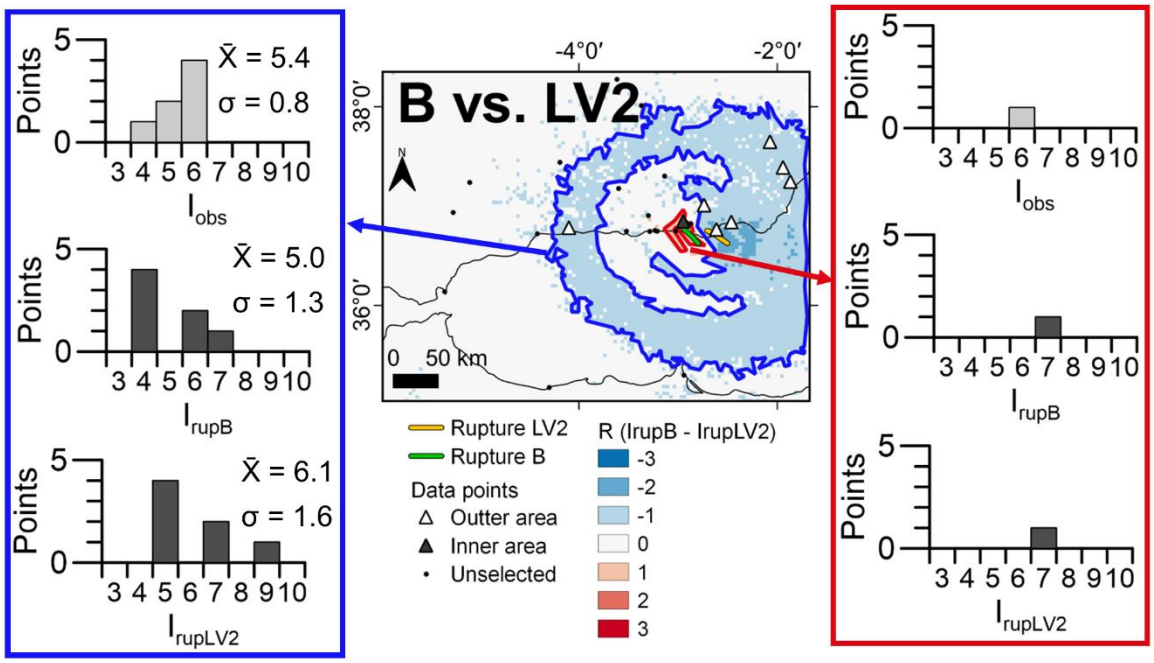

Figure 7. Differential zones for scenarios B and LV2. Histograms represent the distribution of the intensity values inside each differential zone for the observed intensity field (I_{obs}), scenario B (I_{rupB}) and scenario LV2 (I_{rupLV2}).

Differential zones for scenarios A3 and LV2 are presented in Figure 8. There are three differential zones, two to the northeast where scenario LV2 shows higher intensities than A3 (these two will be considered as the same zone for practical purposes), and the other to the southwest where it is the other way around. Histograms in Figure 8 represent the value distribution of the observed intensity (I_{obs}), scenario A3 (I_{rupA3}) and scenario LV2 (I_{rupLV2}) inside the differential zones. I_{rupA3}'s distributions seem to be slightly more similar to I_{obs} than I_{rupLV2}. However, there are only six I_{obs} points within the SW zone and seven within the NE zone, which again is not enough to perform a robust statistical test. Because of this, this step of the analysis cannot be applied to this pair of competing scenarios either.

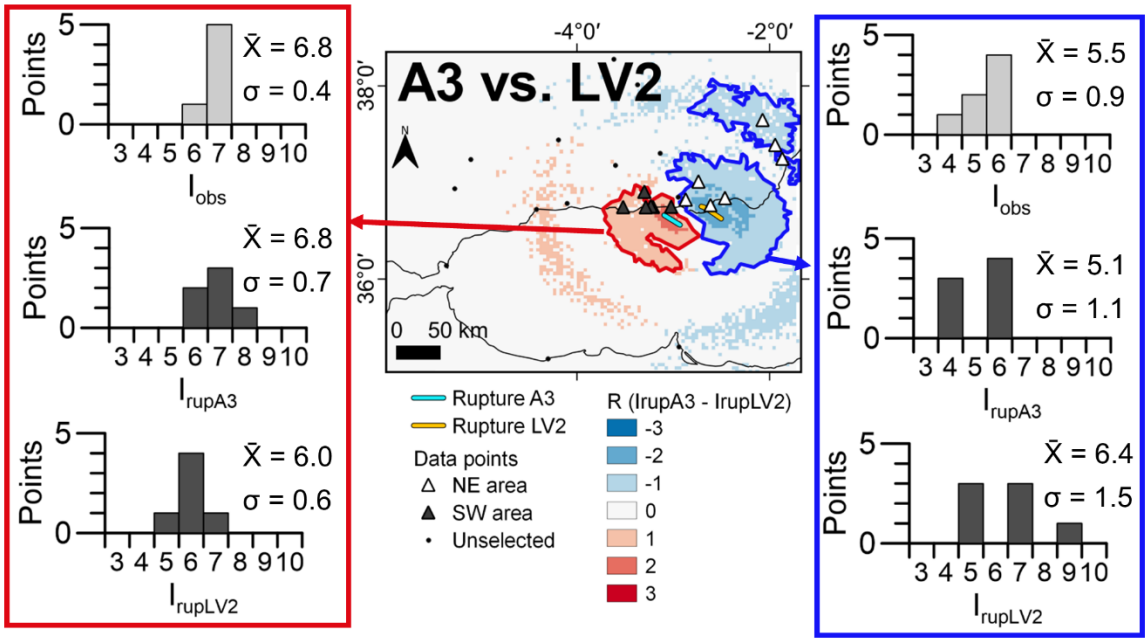

Figure 8. Differential zones for scenarios A3 and LV2. Histograms represent the distribution of the intensity values inside each differential zone for the observed intensity field (I_{obs}), scenario A3 (I_{rupA3}) and scenario LV2 (I_{rupLV2}).

Figure 9 shows the differential zones for scenarios AI and LV2. Again there are three differential zones: a bigger one to the SW where scenario AI shows higher intensity values, and two smaller ones to the NE where scenario LV2 shows higher values. As in the case of scenarios A3 and LV2, these two smaller zones will be considered as the same one for practical purposes. Histograms in Figure 9 represent the value distribution of the observed intensity (I_{obs}), scenario AI (I_{rupAI}) and scenario LV2 (I_{rupLV2}) inside the differential zones. I_{rupAI}'s distributions seem to be slightly more similar to I_{obs}, although once again the amount of I_{obs} points inside both areas is not enough to perform statistical analysis: six points in the SW zone, and eight in the NE zone. Thus we proceed on to step 4 of the methodology.

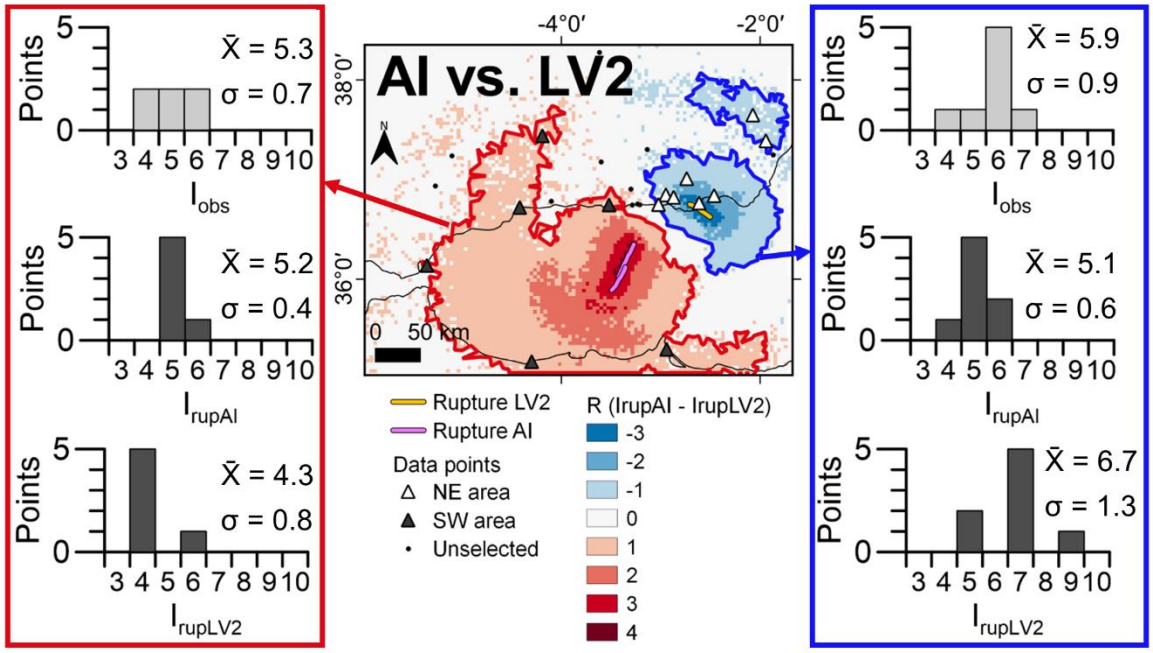

Figure 9. Differential zones for scenarios AI and LV2. Histograms represent the distribution of the intensity values inside each differential zone for the observed intensity field (I_{obs}), scenario AI (I_{rupAI}) and scenario LV2 (I_{rupLV2}).

4.4. Coulomb stress transfer

In this step, we model the static stress change (ΔCFS) produced by ruptures A3, AI, B and LV2 on the 25th August shock's rupture, which we call rupture D. Assuming from their closeness in time and space that the 13th January and the 25th August shocks are related by a triggering process, the rupture which causes ΔCFS > 0 on the most part of rupture D's surface would be the most likely source of the January shock. Rupture D has been tapered into 1 km^2 tiles in order to measure the "loaded" surface.

Figures 10, 11, 12 and 13 show the ΔCFS models from source rupture B to receiver rupture D, from source A3 to receiver D, from source LV2 to receiver D, and from source AI to receiver D, respectively. Rupture D involves the rupture of two faults: LVF and the nearby Llano del Águila Fault (LLAF). Two different views are presented in each figure in order to show both rupture surfaces. Rupture B caused ΔCFS > 0 in a total of 83 tiles of rupture D, which is a 15 % of rupture D's surface. Rupture A3 on the other hand

caused ΔCFS > 0 in 353 tiles, which is a 65 % of rupture D's surface. Rupture LV2 caused ΔCFS > 0 in the largest area: 394 tiles, which is a 73 % of rupture D's surface. Finally, rupture AI caused ΔCFS > 0 in 242 tiles, a 45 % of rupture D's surface.

460 Assuming the Alborán shock triggered the Dalías shock, this could point to rupture LV2 as the best candidate, although rupture A3 could also be a possible source of the Alborán earthquake.

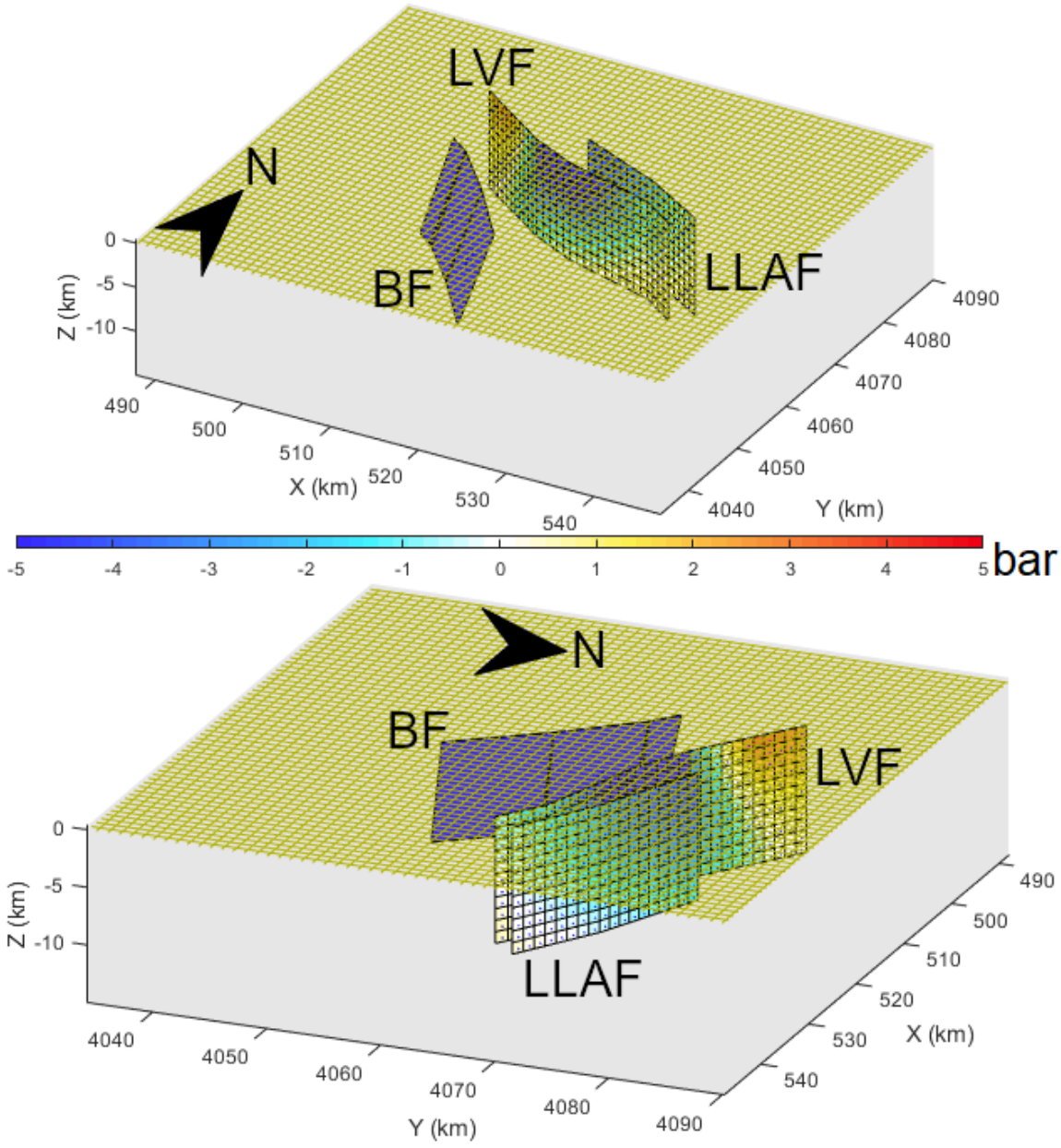

Figure 10. Coulomb static stress change model in rupture D (LVF+LLAF) caused by rupture B (BF).
465 BF: Balanegra Fault. LVF: Loma del Viento Fault. LLAF: Llano del Águila Fault.

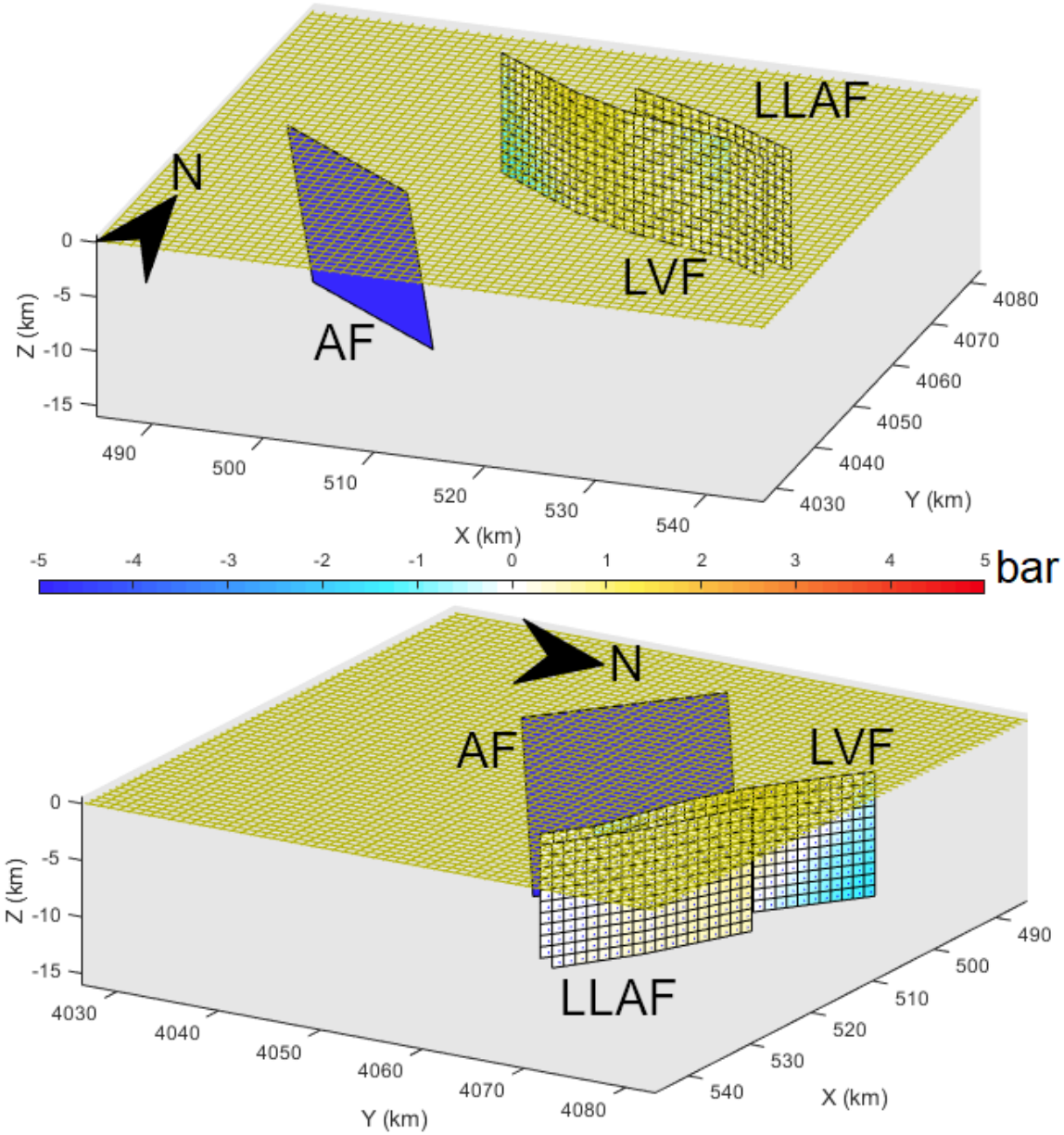

Figure 11. Coulomb static stress change model in rupture D (LVF+LLAF) caused by rupture A3 (AF).
AF: Adra Fault. LVF: Loma del Viento Fault. LLAF: Llano del Águila Fault.

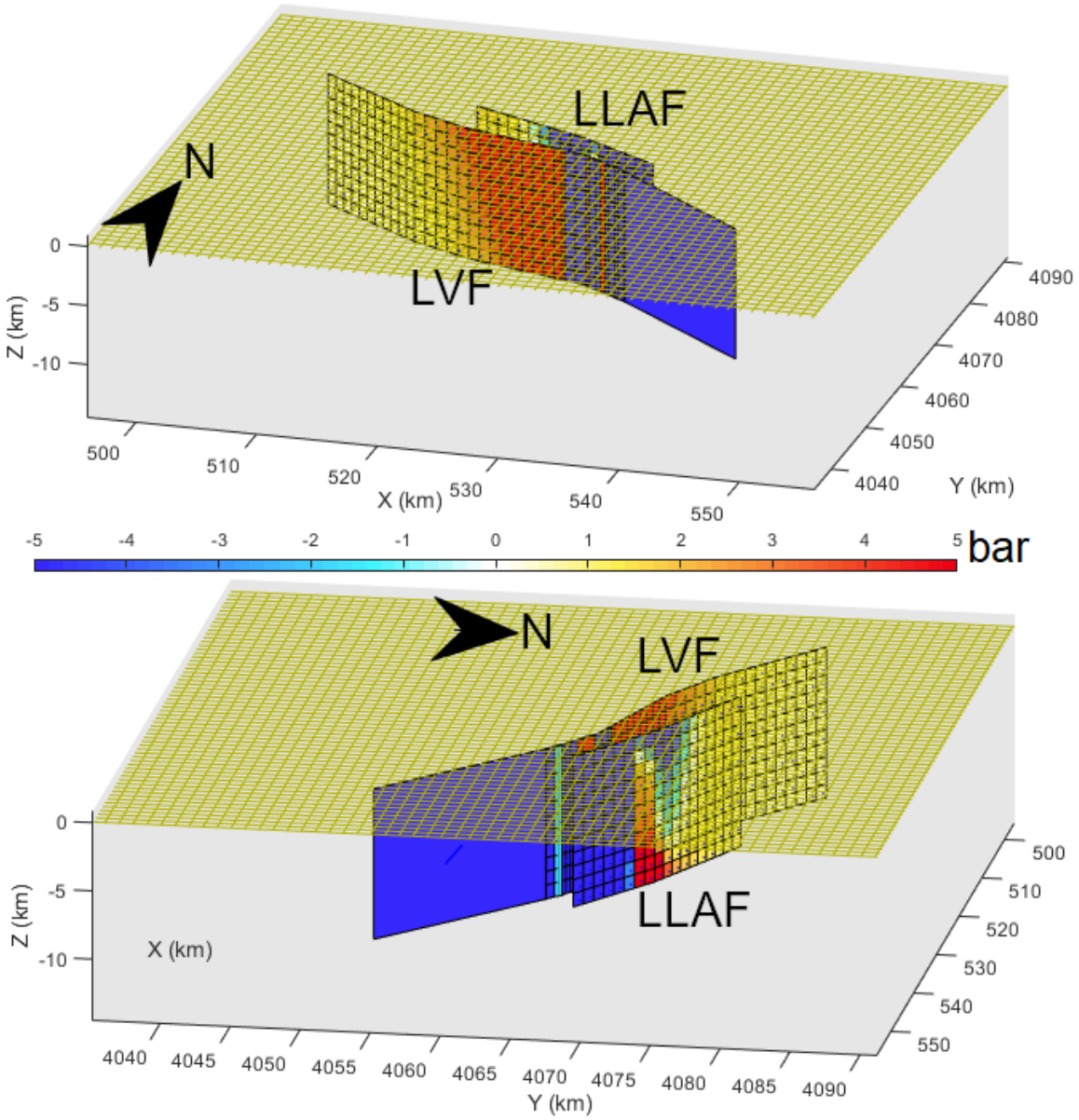

Figure 12. Coulomb static stress change model in rupture D (LVF+LLAF) caused by rupture LV2 (LVF's sea extension). LVF: Loma del Viento Fault. LLAF: Llano del Águila Fault.

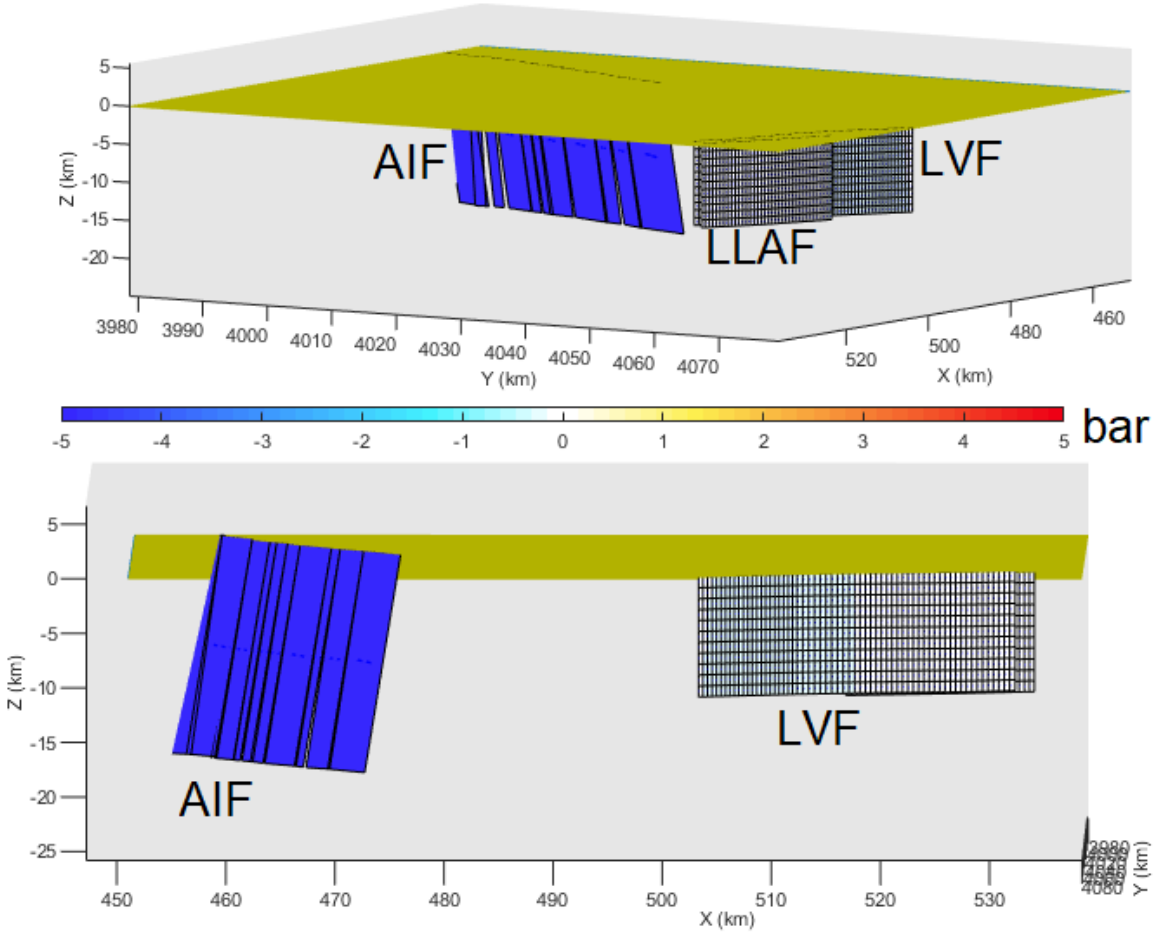

Figure 13. Coulomb static stress change model in rupture D (LVF+LLAF) caused by rupture AI (northern and central segments of Al-Idrissi Fault). LVF: Loma del Viento Fault. LLAF: Llano del Águila Fault. AIF: Al-Idrissi Fault.

4.5. ΔCFS of the 25th August earthquake

After calculating the local ΔCFS caused by rupture D on ideally oriented fault planes, we automatically detected the areas with ΔCFS > 0 bar, which are considered loaded zones, and those with ΔCFS < 0 bar, which are considered shadow zones. We then counted the number of located hypocenters in Instituto Geográfico Nacional (IGN)'s seismic catalogue inside loaded zones and shadow zones. If there is a significantly higher percentage of epicenters inside the loaded zones, it could point to an influence of the ΔCFS generated by the 25th August shock on the posterior seismicity.

IGN's seismic catalog includes a total of 251 events with $M_w > 3$ and hypocentral depth < 20 km in the study area since 25th August 1804 up to present times. Because hypocenter depth in the IGN's catalog can have uncertainties of several kilometers (especially for pre-instrumental earthquakes), we did the ΔCFS calculation for rupture D from 2 to 10 km deep. Figure 14 shows the ΔCFS induced by this earthquake on ideally oriented fault planes at three depths: 2 km, 5 km and 10 km. Epicenters for the 251 events are plotted as well in Figure 14. We found a total of 152 epicenters inside loaded zones (ΔCFS > 0 bar), and 34 events inside shadow zones (ΔCFS < 0 bar). This means that 61 % of the shallow main events in the catalog since 1804 are located inside areas that could have been loaded after the Dalías earthquake of 1804, while only a 13 % of the events after the earthquake occurred inside shadow zones, where we can expect a lesser seismicity rate. This could point to an influence of this region's last great earthquake of $M_w > 6.4$ in the posterior seismicity distribution, including earthquakes occurred during the time of instrumental records.

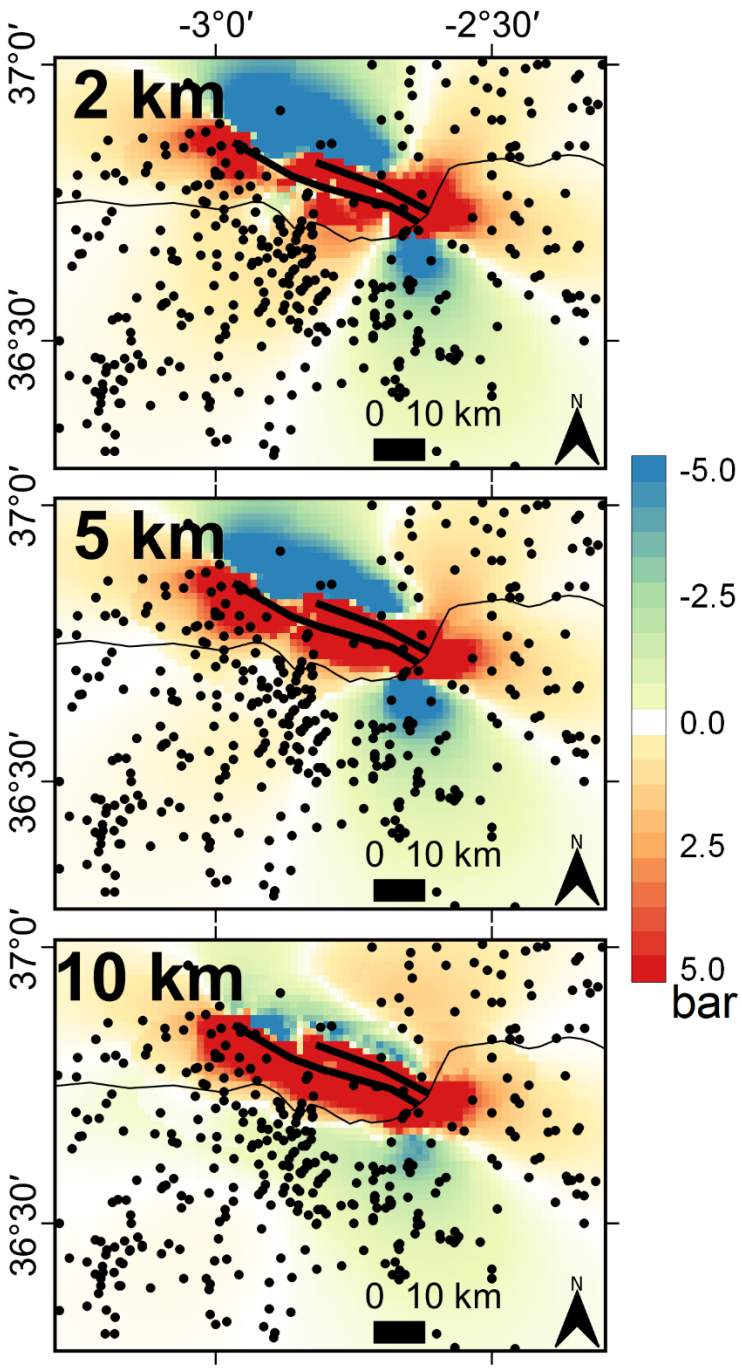

Figure 14. Coulomb static stress change model for rupture D of the Dalías earthquake (25th August 1804) at 2 km, 5 km and 10 km deep. Black dots correspond to epicenters of earthquakes recorded in IGN's seismic catalog of Mw > 3 and hypocentral depth < 20 km occurred from 1804 to 2013. σ_1 00º//158º, σ_3 00º//068º.

5. Discussion

In this work, we have searched for the most likely source of the 13th January 1804 Alborán earthquake combining different methodologies. First, we try to use Gasperini et

al. (1999, 2010)'s method to identify the most likely strike and area where the responsible source might be located. Then, we build intensity scenarios for several possible candidates to be the earthquake source and compare each of them with the observed intensity field, searching for the scenario that best fits the actual earthquake effects, following de Pro-Díaz et al. (2022, 2023)'s method. Finally, we use static Coulomb stress change calculations to refine the results.

The boxer calculated with Gasperini et al. (1999, 2010)'s method for the Alborán earthquake did not match any known active fault. Considering the amount of active tectonics studies conducted in the past in this area, most of which are referenced in the geological context of this work, the possibility of an unknown and unmapped active fault which would match the boxer in position and strike is highly unlikely. A more likely occurrence is a deviation of the boxer due to the intensity data points distribution over the study area: Boxer is known to show a geographical bias towards areas with a more dense population of intensity data points (de Pro-Díaz et al., 2023). As there are no data points offshore, the boxer has clearly been biased towards the Iberian coast, on which there are significantly more points than on the African coast. But this spatial bias is not the only issue with Gasperini et al. (1999, 2010)'s method detected in this work: Boxer also greatly underestimated the magnitude of the Alborán earthquake. This underestimation has been observed before in the Betics in the 1804 Dalías, the 2011 Lorca and the 1680 Málaga earthquakes (de Pro-Díaz et al., 2023) and is probably also related to the intensity data points distribution, or more precisely, to the absence of intensity data offshore, where the seismic source was most likely located. From these results, we suggest it is not possible to obtain valid results using Gasperini et al. (1999, 2010)'s method to study

earthquakes with intensity fields showing such poor azimuthal coverage as this one. Because of this, we did not take into account Boxer's results for the selection of candidate ruptures, and instead searched among the Quaternary active known faults for the ones which might match other authors' proposed sources.

None of the scenarios built for the Alborán earthquake show a perfect correlation with the intensity field's distribution when using the seismic scenario method, as seen in earlier works (de Pro-Díaz et al., 2022, 2023). During our first try building the scenarios with Campbell & Bozorgnia (2014)'s GMM, none of the candidate ruptures generated intensities high enough to match the observed earthquake effects, not even with M_w higher than those proposed by other authors (Figure AP3). We considered three possible explanations to this underprediction of the scenarios: a) the earthquake rupture might be longer than the ones we were using, which would also increase the magnitude; b) this earthquake could be a case in which complex ruptures involving several faults or fault segments lead to a higher energy release, and thus to heavier damage than expected, as it happened in the Kaikoura earthquake of 2016 (e. g. Goded et al., 2017; Kaiser et al., 2017; Stirling et al., 2017; Hamling, 2019); c) the best candidate was another, unknown fault we were not trying; and d) the GMM was underpredicting the ground motion, which in turn led to an underprediction of the intensity. We cast away option *a* because there was no geomorphologic evidence to further extend the fault traces of the BF, AF or LVF, and extending rupture AI further down the south of the AIF did not affect the predicted intensity distribution in the Iberian Peninsula, only in the African coast. Exploring option *b* would require another separate study on its own, so we will not address this option in this work. As for option *c*, the aforementioned absence of evidence for this hypothetical

unknown fault's existence despite intense active tectonics study in the area made this option highly unlikely. We were then down to option *d*: the GMM being the source of the issue. To address this possibility we rebuilt the scenarios using another GMM, Akkar & Bommer (2010), and the predicted intensities increased significantly in all of the scenarios, with some of them showing a rather good match (although not perfect) with the observed intensity distribution. We chose Akkar & Bommer (2010)'s GMM because it was built using data from the study area, as well as the rest of the Mediterranean.

It is noteworthy, though, how even with the GMM change, every scenario using a M_w equal to the ones calculated by other authors seems to significantly underestimate the intensity values. Both Molina et al. (2018) and Martínez Solares & Mezcua Rodríguez (2002) estimated this earthquake's magnitude using mainly intensity data and methodologies similar to that of Gasperini et al. (1999, 2010). The unreliability of this kind of calculation when intensity data are scarce and so heterogeneously distributed over the study area as in this case has been shown before in this work and earlier ones (de Pro-Díaz et al., 2023), so it is possible that Molina et al. (2018) and Martínez Solares & Mezcua Rodríguez (2002) underestimated this earthquake's magnitude. In addition to this, according to the equations of Stirling et al. (2002) and Wells & Coppersmith (1994), $M_w \geq 6.9$ is plausible for the considered rupture areas in the best performing scenarios in this work, and in the case of the AIF, also highlight this fault's potential to generate $M_w \geq 7$ earthquakes. Whether the real M_w was 6.9, or 7.0, or another number altogether, is something we may never know with precision, considering this is a pre-instrumental earthquake. However, our results show that $M_w < 6.9$ does not explain the observed

damage distribution, but higher magnitudes in any of the nearby faults do. This should be considered in future seismic hazards assessments in this area.

The statistical tests could not be applied in the differential zones step for any of the competing scenarios for this earthquake. This is due to the reduced amount of intensity data points inside the differential areas (less than 10 in all cases), which has proven to be the main limitation of the seismic scenario methodology. A similar issue appeared while studying the 1680 Málaga earthquake (de Pro-Díaz et al., 2023), another earthquake which showed an azimuthal coverage of 180º or less on its intensity field and a high dispersion of the data points over a wide area. Poor azimuthal coverage combined with high point dispersion of the intensity field are clearly the main limitations of this methodology. These characteristics are typically present in offshore earthquakes, due to the spatial bias of intensity data; although some earthquakes of $M_w > 7$ may cause such shaking that even if the seismic source is located offshore, there could be enough intensity points inland to apply this methodology. This was the case of the 1755 Lisbon earthquake, which was studied by Silva et al. (2023) using a methodology slightly different to the one used here but also based on building seismic scenarios and comparing them with the observed effects of the earthquake.

The implementation of the Coulomb stress transfer analysis step into the methodology is a parallel approach to strengthen the results and try to discern the best candidate rupture when the intensity data's azimuthal coverage is too poor. In this case study, if we assume, considering their closeness in both space and time, that there was a triggering effect between the Alborán earthquake of January and the Dalías earthquake of August, based solely on our results with the Coulomb stress transfer, the sea extension of the LVF would

be the most likely source for the January shock. The AF would also be a plausible source nonetheless, since it also charged a significant percentage of the Dalías rupture's plane. However, we must bear in mind that this triggering is an assumption, and its occurrence has not been proved. We must also remember that despite none of the scenarios tried in this work shows a perfect match with the intensity field, the intensity spatial distribution of scenarios from the AF and the AIF seem to be more similar to the observed intensity distribution than the scenario from the LVF is.

Our results do not allow us to tell apart one best candidate for the Alborán earthquake, despite the different approaches that have been tried. Nevertheless, we were able to discard six out of ten possible candidates. Based on our results, either one of the AF, the LVF, the BF or the AIF are plausible sources for this earthquake. However, if we had to decide for one of them, our preferred candidate would be the AF, because scenario A3 strikes a balance between the triggering hypothesis and a somewhat good match with the observed intensity's spatial distribution. Until more data is available for this earthquake and based on our results, we propose the Adra Fault as the most likely source for the Alborán earthquake of 13th January 1804, although bearing in mind that the Al-Idrissi, Balanegra and Loma del Viento Faults cannot be cast aside as possible sources.

In this work we have also performed a simple analysis to check for initial evidence of a possible influence of the Coulomb stress transfer caused by the Dalías shock of August on the posterior local seismicity. Our results show a correlation between positive stress change and the post-1804 seismicity rate. This correlation could persist at the present day, especially considering the low tectonic rate of this region that favors a longer-term influence of dynamic changes.

6. Conclusions

We have applied the Gasperini method, the seismic scenario method and Coulomb stress transfer analysis to investigate the most likely source of the Alborán earthquake from 1804. The Gasperini method produced results which were incompatible with the consensus of an offshore source accepted by all independent authors in the bibliography, so we decided against taking those results into account for this work. The seismic scenario method allowed us to discard six out of ten possible candidate ruptures, but the observed intensity field was too scarce and lacked the azimuthal coverage needed to discern the best candidate among the remaining four. The results of the Coulomb stress transfer analysis allowed us to rank these four candidates, but only with the assumption of a triggering effect between the Alborán shock of 13th January and the Dalías shock of 25th August. In the end, we lack enough data to select one best candidate among the Al-Idrissi, Adra, Balanegra and Loma del Viento Faults. The Adra Fault is the one which strikes the best balance between all the proposed hypothesis, but the other three are also plausible candidates to be the source of this earthquake.

We also investigated the possible influence of the stress transfer caused by the Dalías earthquake of 1804 on the local seismicity rate. This influence might still prevail in the present day, although more research is needed on this subject.

Acknowledgements

This work has been funded thanks to a predoctoral research contract from Universidad Complutense de Madrid (2019) and its following Postdoctoral Orientation Period (POP), as well as the research project “Análisis del ciclo sísmico a largo plazo a partir de datos geológicos y modelado” with reference number PID2021-124155NB-C31.

Data and code availability

Data used in this work was not compiled by the authors. The authors used data from Murphy Corella (2019), which is an open-access book available in the digital archive of the Instituto Geográfico Nacional (https://www.ign.es/web/libros-digitales/terremotos-almeria-1804).

Competing interests

The authors have no competing interests.

References

Abrahamson, N. A., Silva, W. J., & Kamai, R. (2014). Update of the AS08 Ground-Motion Prediction equations based on the NGA-west2 data set. *Pacific Engineering Research Center Report*, *May*, 174. http://scholar.google.com/scholar?hl=en&btnG=Search&q=intitle:Update+of+the+AS08+Ground-Motion+Prediction+Equations+Based+on+the+NGA-West2+Data+Set#0

Akkar, S., Sandıkkaya, M. A., & Bommer, J. J. (2014). Empirical ground-motion models for point- and extended-source crustal earthquake scenarios in Europe and the Middle East. *Bulletin of Earthquake Engineering*, *12*(1), 359–387. https://doi.org/10.1007/s10518-013-9461-4

Akkar, Sinan, & Bommer, J. J. (2010). Empirical equations for the prediction of PGA, PGV, and spectral accelerations in Europe, the mediterranean region, and the Middle East. *Seismological Research Letters*, *81*(2), 195–206. https://doi.org/10.1785/gssrl.81.2.195

Álvarez-Gómez, José A., Herrero-Barbero, P., & Martínez-Díaz, J. J. (2023). Seismogenic potential and tsunami threat of the strike-slip Carboneras fault in the western Mediterranean from physics-based earthquake simulations. *Natural Hazards and Earth System Sciences*, *23*(6), 2031–2052. https://doi.org/10.5194/nhess-23-2031-2023

Álvarez-Gómez, Jose Antonio, Martín, R., Pérez-López, R., Stich, D., Cantavella, J. V., Martínez-Díaz, J. J., Morales Soto, J., Martínez-García, P., Soto, J. I., & Carreño, E. (2016). La serie sísmica de Alhucemas 2016. Partición de la deformación e interacción de estructuras en un límite de placas difuso. *Geo-Temas*, *16*(2), 491–494.

Ambraseys, N. N., Douglas, J., Sarma, S. K., & Smit, P. M. (2005). Equations for the estimation of strong ground motions from shallow crustal earthquakes using data from Europe and the middle east: Horizontal peak ground acceleration and spectral acceleration. *Bulletin of Earthquake Engineering*, *3*(1), 1–53. https://doi.org/10.1007/s10518-005-0183-0

Ambraseys, N. N., & Jackson, J. A. (1998). Faulting associated with historical and recent earthquakes in the Eastern Mediterranean region. *Geophysical Journal International*, *133*(2), 390–406. https://doi.org/10.1046/j.1365-246X.1998.00508.x

Ammar, A., Mauffret, A., Gorini, C., & Jabour, H. (2007). The Tectonic Structure Of The Alboran Margin Of Morocco. *Revista de La Sociedad Geológica de España*, *20*(3–4), 247–271.

Atkinson, G. M., & Kaka, S. L. I. (2007). Relationships between felt intensity and

instrumental ground motion in the Central United States and California. *Bulletin of the Seismological Society of America*, *97*(2), 497–510. https://doi.org/10.1785/0120060154

Atkinson, G. M., & Wald, D. J. (2007). “Did You Feel It?” intensity data: a surprisingly good measure of earthquake ground motion. *Seismological Research Letters*, *78*(3), 362–368.

Basili, R., Valensise, G., Vannoli, P., Burrato, P., Fracassi, U., Mariano, S., Tiberti, M. M., & Boschi, E. (2008). The Database of Individual Seismogenic Sources (DISS), version 3: Summarizing 20 years of research on Italy’s earthquake geology. *Tectonophysics*, *453*(1–4), 20–43. https://doi.org/10.1016/j.tecto.2007.04.014

Campbell, K. W. (2003). Prediction of strong ground motion using the hybrid empirical method and its use in the development of ground-motion (attenuation) relations in Eastern North America. *Bulletin of the Seismological Society of America*, *93*(3), 1012–1033. https://doi.org/10.1785/0120020002

Campbell, K. W., & Bozorgnia, Y. (2014). NGA-West2 ground motion model for the average horizontal components of PGA, PGV, and 5% damped linear acceleration response spectra. *Earthquake Spectra*, *30*(3), 1087–1114. https://doi.org/10.1193/062913EQS175M

Canora, C., Martínez-Díaz, J. J., Villamor, P., Berryman, K., Álvarez-Gómez, J. A., Pullinger, C., & Capote, R. (2010). Geological and seismological analysis of the 13 february 2001 Mw 6.6 el salvador earthquake: Evidence for surface rupture and

implications for seismic hazard. *Bulletin of the Seismological Society of America*, *100*(6), 2873–2890. https://doi.org/10.1785/0120090377

Canora, C., Vilanova, S. P., de Pro-Díaz, Y., Pina, P., & Heleno, S. (2021). Evidence of surface rupture associated with historical earthquakes in the Lower Tagus Valley, Portugal. Implications for seismic hazard in the Greater Lisbon Area. *Frontiers in Earth Science, 9:620778*. https://doi.org/10.3389/feart.2021.620778

Caprio, M., Tarigan, B., Bruce Worden, C., Wiemer, S., & Wald, D. J. (2015). Ground motion to intensity conversion equations (GMICEs): A global relationship and evaluation of regional dependency. *Bulletin of the Seismological Society of America*, *105*(3), 1476–1490. https://doi.org/10.1785/0120140286

Caputo, R., Sboras, S., Pavlides, S., & Chatzipetros, A. (2015). Comparison between single-event effects and cumulative effects for the purpose of seismic hazard assessment. A review from Greece. *Earth-Science Reviews, 148*, 94–120. https://doi.org/10.1016/j.earscirev.2015.05.004

d'Acremont, E., Gutscher, M. A., Rabaute, A., Mercier de Lépinay, B., Lafosse, M., Poort, J., Ammar, A., Tahayt, A., Le Roy, P., Smit, J., Do Couto, D., Cancouët, R., Prunier, C., Ercilla, G., & Gorini, C. (2014). High-resolution imagery of active faulting offshore Al Hoceima, Northern Morocco. *Tectonophysics, 632*(C), 160–166. https://doi.org/10.1016/j.tecto.2014.06.008

De Larouzière, F. D., Bolze, J., Bordet, P., Hernandez, J., Montenat, C., & Ott d'Estevou, P. (1988). The Betic segment of the lithospheric Trans-Alboran shear zone during

the Late Miocene. *Tectonophysics*, *152*(1–2), 41–52. https://doi.org/10.1016/0040-1951(88)90028-5

de Pro-Díaz, Y., Perea, H., Insua-Arévalo, J. M., Martínez-Díaz, J. J., & Canora, C. (2023). Constraining earthquake fault sources through the use of intensity data and seismic scenarios: application to the Betic Cordillera (South Spain). *Frontiers in Earth Science, 11:1214836*. https://doi.org/10.3389/feart.2023.1214836

de Pro-Díaz, Y., Vilanova, S., & Canora, C. (2022). Ranking Earthquake Sources Using Spatial Residuals of Seismic Scenarios: Methodology Application to the 1909 Benavente Earthquake. *Bulletin of the Seismological Society of America*, *113*(2), 710–731. https://doi.org/10.1785/0120220067

Delavaud, E., Scherbaum, F., Kuehn, N., & Riggelsen, C. (2009). Information-theoretic selection of ground-motion prediction equations for seismic hazard analysis: An applicability study using californian data. *Bulletin of the Seismological Society of America*, *99*(6), 3248–3263. https://doi.org/10.1785/0120090055

DeMets, C., Gordon, R. G., & Argus, D. F. (2010). Geologically current plate motions. *Geophysical Journal International*, *181*(1), 1–80. https://doi.org/10.1111/j.1365-246X.2009.04491.x

Echeverria, A., Khazaradze, G., Asensio, E., & Masana, E. (2015). Geodetic evidence for continuing tectonic activity of the Carboneras fault (SE Spain). *Tectonophysics*, *663*, 302–309. https://doi.org/10.1016/j.tecto.2015.08.009

Espinar Moreno, M. (1994). Los estudios de sismicidad histórica en Andalucía: los

terremotos históricos de la provincia de Almería. In *El estudio de los terremotos en Almería* (pp. 115–180). Instituto de EStudios Almerienses. https://dialnet.unirioja.es/servlet/articulo?codigo=2767758

Ferrater, M., Ortuño, M., Masana, E., Martínez-Díaz, J. J., Pallàs, R., Perea, H., Baize, S., García-Meléndez, E., Echeverria, A., Rockwell, T., Sharp, W. D., & Arrowsmith, R. (2017). Lateral slip rate of Alhama de Murcia fault (SE Iberian Peninsula) based on a morphotectonic analysis: Comparison with paleoseismological data. *Quaternary International*, *451*, 87–100. https://doi.org/10.1016/j.quaint.2017.02.018

Ferrater, M., Ortuño, M., Masana, E., Pallàs, R., Perea, H., Baize, S., García-Meléndez, E., Martínez-Díaz, J. J., Echeverria, A., Rockwell, T. K., Sharp, W. D., Medialdea, A., & Rhodes, E. J. (2016). Refining seismic parameters in low seismicity areas by 3D trenching: The Alhama de Murcia fault, SE Iberia. *Tectonophysics*, *680*, 122–128. https://doi.org/10.1016/j.tecto.2016.05.020

Fracassi, U., & Valensise, G. (2007). Unveiling the sources of the catastrophic 1456 multiple earthquake: Hints to an unexplored tectonic mechanism in southern Italy. *Bulletin of the Seismological Society of America*, *97*(3), 725–748. https://doi.org/10.1785/0120050250

García-Mayordomo, J., Insua-Arévalo, J. M., Martínez-Díaz, J. J., Jiménez-Díaz, A., Martín-Banda, R., Martín-Alfageme, S., Álvarez-Gómez, J. A., Rodríguez-Peces, M., Pérez-López, R., Rodríguez-Pascua, M. A., Masana, E., Perea, H., Martín-González, F., Giner-Robles, J., Nemser, E. S., Cabral, J., & The_QAFI_Compilers_Working_Group. (2012). The Quaternary Faults Database of

Iberia (QAFI v.2.0). *Journal of Iberian Geology*, *38*(1), 285–302.

Gasperini, P., Bernardini, F., Valensise, G., & Boschi, E. (1999). Defining seismogenic sources from historical earthquake felt reports. *Bulletin of the Seismological Society of America*, *89*(1), 94–110.

Gasperini, P., Vannucci, G., Tripone, D., & Boschi, E. (2010). The location and sizing of historical earthquakes using the attenuation of macroseismic intensity with distance. *Bulletin of the Seismological Society of America*, *100*(5 A), 2035–2066. https://doi.org/10.1785/0120090330

Goded, T., Horspool, N., Canessa, S., & Gerstenberger, M. (2017). Modified Mercalli intensities for the M7.8 Kaikōura (New Zealand) 14 November 2016 earthquake derived from "felt detailed" and "felt rapid" online questionnaires. *Bulletin of the New Zealand Society for Earthquake Engineering*, *50*(2), 352–362. https://doi.org/10.5459/bnzsee.50.2.352-362

Gómez-Novell, O., García-Mayordomo, J., Ortuño, M., Masana, E., & Chartier, T. (2020). Fault System-Based Probabilistic Seismic Hazard Assessment of a Moderate Seismicity Region: The Eastern Betics Shear Zone (SE Spain). *Frontiers in Earth Science*, *8*(December). https://doi.org/10.3389/feart.2020.579398

Gómez de la Peña, L., Gràcia, E., Maesano, F. E., Basili, R., Kopp, H., Sánchez-Serra, C., Scala, A., Romano, F., Volpe, M., Piatanesi, A., & R. Ranero, C. (2022). A first appraisal of the seismogenic and tsunamigenic potential of the largest fault systems in the westernmost Mediterranean. *Marine Geology*, *445*(February).

https://doi.org/10.1016/j.margeo.2022.106749

Gràcia, E., Bartolome, R., Lo Iacono, C., Moreno, X., Stich, D., Martínez-Diaz, J. J., Bozzano, G., Martínez-Loriente, S., Perea, H., Diez, S., Masana, E., Dañobeitia, J. J., Tello, O., Sanz, J. L., & Carreño, E. (2012). Acoustic and seismic imaging of the Adra Fault (NE Alboran Sea): In search of the source of the 1910 Adra earthquake. *Natural Hazards and Earth System Sciences*, *12*(11), 3255–3267. https://doi.org/10.5194/nhess-12-3255-2012

Gràcia, E., Grevemeyer, I., Bartolomé, R., Perea, H., Martínez-Loriente, S., Gómez de la Peña, L., Villaseñor, A., Klinger, Y., Lo Iacono, C., Diez, S., Calahorrano, A., Camafort, M., Costa, S., d'Acremont, E., Rabaute, A., & Ranero, C. R. (2019). Earthquake crisis unveils the growth of an incipient continental fault system. *Nature Communications*, *10*(1), 1–12. https://doi.org/10.1038/s41467-019-11064-5

Gràcia, E., Pallàs, R., Soto, J. I., Comas, M., Moreno, X., Masana, E., Santanach, P., Diez, S., García, M., Dañobeitia, J., Bartolomé, R., Farrán, M., Gómez, M., Alpiste, M. J. R., Lastras, G., Wilmott, V., Perea, H., Blondel, P., Gómez, O., … Roque, C. (2006). Active faulting offshore SE Spain (Alboran Sea): Implications for earthquake hazard assessment in the Southern Iberian Margin. *Earth and Planetary Science Letters*, *241*(3–4), 734–749. https://doi.org/10.1016/j.epsl.2005.11.009

Griffin, J., Nguyen, N., Cummins, P., & Cipta, A. (2019). Historical earthquakes of the eastern sunda arc: Source mechanisms and intensity-based testing of Indonesia's national seismic hazard assessment. *Bulletin of the Seismological Society of America*, *109*(1), 43–65. https://doi.org/10.1785/0120180085

Grünthal, G. (1998). *European Macroseismic Scale 1998* (Vol. 15). European Seismological Commission (ESC). http://lib.riskreductionafrica.org/bitstream/handle/123456789/1193/1281.European Macroseismic Scale 1998.pdf?sequence=1

Hamling, I. J. (2019). A review of the 2016 Kaikōura earthquake: insights from the first 3 years. *Journal of the Royal Society of New Zealand*, *50*(2), 226–244. https://doi.org/10.1080/03036758.2019.1701048

Harris, R. A. (1998). Introduction to special section: Stress triggers, stress shadows, and implications for seismic hazard. *Journal of Geophysical Research: Solid Earth*, *103*(B10), 24347–24358. https://doi.org/10.1029/98jb01576

Herrero-Barbero, P., Álvarez-Gómez, J. A., Williams, C., Villamor, P., Insua-Arévalo, J. M., Alonso-Henar, J., & Martínez-Díaz, J. J. (2021). Physics-based earthquake simulations in slow-moving faults: a case study from the Eastern Betic Shear Zone (SE Iberian Peninsula). *Journal of Geophysical Research: Solid Earth*, *126*(5), 1–25. https://doi.org/10.1029/2020JB021133

Herrero Barbero, P. (2021). *Modelización 3D de la estructura, la cinemática y el comportamiento sismogénico del sistema de fallas de las Béticas Orientales. Aplicación a la amenaza sísmica*. Universidad Complutense de Madrid.

Hough, S. E., & Graves, R. W. (2020). The 1933 Long Beach Earthquake (California, USA): Ground Motions and Rupture Scenario. *Scientific Reports*, *10*(1), 1–10. https://doi.org/10.1038/s41598-020-66299-w

Huerta, P., Silva, P. G., Giner-Robles, J. L., Rodríguez-Pascua, M. A., & Bautista Davila, M. B. (2015). Efectos geológicos del terremoto de Dalías-Berja 1804 AD. (Almería, SE España). *XIV Reunión Nacional de Cuaternario*, *1*, 194–197.

IGN-UCM. (2013). *Actualización de mapas de peligrosidad sísmica de España 2012 (Vol. 267)* (p. 272). Centro Nacional de Información Geográfica (CNIG). https://doi.org/10.7419/162.05.2017

Insua-Arévalo, J. M., García-Mayordomo, J., Salazar, A., Rodríguez-Escudero, E., Martín-Banda, R., Álvarez-Gómez, J. A., Canora, C., & Martínez-Díaz, J. J. (2015). Paleoseismological evidence of holocene activity of the los tollos fault (Murcia, se Spain): A lately formed quaternary tectonic feature of the eastern betic shear zone. *Journal of Iberian Geology*, *41*(3), 333–350. https://doi.org/10.5209/rev_JIGE.2015.v41.n3.49948

Kaiser, A., Balfour, N., Fry, B., Holden, C., Litchfield, N., Gerstenberger, M., D'Anastasio, E., Horspool, N., McVerry, G., Ristau, J., Bannister, S., Christophersen, A., Clark, K., Power, W., Rhoades, D., Massey, C., Hamling, I., Wallace, L., Mountjoy, J., … Gledhill, K. (2017). The 2016 Kaikōura, New Zealand, earthquake: Preliminary seismological report. *Seismological Research Letters*, *88*(3), 727–739. https://doi.org/10.1785/0220170018

Kaka, S. L. I., & Atkinson, G. M. (2004). Relationships between instrumental ground-motion parameters and modified Mercalli intensity in eastern North America. *Bulletin of the Seismological Society of America*, *94*(5), 1728–1736. https://doi.org/10.1785/012003228

King, G. C. P., Stein, R. S., & Jian Lin. (1994). Static stress changes and the triggering of earthquakes. *Bulletin - Seismological Society of America*, *84*(3), 935–953. https://doi.org/10.1016/0148-9062(95)94484-2

Lafosse, M., D'Acremont, E., Rabaute, A., Estrada, F., Jollivet-Castelot, M., Vázquez, J. T., Galindo-Zaldivar, J., Ercilla, G., Alonso, B., Smit, J., Ammar, A., & Gorini, C. (2020). Plio-Quaternary tectonic evolution of the southern margin of the Alboran Basin (Western Mediterranean). *Solid Earth*, *11*(2), 741–765. https://doi.org/10.5194/se-11-741-2020

Lozos, J. C. (2016). A case for historic joint rupture of the San Andreas and San Jacinto faults. *Science Advances*, *2*(3), 1–8. https://doi.org/10.1126/sciadv.1500621

Marín-Lechado, C., Galindo-Zaldívar, J., Gil, A. J., Borque, M. J., de Lacy, M. C., Pedrera, A., López-Garrido, A. C., Alfaro, P., García-Tortosa, F., Ramos, M. I., Rodríguez-Caderot, G., Rodríguez-Fernández, J., Ruiz-Constán, A., & de Galdeano-Equiza, C. S. (2010). Levelling profiles and a GPS network to monitor the active folding and faulting deformation in the campo de dalias (Betic Cordillera, Southeastern Spain). *Sensors*, *10*(4), 3504–3518. https://doi.org/10.3390/s100403504

Marín-Lechado, C., Galindo-Zaldívar, J., Rodríguez-Fernández, L. R., Serrano, I., & Pedrera, A. (2005). Active faults, seismicity and stresses in an internal boundary of a tectonic arc (Campo de Dalías and Níjar, southeastern Betic Cordilleras, Spain). *Tectonophysics*, *396*(1–2), 81–96. https://doi.org/10.1016/j.tecto.2004.11.001

Martín-Banda, R., García-Mayordomo, J., Insua-Arévalo, J. M., Salazar, Á. E., Rodríguez-Escudero, E., Álvarez-Gõmez, J. A., Medialdea, A., & Herrero, M. J. (2016). New insights on the seismogenic potential of the Eastern Betic Shear Zone (SE Iberia): Quaternary activity and paleoseismicity of the SW segment of the Carrascoy Fault Zone. *Tectonics*, *35*(1), 55–75. https://doi.org/10.1002/2015TC003997

Martínez-Díaz, J. J. (1999). *Neotectónica y Tectónica Activa del Sector Centro-Occidental de la Región de Murcia y Sur de Almería (Cordillera Bética - España)*. Universidad Complutense de Madrid.

Martínez-Díaz, J. J., & Hernández-Enrile, J. L. (2004). Neotectonics and morphotectonics of the southern Almería region (Betic Cordillera-Spain) kinematic implications. *International Journal of Earth Sciences*, *93*(2), 189–206. https://doi.org/10.1007/s00531-003-0379-y

Martínez-Díaz, J. J., Masana, E., & Ortuño, M. (2012). Active tectonics of the Alhama de Murcia fault, Betic Cordillera, Spain. *Journal of Iberian Geology*, *38*(1), 253–270. https://doi.org/10.5209/rev_jige.2012.v38.n1.39218

Martínez-García, P., Comas, M., Soto, J. I., Lonergan, L., & Watts, A. B. (2013). Strike-slip tectonics and basin inversion in the Western Mediterranean: The Post-Messinian evolution of the Alboran Sea. *Basin Research*, *25*(4), 361–387. https://doi.org/10.1111/bre.12005

Martínez-García, P., Soto, J. I., & Comas, M. (2011). Recent structures in the Alboran

Ridge and Yusuf fault zones based on swath bathymetry and sub-bottom profiling: Evidence of active tectonics. *Geo-Marine Letters*, *31*(1), 19–36. https://doi.org/10.1007/s00367-010-0212-0

Martínez-Martínez, J. M. (2006). Lateral interaction between metamorphic core complexes and less-extended, tilt-block domains: the Alpujarras strike-slip transfer fault zone (Betics, SE Spain). *Journal of Structural Geology*, *28*(4), 602–620. https://doi.org/10.1016/j.jsg.2006.01.012

Martínez Solares, J. M., & Mezcua Rodríguez, J. (2002). *Catálogo sísmico de la Península Ibérica (880 a. C. - 1900)*. Instituto Geográfico Nacional.

McCalpin, J. P., & Nelson, A. S. (1996). *Paleoseismology* (J. P. McCalpin (ed.)). Academic Press.

Mezcua, J., Rueda, J., & García Blanco, R. M. (2013). Iberian peninsula historical seismicity revisited: An intensity data bank. *Seismological Research Letters*, *84*(1), 9–18. https://doi.org/10.1785/0220120097

Michetti, A. M., Esposito, E., Guerrieri, L., Porfido, S., Serva, L., Tatevossian, R., Vittori, E., Audemard, F., Azuma, T., Clague, J., Comerci, V., Gürpinar, A., McCalpin, J., Mohammadioun, B., Mörner, N. A., Ota, Y., & Roghozin, E. (2007). *INQUA Environmental Seismic Intensity Scale 2007 (ESI-2007)* (L. Guerrieri & E. Vittori (eds.)). Servizio Geológico d'Italia - Dipartamento Difensa del Suolo.

Molina, S., Navarro, M., Martínez-Pagan, P., Pérez-Cuevas, J., Vidal, F., Navarro, D., & Agea-Medina, N. (2018). Potential damage and losses in a repeat of the 1910 Adra

(Southern Spain) earthquake. *Natural Hazards*, *92*(3), 1547–1571. https://doi.org/10.1007/s11069-018-3263-6

Molins-Vigatà, J., García-Mayordomo, J., Ortuño, M., García-Sellés, D., & Gómez-Novell, O. (2022). Caracterización geológica de la falla del Llano del Águila en Campo Dalías (Almería): posible fuente sismogénica del terremoto de 1804. *Revista de La Sociedad Geológica de España*, *35*(1), 71–83. https://doi.org/10.55407/rsge.94908

Moreno Mota, X. (2011). *Neotectonic and Paleoseismic onshore-offshore integrated study of the Carboneras Fault (Eastern Betics, SE Iberia)*. Universitat de Barcelona.

Moreno, X., Gràcia, E., Bartolomé, R., Martínez-Loriente, S., Perea, H., de la Peña, L. G., Iacono, C. Lo, Piñero, E., Pallàs, R., Masana, E., & Dañobeitia, J. J. (2016). Seismostratigraphy and tectonic architecture of the Carboneras Fault offshore based on multiscale seismic imaging: Implications for the Neogene evolution of the NE Alboran Sea. *Tectonophysics*, *689*, 115–132. https://doi.org/10.1016/j.tecto.2016.02.018

Moreno, X., Masana, E., Pallàs, R., Gràcia, E., Rodés, Á., & Bordonau, J. (2015). Quaternary tectonic activity of the Carboneras Fault in the La Serrata range (SE Iberia): Geomorphological and chronological constraints. *Tectonophysics*, *663*, 78–94. https://doi.org/10.1016/j.tecto.2015.08.016

Muñoz Clares, M., Fernández Carrascosa, M., Alcolea López, M. O., Arcas Navarro, M. C., Arcas Ruiz, N., Caro del Vas, P., Cruz López, M. T., García Poveda, M., García

Valera, M. A., Llamas Martínez, B., & Ruiz Llanes, A. E. (2012). Sismicidad histórica y documentación municipal: El caso de Lorca. *Boletin Geologico y Minero*, *123*(4), 415–429.

Murphy Corella, P. (2019). *Los terremotos de Almería de 1804 en el archivo histórico nacional*. Instituto Geográfico Nacional. https://www.ign.es/web/libros-digitales/terremotos-almeria-1804

Nocquet, J. M., & Calais, E. (2004). Geodetic measurements of crustal deformation in the Western Mediterranean and Europe. *Pure and Applied Geophysics*, *161*(3), 661–681. https://doi.org/10.1007/s00024-003-2468-z

Okada, Y. (1992). Internal deformation due to shear and tensile faults in a half-space. *Bulletin - Seismological Society of America*, *82*(2), 1018–1040. https://doi.org/10.1785/bssa0820021018

Ortuño, M., Masana, E., García-Meléndez, E., Martínez-Díaz, J., Štěpančíková, P., Cunha, P. P., Sohbati, R., Canora, C., Buylaert, J. P., & Murray, A. S. (2012). An exceptionally long paleoseismic record of a slow-moving fault: The Alhama de Murcia fault (Eastern Betic shear zone, Spain). *Bulletin of the Geological Society of America*, *124*(9–10), 1474–1494. https://doi.org/10.1130/B30558.1

Pagani, M., Monelli, D., Weatherill, G., Danciu, L., Crowley, H., Silva, V., Henshaw, P., Butler, L., Nastasi, M., Panzeri, L., Simionato, M., & Vigano, D. (2014). Openquake engine: An open hazard (and risk) software for the global earthquake model. *Seismological Research Letters*, *85*(3), 692–702.

https://doi.org/10.1785/0220130087

Palano, M., González, P. J., & Fernández, J. (2015). The Diffuse Plate boundary of Nubia and Iberia in the Western Mediterranean: Crustal deformation evidence for viscous coupling and fragmented lithosphere. *Earth and Planetary Science Letters*, *430*, 439–447. https://doi.org/10.1016/j.epsl.2015.08.040

Pedrera, A., Marín-Lechado, C., Stich, D., Ruiz-Constán, A., Galindo-Zaldívar, J., Rey-Moral, C., & de Lis Mancilla, F. (2012). Nucleation, linkage and active propagation of a segmented Quaternary normal-dextral fault: The Loma del Viento fault (Campo de Dalías, Eastern Betic Cordillera, SE Spain). *Tectonophysics*, *522–523*, 208–217. https://doi.org/10.1016/j.tecto.2011.12.001

Perea, H, Roldán, J. L., Sánchez-Lozano, L., Álvarez-Gómez, J. A., & P. Herrero-Barbero1, M.J. Jiménez4, S. Martínez-Loriente2, A. C. y J. L. (2022). Serie sísmica del sur del Mar de Alborán del 2021-2022: relocalización de los eventos e implicaciones sismotectónicas. *IV Reunión Ibérica Sobre Fallas Activas y Paleosismología*, 141–144.

Perea, Hector. (2009). The Catalan seismic crisis (1427 and 1428; NE Iberian Peninsula): Geological sources and earthquake triggering. *Journal of Geodynamics*, *47*(5), 259–270. https://doi.org/10.1016/j.jog.2009.01.002

Pezeshk, S., Zandieh, A., Campbell, K. W., & Tavakoli, B. (2018). Ground-motion prediction equations for central and eastern north America using the hybrid empirical method and NGA-west2 empirical ground-motion models. *Bulletin of the*

Seismological Society of America, *108*(4), 2278–2304. https://doi.org/10.1785/0120170179

Posadas, A., Vidal, F., & Navarro, M. (2006). The M = 6.3 Earthquake of January 13 (1804) in Motril (Spain). *Proceedings of the First Europen Conference on Earthquake Engineering and Seismology*, *91*, 1–8.

Rodríguez-Pascua, M. A., Silva, P. G., Perucha, M. A., Robles, J. L. G., Elez, J., & Roquero, E. (2017). El escenario sísmico del terremoto de Arenas del Rey de 1884. *IX Reunião Do Quaternário Ibérico*, 49–52.

Sanz de Galdeano, C. (1983). Los accidentes y fracturas principales de las Cordilleras Béticas. *Estudios Geológicos*, *39*(3–4), 157–165.

Sanz de Galdeano, C., Azañón, J. M., Cabral, J., Ruano, P., Alfaro, P., Canora, C., Ferrater, M., García Tortosa, F. J., García-Mayordomo, J., Gràcia, E., Insua-Arévalo, J. M., Jiménez Bonilla, A., Lacan, P. G., Marín-Lechado, C., Martín-Banda, R., Martín González, F., Martínez-Díaz, J. J., Martín-Rojas, I., Masana, E., … Simón, J. L. (2020). Active faults in Iberia. In *The geology of Iberia: a geodynamic approach. Volume 5: Active Processes: seismicity, active faulting and relief* (pp. 33–75).

Sanz de Galdeano, C., Rodriguez-Fernandez, J., & Lopez-Garrido, A. C. (1985). A strike-slip fault corridor within the Alpujarra Mountains (Betic Cordilleras, Spain). *Geologische Rundschau*, *74*(3), 641–655. https://doi.org/10.1007/BF01821218

Serpelloni, E., Vannucci, G., Pondrelli, S., Argnani, A., Casula, G., Anzidei, M., Baldi,

P., & Gasperini, P. (2007). Kinematics of the Western Africa-Eurasia plate boundary from focal mechanisms and GPS data. *Geophysical Journal International*, *169*(3), 1180–1200. https://doi.org/10.1111/j.1365-246X.2007.03367.x

Silva, P.G., Goy, J. L., Somoza, L., Zazo, C., & Bardají, T. (1993). Landscape response to strike-slip faulting linked to collisional settings: Quaternary tectonics and basin formation in the Eastern Betics, southeastern Spain. *Tectonophysics*, *224*(4), 289–303. https://doi.org/10.1016/0040-1951(93)90034-H

Silva, Pablo G., Elez, J., Giner-Robles, J. L., Rodríguez-Pascua, M. A., Pérez-López, R., Roquero, E., Bardají, T., & Martínez-Graña, A. (2017). ESI-07 ShakeMaps for instrumental and historical events in the Betic Cordillera (SE Spain): An approach based on geological data and applied to seismic hazard. *Quaternary International*, *451*, 185–208. https://doi.org/10.1016/j.quaint.2016.10.020

Silva, Pablo G., Elez, J., Pérez-López, R., Giner-Robles, J. L., Gómez-Diego, P. V., Roquero, E., Rodríguez-Pascua, M. Á., & Bardají, T. (2023). The AD 1755 Lisbon Earthquake-Tsunami: Seismic source modelling from the analysis of ESI-07 environmental data. *Quaternary International*, *651*, 6–24. https://doi.org/10.1016/j.quaint.2021.11.006

Stein, R. S. (1999). The role of stress transfer in earthquake occurrence. *Nature*, *402*, 605–609.

Stein, R. S. (2003). Earthquake conversations. *Scientific American*, *288*(1), 72–79. https://doi.org/10.1038/scientificamerican0103-72

Stirling, Mark, Rhoades, D., & Berryman, K. (2002). Comparison of earthquake scaling relations derived from data of the instrumental and preinstrumental era. *Bulletin of the Seismological Society of America*, *92*(2), 812–830. https://doi.org/10.1785/0120000221

Stirling, MW, Litchfield, N. J., Villamor, P., Van Dissen, R. J., Nicol, A., Pettinga, J., Barnes, P., Langridge, R. M., Little, T., Barrell, D. J., Mountjoy, J., Ries, W. F., Rowland, J., Fenton, C., Hamling, I., Asher, C., Barrier, A., Benson, A., Bischoff, A., … Zinke, R. (2017). The M(w)7.8 2016 Kaikoura earthquake: sufrace fault rupture and seismic hazard context. *Bulletin of the New Zealand Society for Earthquake Engineering*, *50*(2), 73–84.

Teves-Costa, P., & Batlló, J. (2011). The 23 April 1909 Benavente earthquake (Portugal): Macroseismic field revision. *Journal of Seismology*, *15*(1), 59–70. https://doi.org/10.1007/s10950-010-9207-6

Toda, S., Stein, R. S., Sevilgen, V., & Lin, J. (2011). *Coulomb 3.3 Graphic-rich deformation and stress-change software for earthquake, tectonic, and volcano research and teaching-user guide: U.S. Geological Survey Open-File Report 2011-1060* (p. 63). http://pubs.usgs.gov/of/2011/1060/

Trifunac, M. D., & Brady, A. G. (1975). On the correlation of seismic intensity scales with the peaks of recorded strong ground motion. *Bulletin of the Seismological Society of America*, *65*(1), 139–162. https://doi.org/

Tselentis, G. A., & Danciu, L. (2008). Empirical relationships between modified Mercalli

intensity and engineering ground-motion parameters in Greece. *Bulletin of the Seismological Society of America*, *98*(4), 1863–1875. https://doi.org/10.1785/0120070172

Wald, D. J., Quitoriano, V., Heaton, T. H., & Kanamori, H. (1999). Relationships between peak ground acceleration, peak ground velocity, and modified mercalli intensity in California. In *Earthquake Spectra* (Vol. 15, Issue 3, pp. 557–564). https://doi.org/10.1193/1.1586058

Wells, D. L., & Coppersmith, K. J. (1994). New empirical relationships among magnitude, rupture length, rupture width, rupture area, and surface displacement. *Bulletin - Seismological Society of America*, *84*(4), 974–1002.

Worden, C. B., Gerstenberger, M. C., Rhoades, D. A., & Wald, D. J. (2012). Probabilistic relationships between ground-motion parameters and modified mercalli intensity in California. *Bulletin of the Seismological Society of America*, *102*(1), 204–221. https://doi.org/10.1785/0120110156

Yelles-Chaouche, A. K., Abacha, I., Boulahia, O., Aidi, C., Chami, A., Belheouane, A., Rahmani, S. T. E., & Roubeche, K. (2021). The 13 July 2019 Mw 5.0 Jijel Earthquake, northern Algeria: An indicator of active deformation along the eastern Algerian margin. *Journal of African Earth Sciences*, *177*, 104149. https://doi.org/10.1016/j.jafrearsci.2021.104149

Appendix

Site	I_{EMS-98}	Earthquake effects

Motril	VII-VIII	Part of the building stock was damaged and part was left in ruins. Two casualties. Sea withdrawal of 22 varas (~18 m). The population left their houses for the main square in fear. The different seismic phases are described as follows: first, a strong shaking with perpendicular movement; 14-16 seconds later, trepidation for 4-5 seconds; after that, a strong undulating movement for more than 20 seconds. Total shaking lasted for 40-42 seconds. 11 aftershocks are described in the following days.
Almegíjar	VII	Town hall was destroyed.
Dalías	VI+	Four churches and several private buildings were damaged, the population left their houses and camped outside town in fear. Shaking lasted for 50 seconds. Damage was repaired more than a month afterwards.
Berja		
Adra	VI+	Shaking lasted for 110 seconds. The population left their houses for the streets and squares in fear. Some buildings were damaged.
Roquetas	VI+	The ceiling of the lye storehouse was razed.
Almería	VI+	Generalized damage to the whole building stock.

		Shaking lasted for 30 seconds. No casualties.
Málaga	VI	Population left their houses for the streets and squares in fear.
Gibraltar	V	Shaken furniture inside the houses, loss of balance from standing people.

Table AP1. Translation of earthquake effects reports for different sites studied by Murphy Corella, (2019) and the intensity values he initially assigned to each site.

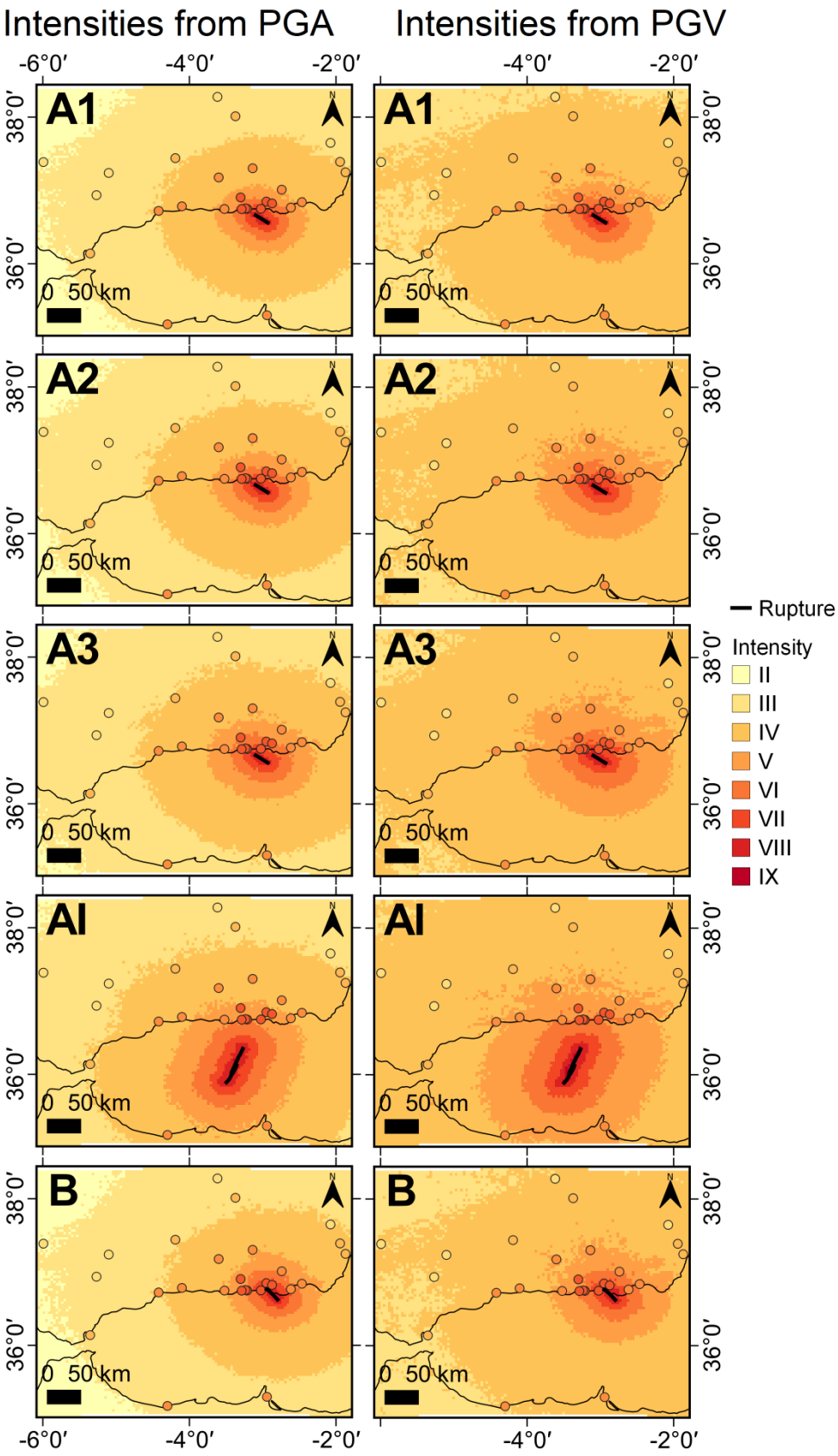

Figure AP1. Seismic scenarios built for candidate ruptures A1 to A3 (Adra Fault), AI (Al-Idrissi

Fault), and B (Balanegra Fault) with the Campbell & Bozorgnia (2014) GMM. The observed intensity field is superimposed in the same color palette.

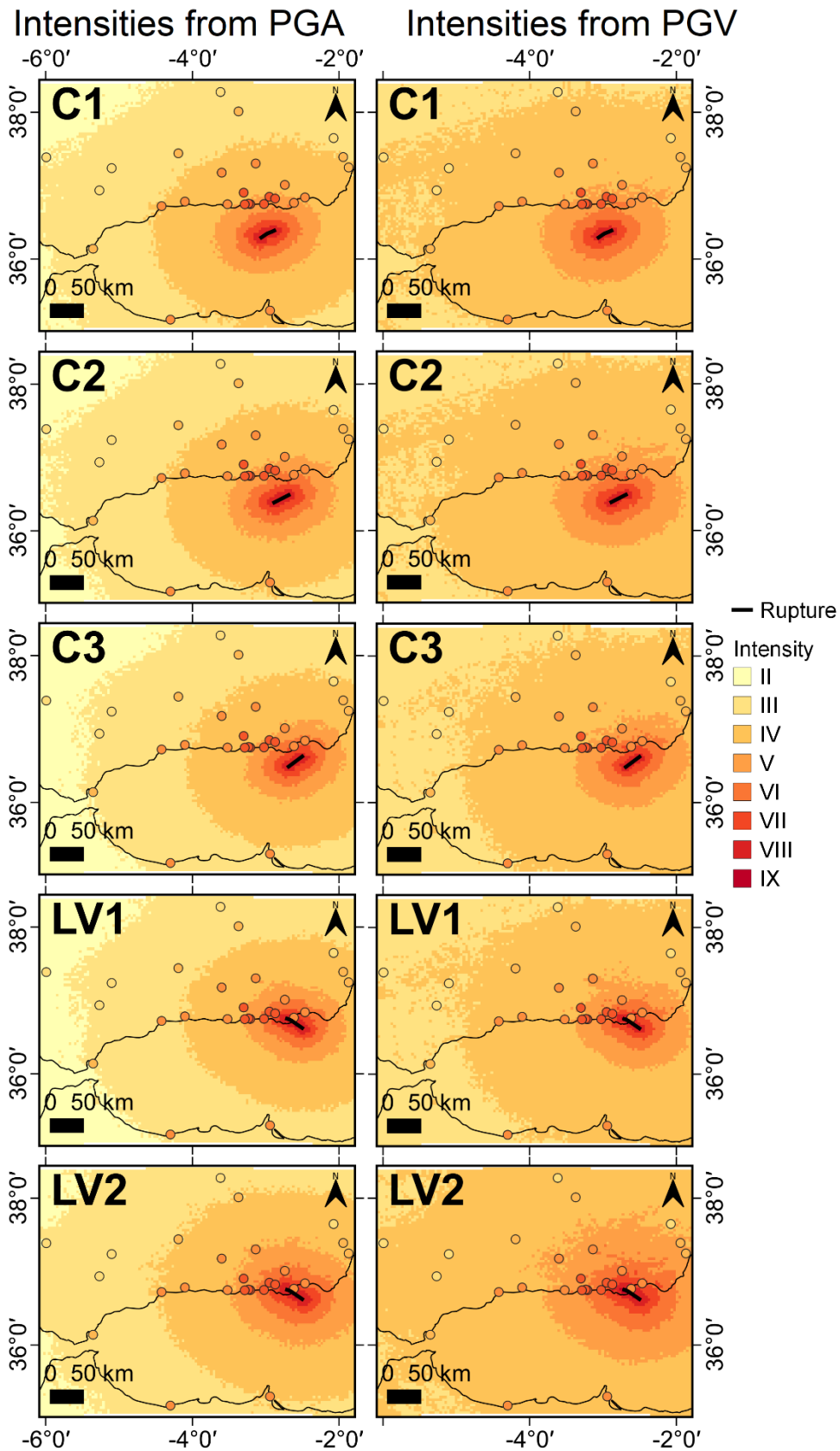

Figure AP2. Seismic scenarios built for candidate ruptures C1 to C3 (Carboneras Fault), and LV1 and

LV2 (Loma del Viento Fault) with the Campbell & Bozorgnia (2014) GMM. The observed intensity field is superimposed in the same color palette.

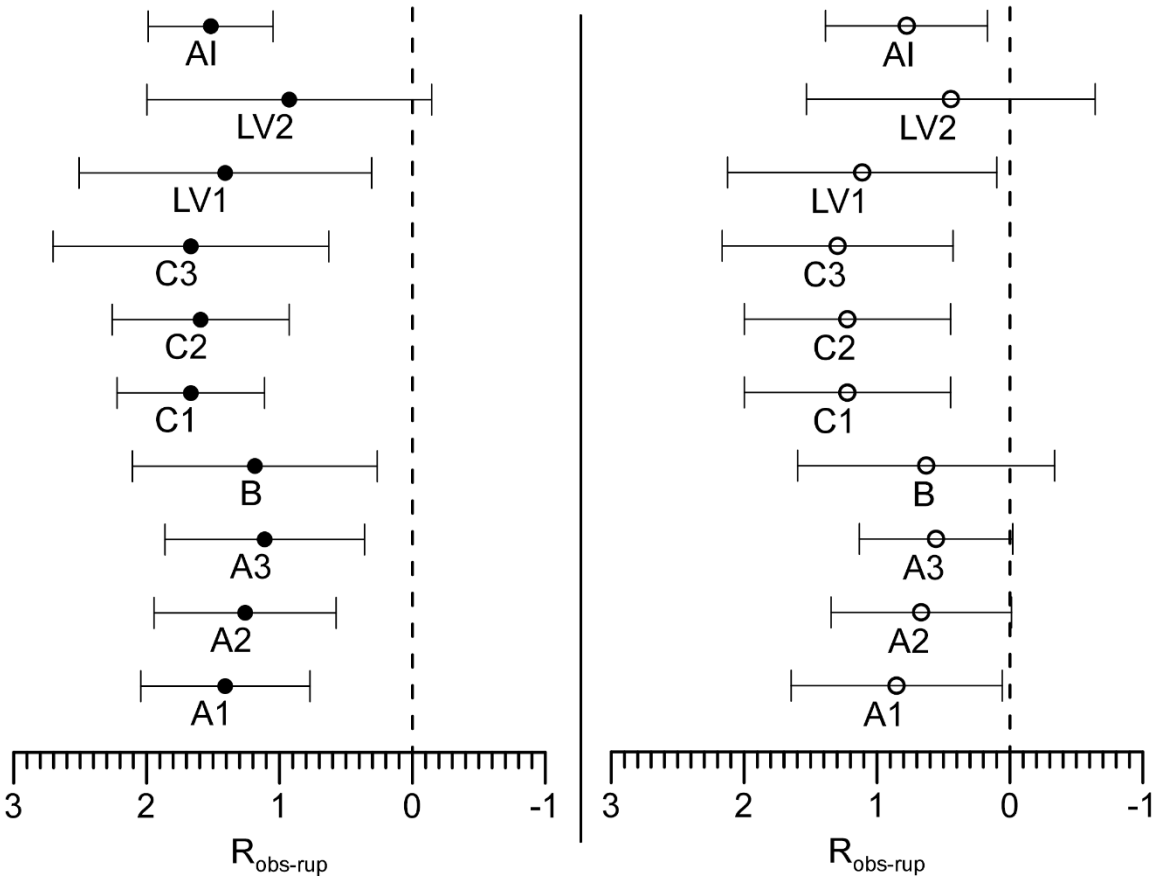

Figure AP3. Residuals $R_{obs-rup}$ for each of the scenarios for the Alborán earthquake built with the Campbell & Bozorgnia (2014) GMM. The average residual is represented with a dot and the bars represent the standard deviation. Black dots correspond to results from scenarios with intensities calculated from PGA, and white dots correspond to results from scenarios with intensities calculated from PGV. Each scenario is labeled below the dot.

The 1804 Alborán seismic series: search for the source using seismic scenarios and static stress interactions

Y. de Pro-Díaz1, J. J. Martínez-Díaz, and C. Canora-Catalán

Comments by Luis Matias

Major comments

Insufficient information provided

Ideally, the information provided in one paper should allow the interested reader to reproduce the presented results. This may not be the case in many circumstances but I found several instances of missing information or incongruence to the quoted sources.

Intensity values

In the paper the authors use 30 observations of intensity as estimated by Murphy Corella, (2019). Nine of these values are described on table AP1 presented in the Appendix. I browsed the Murphy Corella, (2019) work and found Tabla 31 that summarizes his results on the 1804 Alborán earthquake. There we see 26 intensity values greater or equal to 3. Furthermore, the paper table AP1 entries do not coincide with the values reported on Tabla 31. The map representation of Murphy Corella, (2019) results can be found on a interactive web map[1]. Comparing the web map with Figure 2 of the paper we see that 4 additional intensity points were included in the paper, that are not mentioned neither in Tabla 31 or in the web map created by Murphy Corella, (2019). The explanation may lie on the caption of the AP1 table: "Translation of earthquake effects reports for different sites studied by Murphy Corella, (2019) and the intensity values he **initially** assigned to each site". These "initial" values are not easily found on the original reference and an explanation should be given on the differences found between the intensity values used in the paper and the ones on Tabla 31 and the web map.

GMM

The Akkar & Bommer (2010)'s GMM used in the paper requires that parameters defining the type of soil and type of rupture are defined. These parameters should be provided in the paper.

Scaling laws

The authors mention the use of scaling laws presented by Stirling et al. (2002) and Wells & Coppersmith (1994). These two works define a plethora of scaling laws and the authors should detail the ones used in the paper, with a justification if needed.

[1] https://drive.google.com/open?id=1z9Iqxi6gXy7TYDV6xGCkY3nY5uSICBZi&usp=sharing

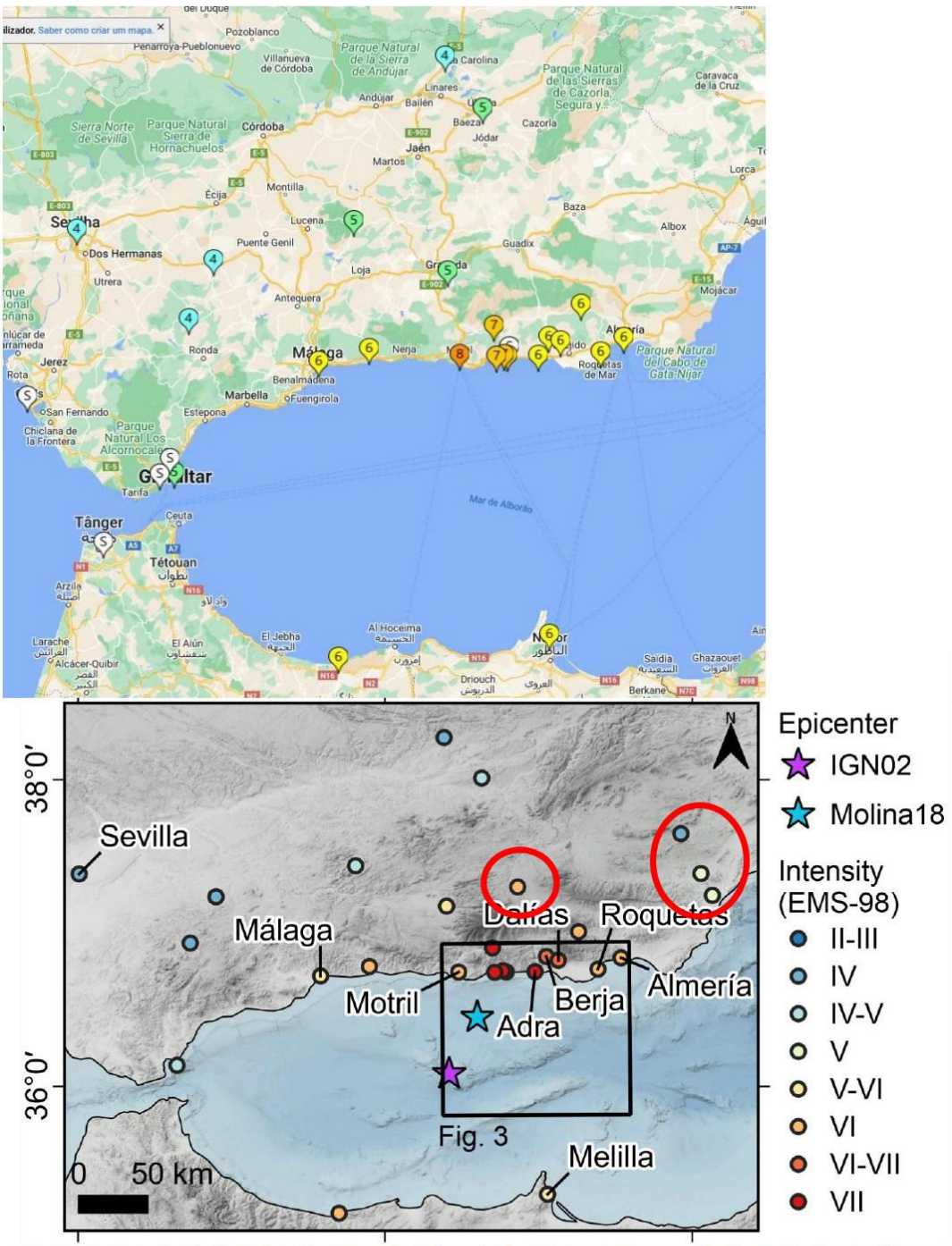

Figure 2. Intensity field of the Alborán earthquake of 13th January, 1804, compiled by Murphy Corella (2019). IGN02: epicenter estimated by Martínez Solares & Mezcua Rodríguez (2002). Molina18: epicenter estimated by Molina et al. (2018).

The untold premise

It is inferred from the paper that there is a perfect knowledge of active faults in the area, onshore and offshore, so that the 1804 Alborán earthquake could only be generated by one of the known faults. Furthermore, given the evidences of a tsunami generated, the fault should be offshore.

This is a very bold assumption given that the region is considered a slow deformation domain with low fault activity. Experience from other more active domains like California should be a more cautious sentence and the rupture of an unknown blind fault should not be ruled out. Furthermore the evidence of seismic activity presented doesn't show any clear relationship between earthquake location and the known active faults. Focal mechanism information is not clear also to support this premise.

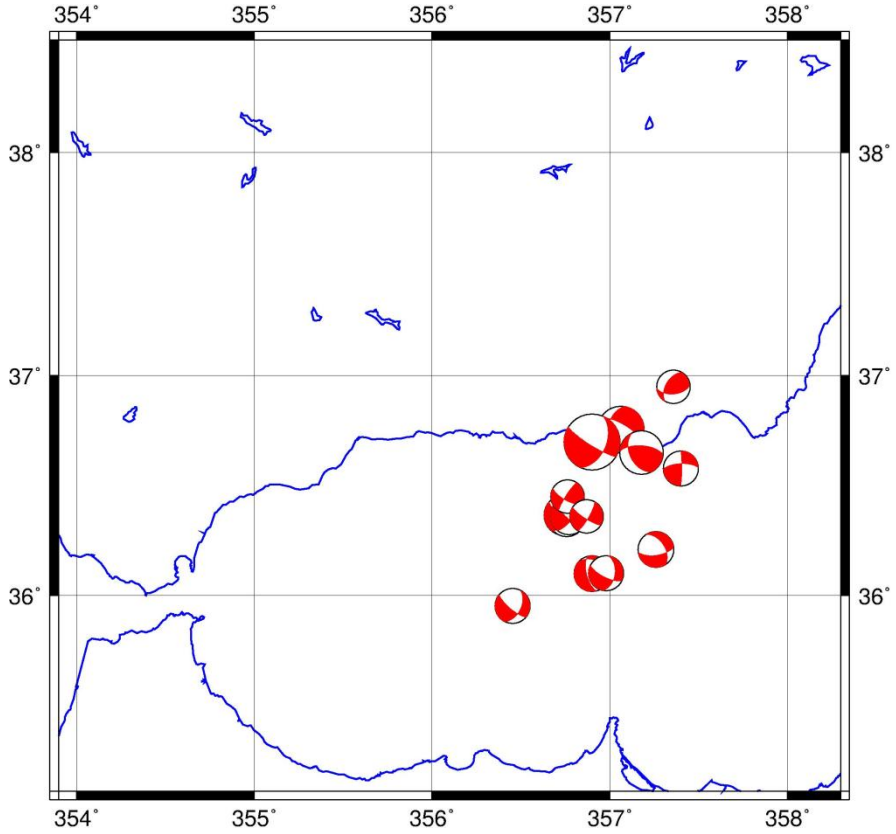

Model development guided by the untold premise

To compare observed to model intensities the authors compute model intensities from one GMM law to obtain either PGA or PGV which ground motion values are then converted to intensity using on GMICE.

Following previous work in the area by de Pro-Díaz et al. (2022, 2023) the authors began to use the Campbell & Bozorgnia (2014)'s GMM. The reasons for the choice of this GMM were detailed in de Pro-Díaz et al. (2023). We recall that this was the GMM used to select rupture

D for the August 1804 earthquake, used in the paper to evaluate the possibility of seismic triggering. Finding out that "none of the candidate ruptures generated intensities high enough to match the observed earthquake effects", then the authors decided to use the Akkar & Bommer (2010)'s GMM because it fitted the untold premise better. Would this GMM fit the August 1804 scenario investigated in de Pro-Díaz et al. (2023) better also? The change from one GMM to another without discussing the previous work is insufficient.

When computing macroseismic intensities from ground motion models, the authors choose PGV instead of PGA ground motion values, again because it fitted better the untold premise.

The fault parameters for the earthquake scenarios were taken from the QAFI database and (we suspect) the moment magnitude inferred by the scaling laws provided by Stirling et al. (2002) and Wells & Coppersmith (1994). For two of the faults investigated (under the untold premise) this magnitude didn't provide intensities similar to the ones observed and so the authors increased the source magnitude 0.4 and 0.5 but didn't discuss the consequences of such decision to the knowledge of the faults parameters or if these values violated the scaling laws used. We finally remark that two out of four of the retained source scenarios are derived from these ad-hoc magnitude increments guided by the obedience to the untold premise.

Model misfit evaluation #1

The authors use as misfit measurement between model and observations simple statistical parameters, average and standard deviation, as applied to the distribution of the differences between observations and models at individual points. This misfit evaluation is prone to several problems not addressed in the paper. Firstly average and standard deviation are enough to characterize a statistical distribution only if that distribution is Gaussian-like, which is not demonstrated. Secondly, this misfit evaluation is not robust to the presence of outliers. I will try to illustrate these problems using examples with a small number of difference values.

Consider the following sets of differences, A=(-2,0) and B = (-5,3). Both sets have an average of -1 but A is clearly better than B. The difference should show up in the values of the standard deviation but the authors do not mention any criteria regarding this issue and neither is applied in the paper. Furthermore there is no support in distribution B to conclude that "on average the model underestimates observations by 1".

To illustrate the influence of outliers, consider know the following sets of differences, A=(-2,-1,5) and B = (1,1,1). Both sets have an average of +1 but it would be difficult to support the conclusion that "on average the model overestimates observations by 1".

The validity of the authors conclusions should be supported by additional information, at least by showing the histogram of the difference values.

We tried to assess these questions by computing the intensity differences under the following assumptions: i) the intensity values are taken from Tabla 31 of Murphy Corella (2019); ii) we assume a log attenuation law for intensity over distance, a functional dependence similar to the conjunction fo the GMM and GMICE used in the paper; iii) we use a single point source with the epicentre taken from the closest to the coast fault point as shown in Figure 3.

The law in (ii) will be derived by least squares fit meaning that the average of residuals will be zero or close to zero, different from the results in the paper. But our aim here is to obtain histograms of the differences to check if they are or not Gaussian-like. The results are shown below where the acronyms stand for LVF: Loma del Viento Fault, BF: Balanegra Fault, AF: Adra Fault and AIF: Al-Idrissi Fault.

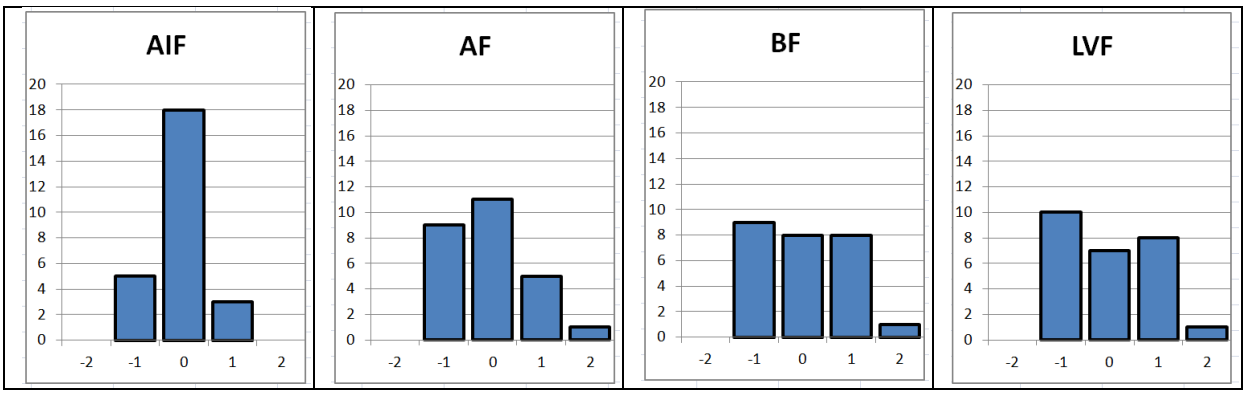

All models show a nearly zero average but they are clearly difference as regards standard deviation. Only AIF model shows a Gaussian-like distribution. Maybe another more usual way of measuirng model misfit, like the root mean square error or the average of the absolute value of differences, could help to choose the best or preferred model, as shown in the table below.

	Average	Standard deviation	Average of |differences|
AIF	-0.077	0.560	0.308
AF	-0.077	0.845	0.615
BF	0.038	0.000	0.731
LVF	0.916	0.938	0.769

Model misfit evaluation #2

As mentioned in the paper, the authors use the model intensity values computed from PGV to select a smaller set of sources for further evaluation. The average and standard deviation of each model are shown graphically but they are not presented in a Table. I recovered these values from Figure 6 and show them on the table below, ordered from the smallest to the largest average value and then ordered on the value of standard deviation. The selected scenarios are shown in bold, rejected models are in red.

scenario	M	ave	std
LV2	**6.9**	**0.26**	**1.06**
A3	**6.9**	**0.45**	**0.64**
A2	6.7	0.56	0.58
AI	**7.0**	**0.56**	**0.67**
B	**6.6**	**0.56**	**0.80**
A1	6.5	0.75	0.69
LV1	6.4	0.78	0.93
C3	6.4	1.07	0.93
C1	6.5	1.14	0.85
C2	6.5	1.15	0.83

I fail to see the reason why scenario A2 was rejected, when it has the same average difference as retained scenarios AI and B while showing a smaller standard deviation. Furthermore, the average difference between the 1st and 2nd retained scenarios is the same as between the last retained scenario and the first rejected. What was the criteria for the decision the accept or reject scenarios? It is not clear in the paper.

Dealing with uncertainty

It is well known that GMM and GMICE laws are uncertain and the statistical dispersion is usually described by the standard deviation. The compound standard deviation of the Akkar & Bommer (2010) laws are 0.279 and 0.278 for PGA and PGV respectively in base 10 logarithmic scale (CGS units). For the GMICE laws used the standard deviation in intensity unis is 0.73 and 0.65 for PGA and PGV respectively. Considering the uncertainties in GMM and GMICE statistically independent, we may estimate the compound standard deviation on the model intensities as 1.2 and 1.1 for PGA and PGV respectively. These values are larger than the standard deviations computed for each source model. If these are taken into consideration, maybe a sizable amount of model values cannot be ascribed a difference value larger than 1. The methodology used deserves some discussion on the influence of GMM and GMICE uncertainties on the final results.

Minor comments

These comments are provided to help on a future submission of the present work.

The authors investigated 5 faults as the possible source for the 1804 Alborán earthquake and, despite the work done, only the Carboneras fault was discarded. The other four faults remained as possible sources. This conclusion should be clearly shown on the abstract, discussion and conclusions.

Following the methodology already used in the area by Pro-Díaz et al. (2023), step 3 implied the statistical investigation of "differential zones". In the case discussed in the paper, this step 3 failed due to the lack of a significant number of observations on these "differential zones". Given this, there is no need to detail the application of this step, the reader will believe the word of the authors. If needed, an example may be provided as supplementary material.

The presentation of the Coulomb stress transfer caused by the 25th August earthquake on instrumental seismicity is a subject that is not relevant to the main purpose of the work and should be omitted in future presentations.

Round 2

Reviewer #1

I have reviewed for the second time the manuscript titled *"The 1804 Alborán Seismic Series: Search for the Source Using Seismic Scenarios and Static Stress Interactions"* by de Pro-Diaz et al., submitted to *Seismica*. The manuscript has significantly improved compared to the initial version. I would like to compliment the authors for their substantial efforts in addressing the concerns raised in my first review and for thoughtfully incorporating the feedback from other reviewers.

In the annotated PDF, I have suggested several minor edits and provided comments that I believe may help further improve the manuscript. While the overall quality has increased, I believe the Discussion section could benefit from additional refinement.

Specifically, I recommend restructuring the Discussion into three clearer subsections: (1) Source Discussion, (2) GMM + GMICE Discussion, and (3) Comparison of Reported vs. Modeled Magnitudes for Offshore Historical Events. Most of this content is already present, so implementing this suggestion should not require extensive rewriting, but it would help enhance the clarity and organization of the discussion.

Please refer to my detailed comments in the annotated PDF, which I hope the authors will find constructive and helpful in finalizing the manuscript.

Reviewer #2

Dear Authors, I had the opportunity to review the second version of your paper. I really appreciated the efforts you made in performing additional analyses and in improving the manuscript. All my comments to the first version of the manuscript were adequately addressed; I think the paper is a nice contribution and provides useful information for the seismic hazard assessment of the region.

I just found a typo at line 150: should be “in Italy” instead of “on Italy”.

Reviewer #3

The authors did a good job reviewing this manuscript, responded satisfactorily to my comments and implemented the required changes. The writing was significantly improved. I think this manuscript is now ready for publication. This will be an important contribution. I just have one last suggestion. Around lines 234-237, the authors refer to an author when citing his work by "he". It would probably be better to adopt a gender neutral language, such as "the author".

João Duarte (University of Lisbon)